1984

Characterization of Iron-Ruthenium Bimetallic Catalyst Systems (Methanation, Moessbauer, Zeolite).

M. Mehdi Akbarnejad
Louisiana State University and Agricultural & Mechanical College

INFORMATION TO USERS

This reproduction was made from a copy of a document sent to us for microfilming. While the most advanced technology has been used to photograph and reproduce this document, the quality of the reproduction is heavily dependent upon the quality of the material submitted.

The following explanation of techniques is provided to help clarify markings or notations which may appear on this reproduction.

1. The sign or "target" for pages apparently lacking from the document photographed is "Missing Page(s)". If it was possible to obtain the missing page(s) or section, they are spliced into the film along with adjacent pages. This may have necessitated cutting through an image and duplicating adjacent pages to assure complete continuity.

2. When an image on the film is obliterated with a round black mark, it is an indication of either blurred copy because of movement during exposure, duplicate copy, or copyrighted materials that should not have been filmed. For blurred pages, a good image of the page can be found in the adjacent frame. If copyrighted materials were deleted, a target note will appear listing the pages in the adjacent frame.

3. When a map, drawing or chart, etc., is part of the material being photographed, a definite method of "sectioning" the material has been followed. It is customary to begin filming at the upper left hand corner of a large sheet and to continue from left to right in equal sections with small overlaps. If necessary, sectioning is continued again—beginning below the first row and continuing on until complete.

4. For illustrations that cannot be satisfactorily reproduced by xerographic means, photographic prints can be purchased at additional cost and inserted into your xerographic copy. These prints are available upon request from the Dissertations Customer Services Department.

5. Some pages in any document may have indistinct print. In all cases the best available copy has been filmed.

University Microfilms International
300 N. Zeeb Road
Ann Arbor, MI 48106

Akbarnejad, M. Mehdi

CHARACTERIZATION OF IRON-RUTHENIUM BIMETALLIC CATALYST SYSTEMS

The Louisiana State University and Agricultural and Mechanical Col. PH.D. 1984

CHARACTERIZATION OF IRON-RUTHENIUM BIMETALLIC CATALYST SYSTEMS

A DISSERTATION

Submitted to the Graduate Faculty of the
Louisiana State University and
Agricultural and Mechanical College
in partial fulfillment of the
requirements for the degree of
Doctor of Philosophy

in

The Department of Chemistry

by
M. Mehdi Akbarnejad
M.S., University of Central Florida, 1977
May 1984

ACKNOWLEDGEMENTS

With gratitude the author acknowledges the determining role played in this research by his dissertation advisor, Dr. Mary L. Good. It has been an invaluable experience professionally and personally to work with you. Your guidence and assistance will always be remembered and sincerely appreciated.

I am thankful to Professors Frank Cartledge, Brian Hales, Teresa Monger, Geoffrey Price and, Steven Watkins for their evaluation of the dissertation.

I wish I could fully express my deep gratitude to my parent for their unending moral support and love. Ms. P. Simon is also due thanks for her assistance and encouragement.

I wish to thank my many colleagues in Dr. Good's research group for their suggestions and assistance especially Dr. John Carter, Dr. M. D. Patial and Dr. Jeffery Donner.

The author is grateful to the National Science Foundation (Grants No. CHE 76-17434 and CHE 79-12999) for financial support.

Finally I wish to acknowledge the financial support of the Dr. Charles E. Coates found for costs pertinent to the publication of this dissertation.

TABLE OF CONTENTS

TABLE OF CONTENTS (cont.)

TABLE OF CONTENTS (cont.)

LIST OF TABLES

LIST OF FIGURES

LIST OF FIGURES (cont.)

LIST OF FIGURES (cont.)

ABSTRACT

Due to the potential of iron-ruthenium bimetallic heterogeneous catalysis in a number of high demand, energy related processes, this study was undertaken to synthesis and characterize a series of bi-metallic Iron-Ruthenium alloy and clusters. A material science approach was taken which relies on the physical and chemical characterization of catalyst material itself rather than the classical chemical kinetics investigation of the catalytic reaction. Various methods have been employed for the determination of surface and bulk properties of catalysts during dehydration - hydration, and oxidation - reduction treatments. In the case of the bimetallic systems, the use of ^{99}Ru and ^{57}Fe double labelled Mossbauer experiments was most useful. Additional information was obtained from ESCA, X-ray diffraction, and infrared spectroscopy. This array of physical techniques provided complementery details for the complete characterization of the systems of interest.

It is known that iron cannot be reduced beyond the ferrous state when ion exchanged in Y-zeolite. Thus, the reduction behavior of iron on zeolite surfaces is considered a classical problem in catalytic research. Several attempts were made to modify the reduction behavior of iron. One approach was to introduce ruthenium into the system to encourage hydrogen spillover which should provide the reactive hydorgen atom as the reducing agent. Utilizing the preparation method designated as "Homogeneous-Deposition", the iron was reduced and the formation of hcp iron-ruthenium clusters on the surface of Y-zeolite was confirmed.

To elucidate the nature of the interaction between iron and ruthenium and to evaluate the chemical differences of the solid state reaction during the preparation of bimetallic iron-ruthenium, the products formed when ruthenium trichloride is mixed with a variety of iron salts and oxides were investigated. The anions associated with the metal in the initial material influenced the formation and the nature of bimetallic particles.

A unique preparative method based on the reaction of a cation exchanged zeolite with a metal-containing coordination complex anion was extended to synthesize the mixed iron-ruthenium cyanide polynuclear complexes directly on the zeolite. Under reduction conditions hcp iron-ruthenium bimetallic alloy was detected. This preparative method could provide an alternative way to stabilize polymetallic particles on zeolites.

CHAPTER I

INTRODUCTION

A. GENESIS OF IRON AND RUTHENIUM CATALYST SYSTEMS: METHANATION REACTION AND MECHANISM.

Although significant scientific and technological advances in the field of catalysis have been made in recent years, the details of catalytic phenomena are still not generally well understood. Catalytic systems can be divided into two distinct categories: homogeneous catalysis - where the catalyst is in the same phase as the reactants; and heterogeneous catalysis - where a phase boundary separates the catalyst from the reactants. Heterogeneous catalytic systems have been widely utilized in large-scale processes in the chemical and refinery industries. In these systems the reaction takes place on the surface of the catalyst, thus the specific chemical properties of the surface become a critical factor in fully understanding the processes. The surface atoms possess lower coordination numbers than the bulk atoms and chemical adsorption of the reactant molecules takes place as the result of molecular interaction with free valences of surface atoms. The adsorption properties of the surface active sites of the solid depend on the chemical nature of the catalyst components. The understanding of catalytic phenomena at the atomic level is limited due to difficulties associated with characterization of the active site. In recent years, new developments in solid state chemistry and the introduction of many advanced analytical methods have provided new approaches to thorough

investigations of catalytic processes at the microscopic and molecular levels. Evaluation of physical and electronic states of active catalytic centers and correlation of these properties with information concerning the activity and selectivity of the systems under specific reaction conditions provides a clear basic understanding of "how catalysts work". Such insight into catalytic properties and processes is particularly useful in the field of catalytic design, where there is the need to prepare a selective and active catalyst for a specific reaction of interest.

For most heterogenous systems it is particularly efficient and economical to use the catalyst elements in the form of fine metallic particles dispersed on the surface of a high surface area support. The preparation of a supported metal catalyst includes both the loading of metal or metal compound in or on the support material and the treatments governing the final dispersion of the metal. Generally, supported metal catalysts are of more interest than unsupported ones because of their higher degree of dispersion and greater stability. The physical chemical characterization of supported metal catalysts is a challenging problem because of difficulties in obtaining direct information on the chemistry and microstructure of metallic particles of the small size and low concentration typical of practical supported systems. Complexity is also introduced due to the physical chemical nature of the support. The nature of the carrier may influence the reducibility and degree of dispersion of the catalyst particles as well as alter the electronic properties of the metal through metal support interaction. In the presence of such a strong interaction it will be very difficult to generate and stabilize a well dispersed metallic particle on the surface

of the carrier. It is possible to accelerate the reduction of a highly dispersed metal by adding a second metal which is highly active toward hydrogen reduction. However, the importance of the effect of the addition of a second metal to form a bimetallic system goes beyond the ease of reduction. In many cases the properties of binary metal catalysts have shown a remarkable shift in activity and/or an improvement in selectivity and stability when compared to monometallic systems. Because of interesting features with regard to solid state and surface properties, bimetallic catalysts offer many opportunities for significant advances in heterogeneous catalytic systems. Developments in this area are being reported regularly and significant research is underway to explain this aspect of heterogeneous catalysis.

In the field of catalysis, group VIII transition elements have long been recognized as active and selective species for various important industrial proceses. Tremendous research effort has been directed toward the development of desirable catalysts for problem oriented, energy related field such as carbon monoxide hydrogenation. Among the transition elements, iron and ruthenium have been shown to be two of the most active catalysts for synthesis of hydrocarbons via CO-hydrogenation (1-2). In addition, ruthenium-containing catalysts have found utility in a wide selection of reactions such as solar energy conversion (3-4), various hydrogenation processes (5-6), the water gas shift reaction to produce hydrogen (7), and other potentially attractive processes. The importance of iron and ruthenium catalysts and, especially the bimetallic aspect of these two metals, in the technologically interesting area of synthesis reactions of hydrocarbon production will be reviewed in the following section.

In order to compensate for the irreversible rapid depletion of natural reserves of fossil fuels, many new energy sources are being researched (8-9). Considerable interest has been focused on utilizing the tremendous coal reserve as a possible source of gaseous fuel and chemical raw materials (10). One process of interest is the production of synthetic gas containing carbon monoxide and carbon dioxide by the reaction of coal with oxygen and superheated steam, and the subsequent catalytic hydrogenation of the gas to methane and other hydrocarbons (11-13). The production of a wide range of products can be achieved with the appropriate choice of catalyst and reaction conditions (10). The earliest examples of such chemistry were reported for the formation of methane from CO + H_2 in 1902 (14) and synthesis of higher molecular weight hydrocarbon in 1923 (15) by Fischer-Tropsch (F-T) using iron as catalyst.

The still unanswered fundamental question associated with CO + H_2 synthesis involves the problem of selectivity and is closely related to the mechanism of the reaction (12). The reaction mechanism of F-T synthesis has long been the subject of debate and is still a matter of controversy. Many different types of mechanisms have been suggested (16-19). The question of the most applicable model is now believed to depend on the nature of the metal surface involved. The carbide theory was the earliest mechanism model proposed for the reaction over an iron catalyst (15). Rather large amounts of surface and bulk carbide have been detected on the surface of this catalyst during CO-hydrogenation (20-21). Iron, as the most electropositive element among group VIII transition metals, forms a very strong bond with carbon. When carbon monoxide comes into contact with the iron surface, the large binding

energy between iron and carbon causes the molecule to dissociate on the surface, consequently surface carbides are formed (22-23). The surface carbides appear to be the active surface species and at higher temperature they irreversibly convert to carbon bulk deposits characterized as graphite, which deactivates the catalytic site (23-25). There is growing evidence in the literature that hydrocarbon synthesis over both ruthenium and iron procedes via initial formation of surface carbides (25).

Dissociative, as opposed to an associative, adsorption of carbon monoxide is known to occur on the surface of many transition elements (26). This tendency increases moving from right to left across a row in the periodic table and upwards in each group. It has been shown that the vibrational frequency of the C-O bond decreases proceding from right to left across a row. This can be related to a decrease in the C-O bond order in the chemisorbed state. It has been concluded from such spectroscopic work that the stretching of the C-O bond is a prerequisite for the dissociation of carbon monoxide on the surface of transition metals (19). Theoretical calculations indicate that the metal-carbon bond is comprised of two components (27-28). The first is the donation of electrons from the carbon monoxide molecules to the metal through an overlap of occupied 5σ orbitals of CO and unoccupied metal orbitals. With respect to the C-O bond, the 5σ orbital in gaseous CO is essentially nonbonding, so, the donation of electrons is not expected to affect strongly the strength of the C-O bond in the chemisorbed state. The second component of the metal-carbon bond arises from an overlap of occupied metal orbitals and unoccupied $2\pi^*$ orbitals of CO. This results in the donation of electrons from the metal to the molecule. Since $2\pi^*$

orbitals are antibonding with respect to the C-O bond, the donation of electrons into these orbitals leads to a weakened C-O bond. Thus through a greater availability of d-electron density on transition metals the metal-carbon bond becomes strong and the C-O bond strength diminishes as demonstrated by lower C-O vibrational frequencies (29). The dissociative adsorption of carbon monoxide at elevated temperature is usually accompanied by the release of oxygen in the form of CO_2, thus, normally the dissociation of carbon monoxide and formation of CO_2 takes place on the surface of metals which form a stronger metal-carbon bond than the carbon-oxygen bonds in CO_2 (22). Rupture of the C-O bond during adsorption and the formation of CO_2 has been detected and attributed to the disproportion of carbon monoxide on the surface of both ruthenium (30, 31, 35), and iron catalysts (32).

Identification of the processes involved in the chain growth of hydrocarbons during catalytic hydrogenation of carbon monoxide is essential for understanding the chemistry which controls the selectivity of the catalyst. The product selectivity can be expressed by olefin/saturated ratios, length of hydrocarbon chain, and tendency to produce branched chain hydrocarbons. The hydrogenation of carbon deposited by CO disproportionation readily produces methane and higher molecular weight hydrocarbons. The first stage of hydrogenation involves the formation of CH_x (x = 1-3) species by the stepwise addition of atomic hydrogen to singlet carbon atoms, producing adsorbed methylene and methyl groups. These species may be considered as precursors to methane as well as centers for hydrocarbon chain growth (33-34). The hydrogenation of carbon deposited on the surface of the ruthenium catalyst leads to the appearance of ethane, propane and butane in addition to methane

with quantitative consumption of carbon at room temperature (35-36), whereas chemisorbed CO was found to be totally unreactive. On the surface of the iron catalyst, it was noted that the rate of hydrocarbon formation corresponds to the rate of hydrogenation of surface carbon deposits (19-20, 34), thus molecularly adsorbed CO apparently is not involved in the chain growth processes. Further investigation has indicated that the chain growth procedes through the polymerization of partially hydrogenated carbon species (35). The insertion of methylene groups into metal-carbon bonds has been observed (37-39), this process leads to the formation of an ethyl group, and continuation of this type of reaction gives rise to the formation of an adsorbed alkyl group. Alkanes are formed by the reaction of alkyl groups with adsorbed hydrogen. Unsaturated hydrocarbons are produced by β-elimination of the hydrogen atom from the alkyl groups. It has been further noted that, with an increase in the partial pressure of hydrogen, the extent of chain growth is suppressed and olefin content of the product is decreased (39). In the absence of sufficient atomic hydrogen on the catalyst's surface, the CH_x group recombines to form ethylene rather than adding hydrogen to form the methylene group.

Substantial improvement in the selectivity of the reaction, leading to a preferred formation of lower olefins as primary product is one route for making the Fischer-Tropsch synthesis promising and economically feasible (40-41). Development of a catalytic system which maximizes the selectivity toward lower olefin products is one of the major research objectives today in this field. The correlation between catalyst surface basicity and hydrocarbon selectivity has been investigated (42-45). Higher surface basicity, introduced by addition of the alkali

metals promoters to the catalyst, has been correlated with lower methane selectivity. Increased electron density of the transition metal, induced by basic promoters, may enhance the back-donation of electrons from the metal to antibonding orbitals of the C-O bond. The bond is thereby weakened, its dissociative probability is increased and the relative surface concentration of carbide species is increased. The donation of electrons to the metal by alkali promoters also increases the strength of the metal-carbon bond and the relative residence time of carbide species on the surface is subsequently increased, thus permitting a longer chain growth. At the same time, as the surface of the transition metal becomes more basic, the affinity of the surface for hydrogen adsorption decreases. This then decreases the relative hydrogen surface concentration, which gives rise to higher selectivity of the surface for unsaturated hydrocarbons.

The promotion influence of support material on the hydrocarbon selectivity has also been studied (46). The formation of longer chain hydrocarbons has been detected over X zeolite as compared to Y zeolites. This effect is apparently due to the fact that X zeolites are less acidic than Y zeolites. This is indicative of the fact that the zeolite matrix interacts with the metal particles, whereby the metal becomes more electron deficient, thus promoting the chain growth of hydrocarbons under F-T reaction condition.

"Ideal catalysts" should have a moderate affinity for both carbon monoxide and hydrogen adsorption. The metals which adsorb CO most strongly adsorb H_2 most weakly. Adsorption dissociation of carbon monoxide and, consequently, the formation of carbide species takes place to a considerably greater extent on iron than on ruthenium, whereas

adsorption of hydrogen takes place to a greater degree on ruthenium than on iron. One would expect, therefore, that the bimetallic FeRu would show higher efficiency for CO + H_2 reaction. The relative availability of adsorbed H_2 and CO depends on the composition ratio of Fe/Ru on the catalyst surface which determines the catalytic activity and selectivity under F-T reaction conditions (50). CO hydrogenation has been studied over both supported and unsupported FeRu catalysts (47-51). The addition of ruthenium to iron produces effects on selectivity similar to those observed when alkali promotors are added to iron; that is, methane formation is reduced and olefin formation is enhanced (48). When a bimetallic system is used, the hydrogen is apparently adsorbed, activated and supplied by ruthenium metal, thus the carbon deposits on the surface of the iron should be removed with increased amount of hydrogen. This should increase the activity of the catalyst compared to pure iron. Compared with pure ruthenium, the hydrogen concentration on the surface of FeRu bimetallic catalyst is lowered by the addition of iron, which reflects the selectivity of the catalyst through lengthening of the residence time of carbon species on the surface, thereby permitting the carbon chain to grow (50). In the absence of sufficient atomic hydrogen on the surface, the olefin content of the product is increased. This hypothesis leads one to believe than an optimum range of FeRu composition must exist which would maximize olefin production and minimize methane formation. Thus, a higher activity with respect to pure iron and improved selectivity compared with pure ruthenium is expected for the FeRu bimetallic catalytic system under F-T reaction condition.

In this work we shall deal with the bimetallic system of iron and ruthenium. The term "bimetallic cluster" is chosen for referring to

highly dispersed binary metals supported on the surface of a carrier. The term "alloy" is used to designate the metallic system in the absence of support material. The characterization of these catalytic systems has focused on the evaluation of physical and electronic states, as deduced by Mossbauer spectroscopy.

B. MOSSBAUER SPECTROSCOPY AND ITS APPLICATION TO HETEROGENEOUS CATALYSTS

1. A BRIEF INTRODUCTION TO THE MOSSBAUER EFFECT

The Mossbauer effect when utilizd as a spectroscopic method, has a broad range of applications. It has been successfully applied to heterogeneous catalytic systems where detailed chemical information about well dispersed metal particles can be most useful. The technique is applicable to in situ studies and is thus not limited by the necessity to make measurements under conditions not representative of the actual catalytic process. Mossbauer spectroscopy is now a mature technique where instrumentation is readily available, and a good theoretical basis for interpretation of results exists. The resolution of the Mossbauer effect is so great that perturbation of nuclear levels of about 10^{-7}ev can be observed, and chemical, structural and magnetic information can be obtained about atoms on the surface and in the bulk phase of catalyst materials.

The principle of the Mossbauer effect can be described as a nuclear resonance fluorescence process which takes place during the recoil-free emission and resonant absorption of γ-rays (53-63). The experiment consists of the following sequential steps: 1) A source atom decays from an excited nuclear energy level to its ground state emitting a γ-ray of energy equal to the transition energy. 2) The emitted γ-ray

energy is modulated mechanically via the Doppler shift. 3) The modulated energy is then resonantly absorbed by an absorber nucleus of the same element and isotope number. 4) A Mossbauer spectrum is obtained as a plot of the intensity of the detected γ-ray beam transmitted through the absorber versus the modulation energy. Prior to the discovery of the Mossbauer effect (64), the nuclear resonance absorption (step 3) had not been observed because under the conditions of previous experiments the emitted gamma ray (step 1) lost sufficient energy through recoil effects to prevent resonant absorption. Mossbauer discovered that γ-ray emission without a loss of energy from recoil of the nucleus could be achieved by incorporating the nucleus in a crystal lattice. Also, at temperatures below the Debye temperature, the nucleus could emit a gamma ray with no recoil energy lost. Thus the Mossbauer effect is normally observed only in atoms bound in, or on, solids and usually at low temperatures.

The criteria for observation of the Mossbauer effect can be described through a discussion of several characteristic energies involved in the process. The displacement in energy of the emission and absorption distributions is of the order of their line widths. The natural line width of a γ-ray energy distribution is given by the uncertainty principle. For most Mossbauer isotopes, the mean life time of the excited state is of the order of 10^{-7}sec., with a corresponding natural line width of the order of 10^{-8}ev. The difficulties involved in observing nuclear resonance become readily apparent when we consider the line width of the nuclear transition as compared to the loss of recoil energy suffered by the nucleus during the transition process. The necessary condition for the utilization of the effect is that the recoil

energy be smaller than the natural line width. A typical value of recoil energy for an isolated atom is about 10^{-2}ev at room temperature. This value is six orders of magnitude larger than the natural line width, therefore making gas phase nuclear resonance difficult and perhaps impossible. It is possible to observe the γ-ray resonance in the solid state or in viscous liquid. The perturbation of nuclear levels by the chemical environment can be traced by the modulation of the primary recoil free γ-ray. The modulation energy is produced using the Doppler effect when the source is moved relative to the absorbed. A range of source velocities is scanned until maximum absorption occurs. The absorption occurs when the modulated energy is precisely equal to the energy difference between the nuclear ground state and excited state in the absorber. Detection of the γ-ray transmitted through the absorber versus the Doppler velocity produces the Mossbauer spectrum.

2. CATALYTIC INFORMATION DERIVED VIA THE MOSSBAUER EFFECT

The perturbation of the nuclear levels by the chemical environment can be interpreted in terms of chemical effects pertinent to catalysis. The chemical perturbation of the nuclear levels originates from one or more of the following interactions: the coulomb interactions between the positively charged nucleus and the negative electron density at the nucleus; the interaction between the nuclear quadrupole moment and the surrounding electric field; and the interaction between the nuclear magnetic moment and the magnetic field present at the nucleus. If both the source and absorber are located in an exactly identical chemical situation, nuclear levels in both will be the same, no modulation of original energy is needed and absorber resonance will take place at zero relative velocity, Fig.1. If the absorber nucleus is in a different

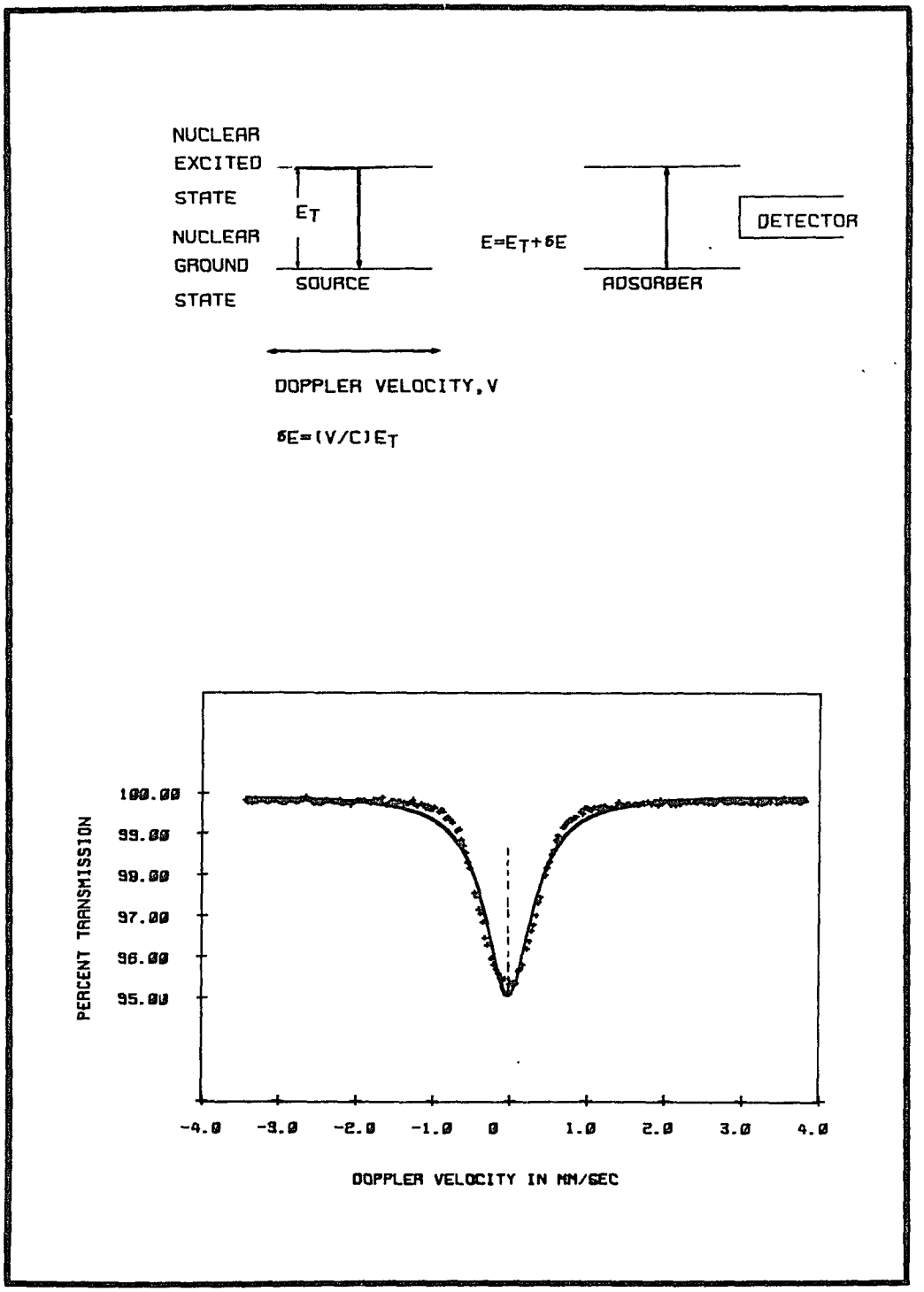

Figure 1. A Mossbauer Spectroscopy experiment.

chemical environment relative to the source nucleus, different perturbations of nuclear levels take place which result in shifts and/or splitting of the Mossbauer spectrum.

(1). Isomer Shift. The Coulomb interaction between the positively charged nucleus and the negative electron density at the nucleus manifests itself as a shift of the nuclear energy levels. For a given source, an absorber with a different electronic structure will have a different perturbation in nuclear levels characterized by a different isomer shift; i.e., shifts of resonance maximum from zero relative velocity, Fig.2. The determination of the isomer shift leads to an evaluation of electron density at the nucleus of the atomic species with respect to that of the source which can be chosen as a standard. The isomer shift is given by the following expression derived from the perturbation theory (55):

$$\text{I.S.} = \text{Nuclear Parameter Constant} \left(\psi(0)_A - \psi(0)_S \right) \qquad [1]$$

$$\text{Nuclear Parameter Constant} = 2/3\pi e^2 Z \left(\langle r^2 \rangle_e - \langle r^2 \rangle_g \right)$$

The isomer shift is a measure of the difference in the nuclear excitation energy between the nuclei in the source and those of the absorber for each Mossbauer isotope. The $(\langle r^2 \rangle_e - \langle r^2 \rangle_g)$ term is the change in the average value of the radius squared of the nuclear charge distribution going from the excited to the ground state. The fractional change in the nuclear radius in the ground and the excited states has been calculated for a number of Mossbauer isotopes and has the value of -1.8×10^{-3} for ^{57}Fe (54). The negative sign indicates that in the case of iron nuclei, the 1/2 ground state radius is larger than the radius of the 3/2 excited state. In this case, the nuclear parameter term has a negative sign. For iron compounds, if there is a larger electronic

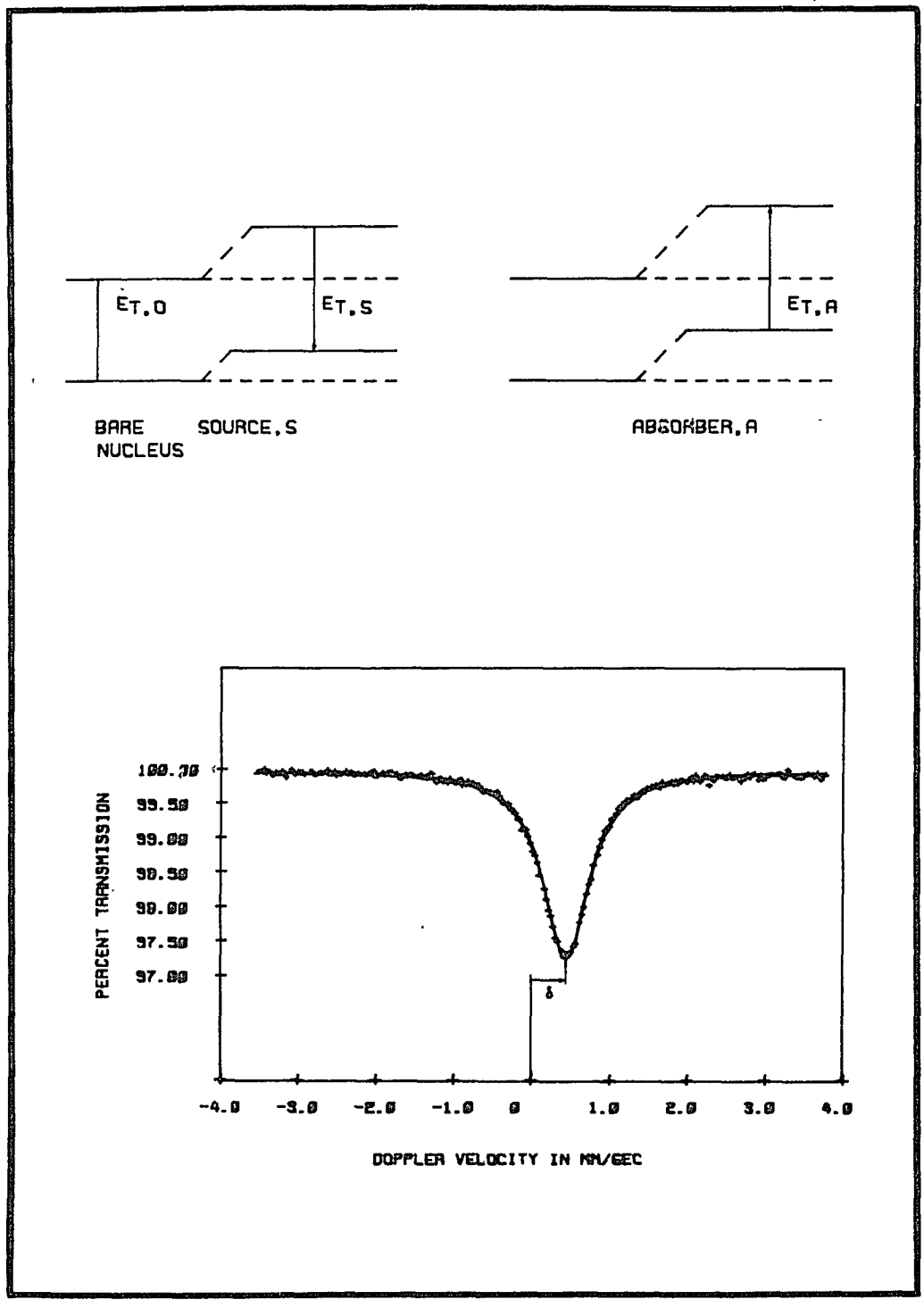

Figure 2. The Isomer Shift.

charge density at the source with respect to the absorber, $\psi_S > \psi_A$, it causes a positive shift of resonance peaks with respect to zero relative velocity.

The only electrons with a nonzero probability for being located at the nucleus are those in the s and $p_{1/2}$ orbitals. The relative importance of the electrons in these two orbitals indicates that the effect of $p_{1/2}$ electrons is often negligible compared to those of s orbitals (65). Thus the isomer shift mainly reflects the s-electron density at the nucleus. Due to shielding effects, the isomer shift is also sensitive to the presence of d and f electrons. The removal of d electrons effectively increases the s-electron density at the nucleus and consequently ferric species will have a smaller shift than ferrous ions, Fig.3. Chemical bonds which involve hybridization of orbitals will exhibit a range of shifts depending on the contribution of s and d orbitals. In these cases the chemical interpretation of the Mossbauer data yields information about the particular chemical bonds or oxidation states involved in the material (66). The isomer shift for iron atoms with the same oxidation state, electronic structure and with identical ligands is dependent on the number and symmetry of the coordinating ligands (67). Tetrahedral iron compounds have a lower isomer shift than octahedral compounds with the same ligands. In most cases, the detailed electronic information from the Mossbauer effect is most effectively supplied by a combined consideration of isomer shift values and the second hyperfine interaction, the electric quadrupole interaction (see the discussion of this effect below).

The temperature dependency of the isomer shift also supplies information of value in catalytic studies. A vibrating atom in the lattice

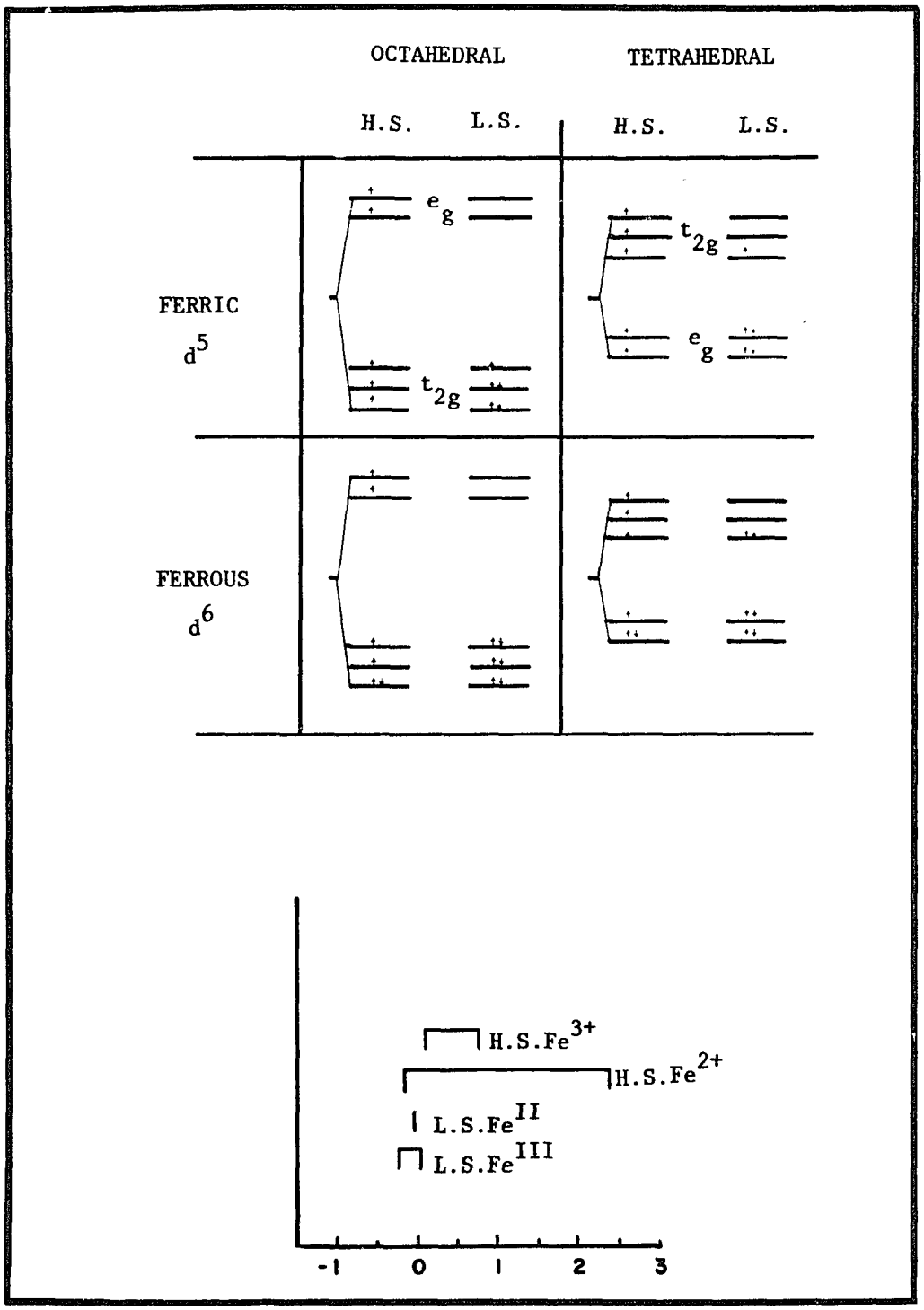

Figure 3. Electron population of the d orital for various electronic configurations and typical Mossbauer line positions for different oxidation states of iron.

sites gives rise to an average velocity equal to zero (the characteristic time scale for vibration is 10^{-12}sec, which is shorter than the time scale of nuclear decay, 10^{-7}sec). The second order velocity term, however, does not average to zero and alters the energy of emitted gamma rays via the Doppler effect. A weakly bonded atom will exhibit a larger velocity term and consequently a larger second order Doppler shift (68). This so called second-order Doppler effect is temperature dependent and provides information about the strength of bonding of the atoms in the lattice.

(2). Nuclear Quadrupole Splitting.

Any nuclear state with spin quantum number I>1/2 is nonspherical and has an ellipsoidal shape characterized by a nuclear quadrupole moment. In a non spherically symmetric electric field, i.e., when the field gradient tensor does not vanish at the nucleus, the interaction between the nuclear quadrupole moment and electric gradient tensor splits the nuclear state into I+1/2 levels having the same center as the unsplit level. In the case of the ^{57}Fe isotope, the excited I=3/2 level splits into two levels where the ground state I=1/2 remains degenerate Fig.4. The transitions between the ground level to these two excited states is displaced as a two line Mossbauer spectrum. The energy difference between two peaks is the quadrupole splitting (Q.S.), where the centroid of the doublet, relative to the source, is the chemical isomer shift. The split spectrum reflects the presence of a non-zero field gradient at the nucleus which is determined primarily by the symmetry of electronic distribution and consequently the symmetry of the bonding distribution about the Mossbauer isotope.

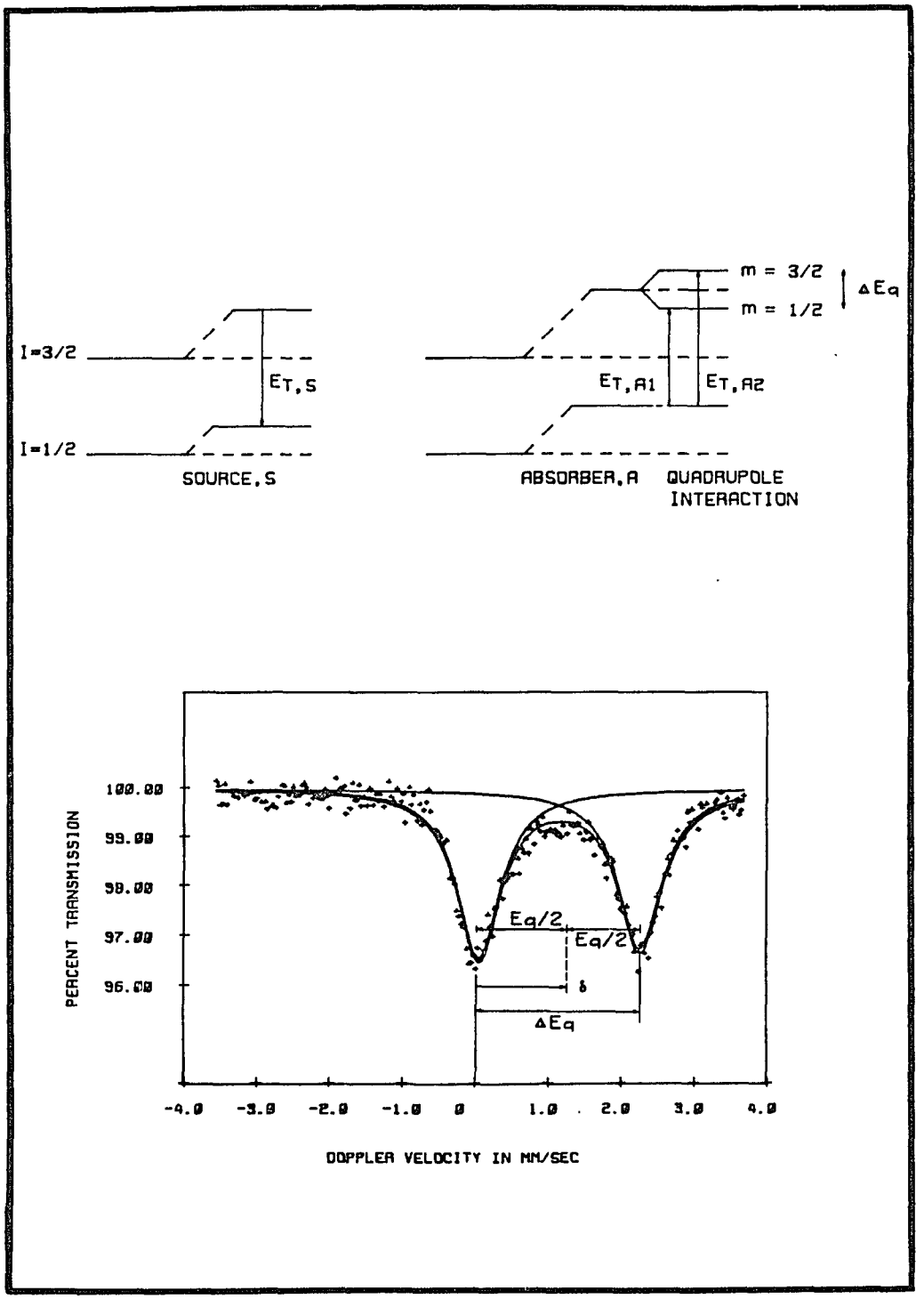

Figure 4. The Quadrupole Splitting.

The electronic symmetry about the nucleus can be affected by the atomic electrons which may fill orbitals in such a manner that the resulting electron spatial distribution produces an electric field gradient. Also the charge distribution, i.e., the crystal field of neighboring lattice sites or ligands and atoms in the crystal structure, may affect the symmetry of the electronic distribution about the nuclei. In the case of the ^{57}Fe isotope, the contribution of 3d valence electrons usually dominates the effect of the charge distribution or crystals field of neighboring ions in the crystal lattice (56, 57). High-spin ferric compounds where the half filled electron shell ($3d^5$) has a spherically symmetric electron distribution have a smaller quadrupole splitting compared to high spin ferrous species, $3d^6$, where large quadrupole splitting rises from the sixth d electron. Low spin Fe(II), has a symmetric valence electron distribution compared to low spin Fe(III) and therefore does not exhibit a significant quadrupole splitting Fig.3. The temperature dependency of the electric field gradient also provides additional information concerning the symmetry of the resonant atom. The crystal field effect of atomic electrons is temperature dependent as given by the appropriate Boltzman exponentials for the population of crystal field split energy levels. For high spin Fe(II) and low spin Fe(III), at higher temperatures, the electronic population around the nucleus becomes more symmetric and the quadrupole splitting will be reduced. For low spin Fe(II) and high spin Fe(III), higher energy is required to excite electrons to new orbitals, thus a smaller temperature dependency of splitting is expected. Unlike the crystal field splitting, the lattice effect is not very sensitive to temperature.

(3). Magnetic Hyperfine Splitting and Superparamagnetism

The interaction between the nuclear magnetic moment and the magnetic field around the nucleus gives rise to magnetic splitting. The magnetic field may be applied externally, or it may result from the electronic structure about the nucleus. In any nuclear state with spin quantum number I>0, the magnetic interaction removes the degeneracy of nuclear substates and splits it into 2I+1 levels. The split in the position of each level is given by

$$\Delta E_m = - g\mu Hm \qquad [2]$$

where g is the nuclear g factor, μ is the nuclear magneton, H is the magnitude of the magnetic field at the nucleus, and m is the quantum number for each magnetic state. In the case of ^{57}Fe the I=3/2 excited state splits into four, and the I=1/2 ground state into two, nuclear energy levels, leading to 6 allowed transitions (Fig.5). In this case the magnetically split absorber against an unsplit spectrum of the source gives a six peak pattern of equal spacing as the result of the magnetic field generated by the ferromagnetic exchange interaction. The separation between the outer two peaks is due to the 330 KG internal field of natural iron which has been found to be equivalent to 10.64 mm sec^{-1} at room temperature.

The effective magnetic field due to the electronic structure about the nucleus is sum of several contributions. The primary contribution arises from the Fermi contact interaction which produces a core polarization field due to the electron spin exchange interaction between polarized outer electrons and inner core s-electrons. This causes a slight imbalance at the nucleus of the density of s electrons with spin up compared to those spin down. In the case of iron, unpaired 4s elec-

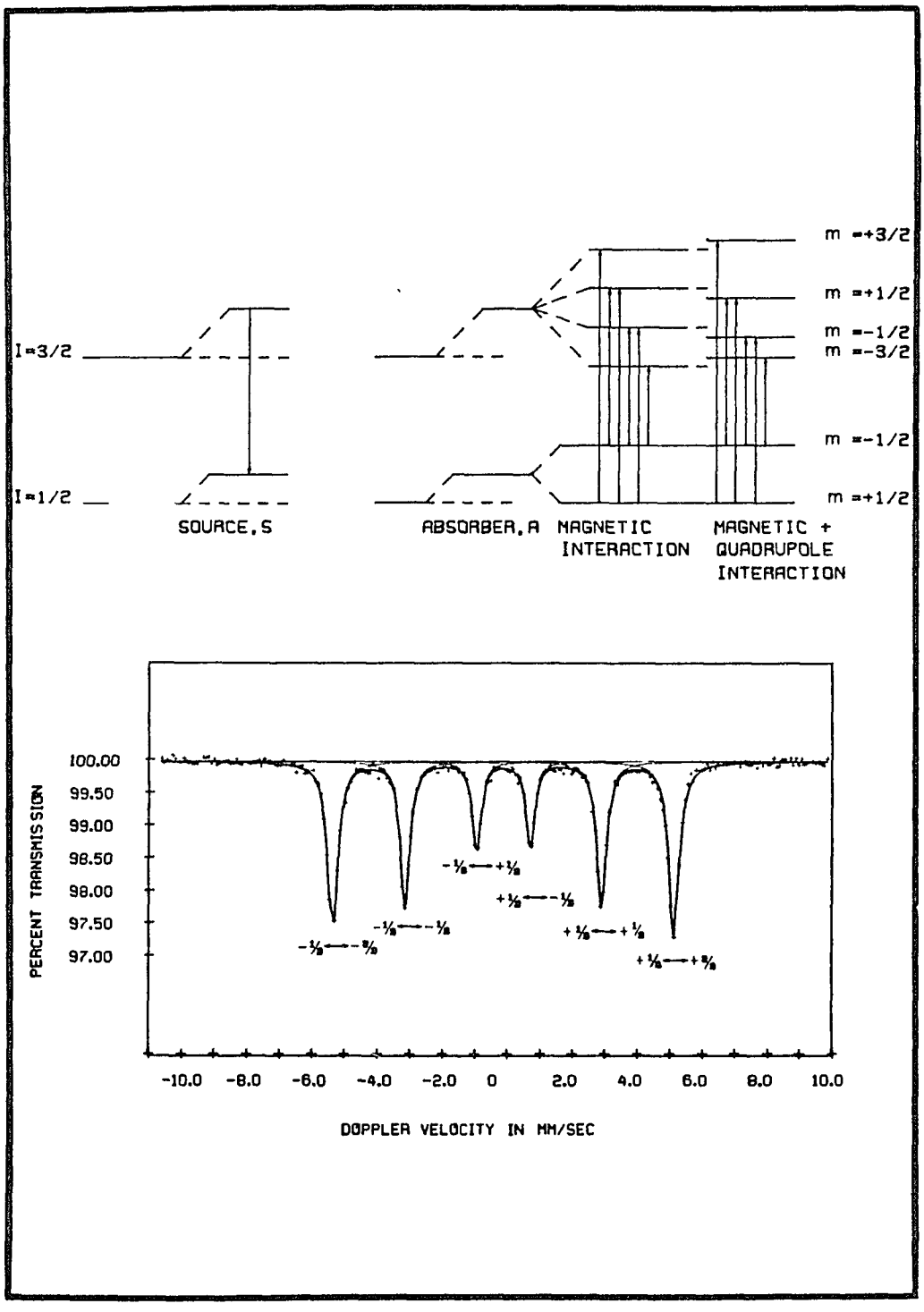

Figure 5. The magnetic hyperfine splitting and the combined quadrupole interaction.

trons make a direct contribution, but the polarization of inner s electrons by unpaired outer shell 3d electrons provides a larger contribution to this effect. The second contribution to the effective magnetic field about the nucleus arises from the orbital angular momentum of the electron distribution, and the third contribution is due to the total electronic spin. From these three magnetic terms, valuable chemical information can be obtained. Through the time dependency of these terms (magnetic relaxation), information concerning the particle size, shape and surface structure can be deduced.

In order to observe a distinct nuclear level splitting by the magnetic dipole interaction, the magnetic splitting must be larger than the line-width of the γ-ray distribution. In other words, the magnetic field must be fixed in space for a time period (life time of nuclear excited state) larger than, or at least of the same order of magnitude, as the time needed for nuclear interaction (the Larmor precession time of the nucleus is about 10^{-8}sec for iron in antiferromagnetic materials). If the magnetic field fluctuates faster than the nuclear precession time, the magnitude of the magnetic field at the stationary nucleus will average to zero (69, 70).

Two relaxation modes are involved in paramagnetic spin systems. One is spin-lattice relaxation and the other is spin-spin relaxation. The characteristic relaxation time for the spin-lattice mode decreases with increasing temperature, whereas the spin-spin relaxation time is usually temperature independent and becomes more important as the concentration of spins increases. At a characteristic Neel or Curie temperature of the solid the ordering of the electron spins breaks down and the directions of the electron spins of individual atoms become free of

order and average to zero during the observation time. Thus the magnetic dipole splitting in the Mossbauer spectrum vanishes. This phenomenon is referred to as superparamagnetism (72-75). The relaxation time of the magnetic moment of single domain particles is temperature (as well as volume) dependent. When the microcrystals are sufficiently small <100 A° (1 Angstrom = 10^{-8}), each particle can often be considered to be a separate spin system and the relaxation of the magnetic field at the nucleus is accompanied by the collective fluctuation of entire spin systems (spin waves) (73-75). The relaxation time of the phenomenon increases with the volume of the particles and decreases with temperature. Using the Mossbauer technique, it is possible to study the transition to superparamagnetism as a function of volume and temperature. For a given particle size, below a certain temperature, the Mossbauer spectrum is magnetically split. Considerably above this characteristic temperature the paramagnetic system with one or two lines is found. Near the characteristic temperature the value or relaxation time is close to the nuclear Larmor precession time and spectra with broadened lines are observed. The change in the direction of the magnetization vector for a single domain spin system is anisotropic with respect to the crystallographic axis (76). The height of the barrier will determine the relaxation time for magnetization fluctuations. Since all of the atoms in the spin system contribute to this magnetic anisotropy, the magnitude of the energy barrier depends on crystal structure, domain shape, and size (57). For small particle sizes the anisotropic energy with respect to temperature decreases, and thus decreases the relaxation time. The measurement of the magnetic anisotropic energy barrier provides information about the size and shape of the spin system, which for

small particles is equivalent to the particle size and shape. The transition from superparamagnetic to magnetically ordered behavior on increasing particle size or decreasing temperature can be quantitatively studied. The resulting data have been used to calculate the anisotropy constant at two temperatures and to obtain a size distribution for Fe_2O_3 (79), Fe_3O_4 (81-82) and metallic iron particles (83-84, 139).

The magnetic properties of α-Fe_2O_3 hematite have been extensively studied (77-80). The structure of bulk α-Fe_2O_3 involves a close-packed oxygen lattice containing ferric ions in octahedral sites. The moments on adjacent atoms are essentially antiferromagnetically coupled but above a characteristic temperature (the Morin temperature, T_M = 263K) the atomic spins aligning with one of the vertical planes of symmetry are slightly centered toward each other making a small angle with the basal plane, and the material exhibits weak ferromagnetism. Below T_M the spins are aligned parallel to vertical planes of symmetry and the material behaves as a normal antiferromagnet. The change in the magnetic behavior of bulk α-Fe_2O_3 in going through the Morin transition as reflected in the position of Mossbauer lines, is presented in Fig.6. These spectra were taken above and below the Morin transition temperature, 473K and 83K respectively. The difference between the spacing of the pairs of the outer peaks gives the quadrupole coupling constant.

(4) Recoil-Free Fraction, Mossbauer Line Intensity and Line Shapes. In general, the fraction of recoil free or zero phonon events, f, is given by

$$f = \exp\{-4\pi^2\langle x^2\rangle/\lambda^2\} \qquad [3]$$

where λ is the γ-ray wavelength, and $\langle x^2\rangle$, the mean square vibrational amplitude of the resonant atom in the direction of the γ-ray, increases

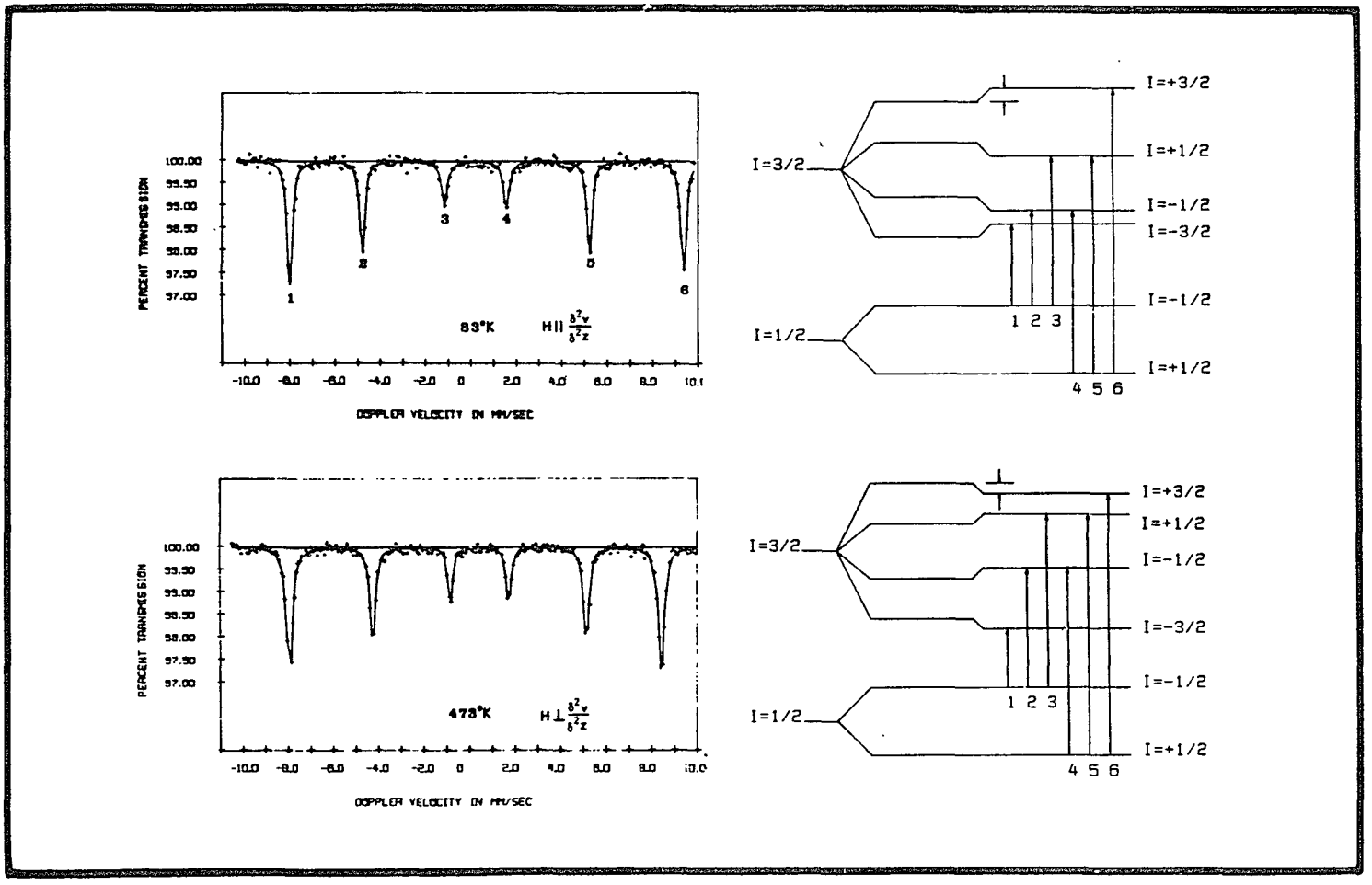

Figure 6. Morin transition effect in α-Fe_2O_3.

with temperature. The decrease in f with increasing temperature is a direct result of the increase of $\langle x^2 \rangle$ with temperature; thus, a measure of f and/or its temperature dependence is a measure of the strength of binding between the resonant atom and its surroundings (56). In microcrystals the recoil-free fraction was found to differ from the corresponding value in macroscopic samples (85).

Additional chemical and structural information can be provided through a careful expamination of the relative γ-ray intensities of the Mossbauer spectrum. In general, the value of Mossbauer transition probabilities, and therefore the relative intensities, depend on the angle between the γ-ray direction and the principal axis of the magnetic field or the electric field gradient tensor (68). For quadrupole splitting in ^{57}Fe, the ratio of two line intensities is given as:

$$\frac{I_{1/2 \rightarrow 3/2}}{I_{1/2 \rightarrow 1/2}} = \frac{1 + \mathrm{Cos}^2\theta}{2/3 + \mathrm{Sin}^2\theta} \qquad [4]$$

If crystallites in a powdered sample have a preferred orientation due to compacting, an unexpected asymmetry of the quadrupole doublet may result (86-87). In addition to the preferred orientation effect, the cause of asymmetry of the quadrupole doublet can be due to the angular dependency of the recoil free fraction as would be the case for anisotropic vibration in the solid. This so-called Gol'danskii-Karyagin effect is of particular interest in catalyst studies. In this case, the vibration of a surface atom parallel to the surface plane can be expected to be different from vibration perpendicular to it (88-89, 135). The anisotropic magnitude of $\langle x^2 \rangle$ for "surface atoms" makes the recoil free fraction angle dependent, thereby affecting the relative γ-ray intensities for different nuclear transitions. A careful study of relative

γ-ray intensities can provide information about the vibrational anisotropy of the atom on the surface and may allow the assignment of the resonant atoms to the surface. For single crystals where the orientation of the sample is known, the orientation of the principle axis of the magnetic field or electric field gradient tensor with respect to the crystographic axis can be determined (68). This effect is temperature dependent and becomes pronounced at higher temperature (89, 135).

Linewidth broadening of the observed resonance lines may also provide chemical information important to catalyst phenomena. The broadening of observed resonance lines is expected to be due to one or more of the following origins. First, if all resonating atoms in the sample are not in an identical chemical environment, e.g., for small catalyst particles, the contribution of the surface atom to the total Mossbauer spectrum can be detected through examination of the linewidth; this provides information about the surface atoms as well as the particle size. The second cause of line broadening can have its origin in the presence of an unresolved quadrupole or magnetic hyperfine splitting, where the magnitude of respective splittings is small and various peaks of the resonance overlap to produce a broadened envelops. A line broadened spectrum can also be produced if the internal magnitude field fluctuates with a characteristic time that is of the same magnitude as the lifetime of the nuclear excited state. The information concerning the magnetic relaxation rate can be obtained by studying the corresponding line width broadening effect (70). An additional cause of line broadening can originate from motion associated with the resonant atom (mobility or diffusivity); a broadening of the γ-ray distribution is expected if the time scale of the motion is of the same order of magni-

tude as the time scale of the γ-ray emission or absorption process. Effective motion of the order of $10^{-8}cm^2sec^{-1}$ can be studied by the Mossbauer effect (90).

(5) Properties of Surface Atoms from the Mossbauer Effect. Knowledge of the electronic environment of surface nuclei is important in understanding the surface chemistry and the nature of catalytic phenomena which the primary research objectives in the field of heterogeneous catalysis. A means to probe the surface electronic, geometric, dynamic and chemisorptive properties under reaction conditions is provided by Mossbauer spectroscopy. A number of articles dealing with the application of the method to solid surface phenomena (58-60), and specific applications to hetrogeneous catalysts have been reviewed (56-57).

In small particle systems (<100 A°), typical of practical catalysts where a sufficiently large fraction of resonating nuclei are located on the surface of the solid, Mossbauer spectroscopy may conventionally be used to investigate the surface phenomena, including those properties associated with the atoms present directly on the surface and also those phenomena which are related to the affect of boundaries of the solid on the properties of internal atoms. The isomer shift may be a sensitive probe of differences between the electronic structure of surface and bulk atoms in small catalyst particles, and effects of chemisorption on the electronic properties of these systems are amenable to study using the isomer shift. The quadrupole splitting of the surface atoms is related to their respective symmetries. Lower symmetry of a surface atom may be reflected in a larger quadrupole splitting for these species compared to that of bulk atoms, allowing these different types of atoms to be distinguished. The lower symmetry of surface atoms compared to

that of the bulk atoms gives rise to the phenomena called "magnetosurface anisotropy" (72). The magnetic anisotropic energy for a surface atom depends on the orientation of magnetization with respect to that of the atom. This makes the magnetic interaction sensitive to the surface structure. The effects of chemisorption on the electronic spin state of the resonant atom located on the surface of the catalyst may lead to a localized surface spin cancellation (or creation), or may lead to a collective change in the spin state of the entire catalyst particle. The first effect would cause a change in the spectrum area, whereas the second effect would be observed by a change in the magnitude of the internal magnetic field for the entire particle. The mean square displacement of a surface atom is expected to be larger than the respective value for a bulk atom, thereby allowing these different types of atoms to be distinguished through their recoil-free fraction temperature dependencies. Also the mean square vibration amplitude for a surface atom may be quite anisotropic, which affects the relative γ-ray intensities for different nuclear transitions; thus, information about the vibrational anisotropy of the atoms on the surface of the particles may be obtained through a careful examination of relative gamma ray intensities and changes thereof upon chemisorption. The ability to monitor the chemical species in the bulk and at the same time to examine the surface composition of the material should provide the ideal tool in heterogeneous catalyst evaluation.

3. THE MOSSBAUER SPECTROMETER AND EXPERIMENTAL CONDITIONS.

Mossbauer measurements are practical only for selected elements (55). Good Mossbauer sources for most active nuclei are now available commercially. The source contains a Mossbauer nucleus in its first

excited state, poised to decay to the ground state and emit a γ-ray. In order to determine the chemical perturbation of the nuclear levels, the emitted γ-ray energy from the source must be modualated by small varying amounts. An electromechanical motion of the source relative to the absorber has been employed to produce the desired energy modulation via the Doppler effect. For Fe^{57} this requires the generation of a precise and controlled motion of the source relative to the absorber in the region of mm $sec.^{-1}$

A variety of differently designed spectrometers has been developed. Most general purpose spectrometers use the constant vibration mode for scanning velocity. In this case, an electromechanical drive is driven by a specified wave form. The drive consists of a drive coil to which a voltage related to the desirable velocity is applied; this causes the drive shaft (which carries the γ-ray source) to move, and a velocity-sensing coil supplies feed back voltage which forces the induced driving voltage to be equal to a desirable periodic reference voltage signal. With a symmetric ramp function as a reference signal, each ramp function is repeated by another ramp of opposite slope. During a two ramp period, the drive shaft velocity then runs linerarly from V_{max} through zero to $-V_{max}$ and reverse. The modulated energy is then resonantly absorbed by the absorber and the transmitted γ-rays counted by the nuclear detective device. The source energy is not always monochromatic. The decay scheme from parent to excited source nucleus to desired excited level to the ground state can generate more than one γ-ray; therefore, an energy selective detector, such as a gas-filled proportional counting tube or scintillation counter, is usually used. The detector of choice for low energy γ-ray energy isotopes, such as

^{57}Fe, is a proportional counter. In this detector the incoming radiation ionizes a gas. As the electrons produced are accelerated to the anode (a wire down the center of the tube), they ionize more gas and generate more electrons. The current produced at the anode is proportional to the γ-ray energy. The detector of choice for high energy isotopes such as 90 Kev ^{99}Ru nuclei, requires a NaI(Tl) scintillation counter. In this detector, light produced by passage of the γ-ray through a Tl activated NaI crystal falls on the photocathode of a photomultiplier tube. The number of electrons in the charge pulse received by the photomultiplier is proportional to the γ-ray energy. The detector is connected to an pulse amplifier and a single channel analyzer (SCA). The SCA detects the height of the pulses coming from the linear amplifier and serves as a energy "window", set by the experimenter, and selects the input pulses which fall within the energy window. The SCA generates a logic pulse which is sent to a multichannel analyzer (MCA). The MCA provides a collection of memory channels (e.g., 512) into which the pulses from the SCA are stored. The periodic drive sweeps through a range of velocities are synchronized to the respective sweep of the multichannel analyzer. In this way, as the drive shaft sweeps through its Doppler velocity cycle, the Multichannel analyzer sweeps through all of its channels, thereby allocating a specific velocity increment to each channel. The storing of counts into various addresses of the memory device according to the instanteous Doppler velocity is done in "time mode" operation. In this mode each of the memory channels is opened for the storage of counts during a constant time interval (e.g., 5μsec.) until the last channel is reached, then the cycle is repeated. Count rates of the order of $10^6 sec^{-1}$ are

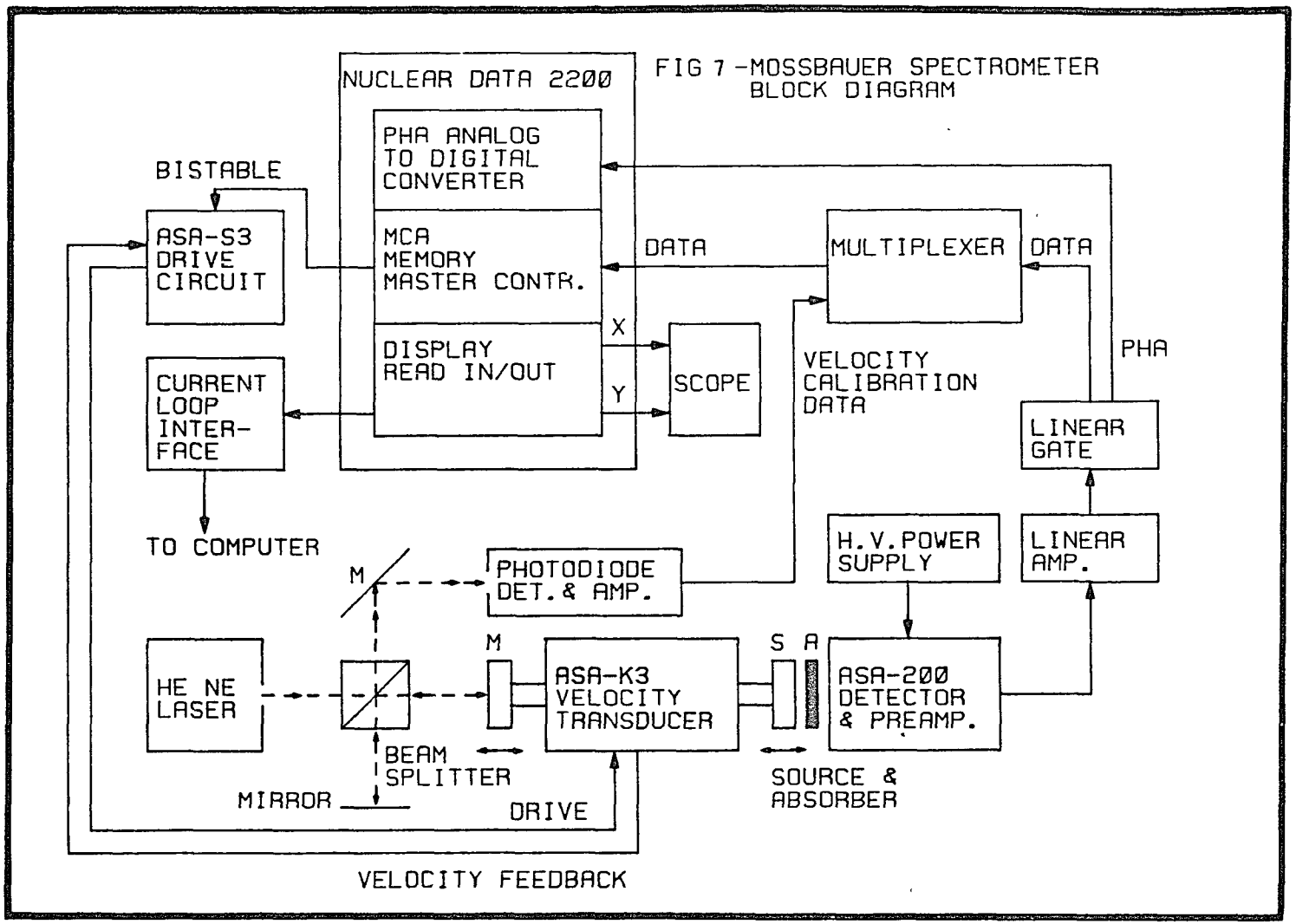

FIG 7 -MOSSBAUER SPECTROMETER BLOCK DIAGRAM

easily handled by this storage device. A block diagram of the spectrometer is shown in Fig.7.

A majority of Mossbauer experiments are performed at low temperatures. A description of appropriate low temperature apparatus is available in the literature (183, 208). Details of sample preparation are also given (57). In order to exploit the in situ study of catalyst behavior, a variety of Mossbauer absorber cells have been designed (91-92).

C. ZEOLITES, METAL-SUPPORT INTERACTION AND REDOX BEHAVIOR OF TRANSITION METALS IN ZEOLITES.

1. ZEOLITES

The unique properties of molecular sieve materials have caused these substances to exhibit an increasingly important role in industrial catalysis (93-95). The zeolites occur naturally (96-97) and they can be made synthetically (97-98) on an industrial scale. There are hundreds of different types of synthetic zeolites. These complex materials are represented by the general formula $M_{x/n}\ (AlO_2)_x\ (SiO_2)_y\ zH_2O$, where M is a metal cation of charge n. The subsequent x, y and z are integers and the ratio x/y (Al/Si) varies between 1/1 to 1/5. The most common species are the Linde X, Y and A type zeolites. The great potential of X, and specially Y type zeolites as highly active catalysts for many important processes such as isomerization and petroleum cracking (99-100) has been recognized for many years. It has been established that these crystalline aluminosilicates are more uniform catalysts than the related amorphous silica-alumina which have wide pore size distributions.

The major source of structural information on zeolites arises from X-ray crystal structure determinations (101). The framework structures of zeolites consist of AlO_4 and SiO_4 tetrahedra linked together in a well defined three dimensional array, composing building units which range from single 4-rings to larger polyhedral assemblies. Fig.8 shows a silicon and aluminum atom with four tetrahedrally coordinated oxygens. Each AlO_4 unit in the framework of the zeolite requires the presence of a cation in order to maintain electrical neutrality. The silicon or aluminum is essentially buried in the center of the tetrahedron, thus the intercrystalline surface of the zeolite consists of oxygen atoms. Also the ports, or windows, are formed with oxygen. Type A, X and Y zeolites are similar. All contain sodalite cages as their basic structural unit. The sodalite cage, Fig.8 consists of 24 (Si/AlO_4) tetrahedra linked together to give a hollow truncated octahedron which contains eight hexagonal faces with a free diameter of 2.2 A°, six square faces, 24 vertices and 36 edges. The free diameter of the cavity is 6.6 A° with an absorption capability of 4 molecules of water. In zeolite A, the six four-membered rings of sodalite are joined to neighboring sodalite cages to give octahedral arrays. In the X and Y zeolites the four six-membered rings of the sodalite cages are joined by oxygen bridges to give a tetrahedral array forming a hexagonal prism between the sodalite cages. The hexagonal prism is composed of two parallel six-rings and six four-membered sides. The void space in the structure, the supercage or faugasite cage, occurs as the main cavity in the X and Y zeolite. Its structure consists of 18 square faces, 4 six-membered rings and 4 twelve-membered rings. The free diameter of this elliptically shaped cavity is 13 A°; it is entered through apertures of dis-

torted chain-shaped 12-membered rings, with a free diameter of 8-9 A°, The supercage has a capacity of 28 molecules of water.

Zeolites X and Y have the same structure. X has a lower Si/Al ratio and consequently a lower acidity than the Y zeolite. As the Si/Al ratio increases, the zeolite becomes more acid resistant and its thermal stability is increased. On the other hand, increasing the Si/Al ratio and thereby decreasing the cation content can alter the ion exchange capacity. In the sodium form of the X zeolite there are 86 cations per unit cell and in a typical sample there are 56 sodium ions per unit cell. The cations can occur in three different positions in the X zeolite. Site I is located in the hexagonal prism faces between the sodalite units with 16 sites per unit cell. Site II is located in the open hexagonal prism with 32 sites per unit cell. Site III is located on the walls of the supercage with 48 sites per unit cell. In the case of Linde Y zeolite, 56 cations occupy the same position just as in the Linde X sieve; type I, 16 per unit cell, type II, 32 per unit cell and type III only 8 per unit cell located on the walls of the supercage.

Single crystals of A and X type zeolites were prepared by Charnell's method (144), and are shown in Fig.9. The crystals are grown by the reaction of appropriate proportions of sodium metasilicate with sodium aluminate, using triethanolamine as a complexing agent. The temperature was maintained at 85°C for 5 weeks. The diameter size of single crystals were in the order of 100 μm (1 micron = 10^4°A). Many attempts to grow single crystals of Y type zeolite were made in different laboratories. The results have not yet been totally successful. Recently a new preparative method was proposed, and the factors which control the crystal growth are discussed in terms of the

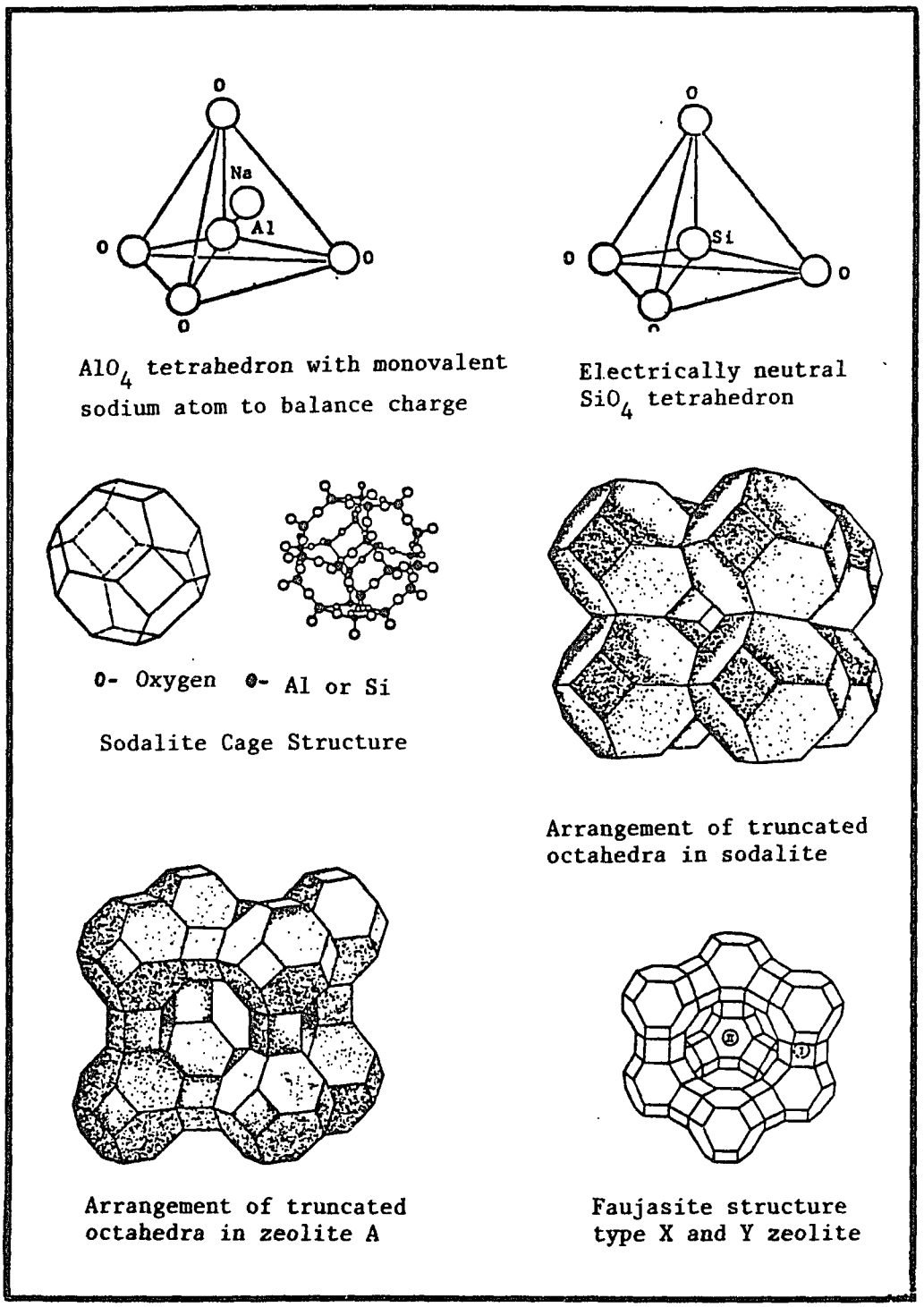

Figure 8. Line drawing of structures of Sodalite, A, X and Y type zeolites.

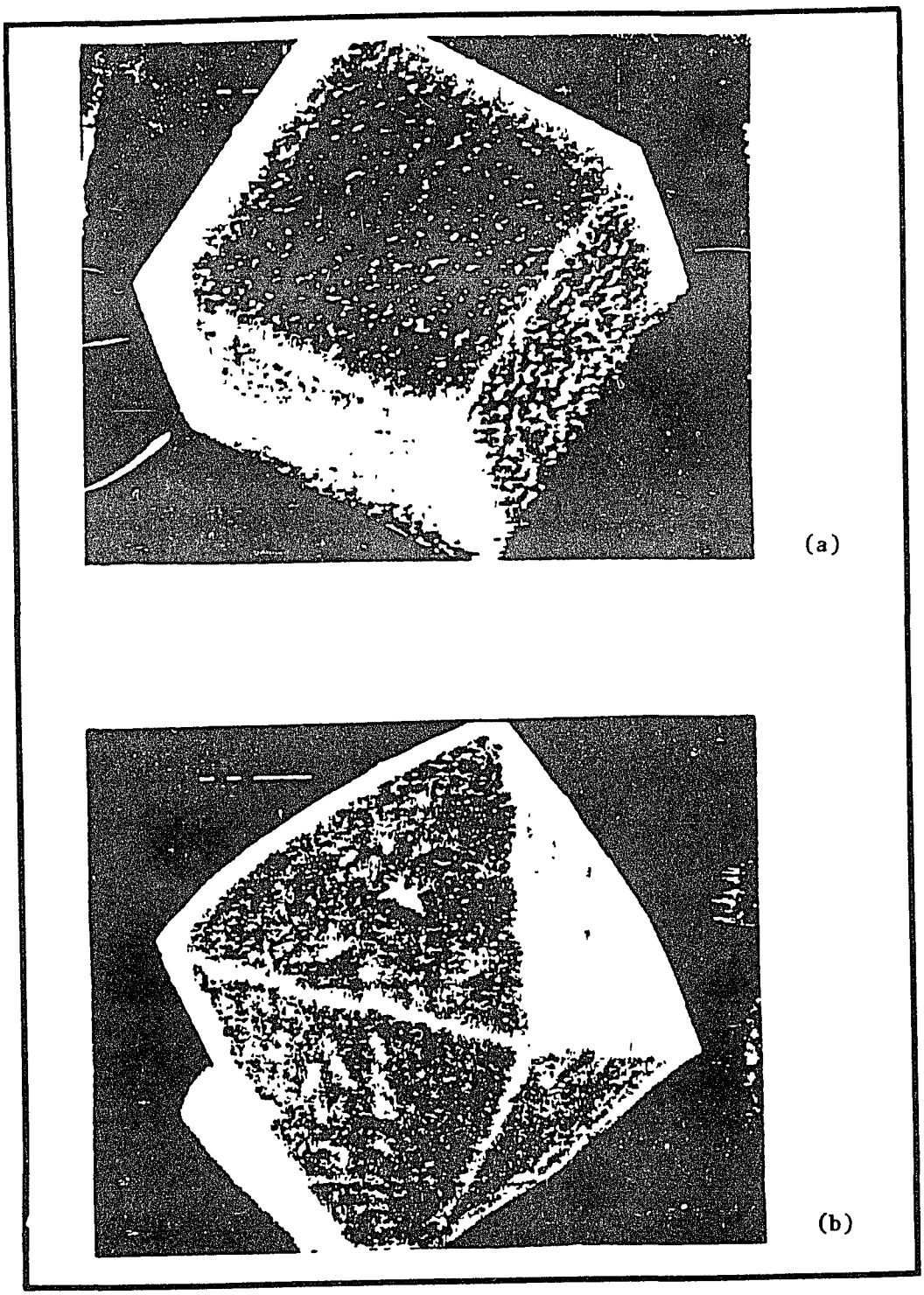

Figure 9. Scanning Electron Micrograph: (a) single crystals of cubic A, and (b) Octahedral X type zeolite.

time required to initiate the crystallization at a given reaction temperature (143).

One of the interesting features of zeolites is their reaction selectivity which is due to their regular, relatively narrow channels and cavities (103-107). Zeolites exert a selective action on the basis of the shape and size of molecules which can enter a cage and have access to catalytically active centers. Great interest has been focused on the selective properties of the zeolites since catalyst selectivity is a central problem in catalytic research. The shape selectivity of zeolites has been studied extensively and is directly related to the size of channels. It can be controlled by selecting the zeolite having an adequate pore size diameter. Zeolites such as ZSM-5, with their interconnected straight channel systems of small size, have exhibited the most pronounced shape selectivity behavior compared to large pore zeolites such as Y zeolite (107-109).

The zeolite structure offers the possibility of introducing into the lattice exchangeable cations which make it possible to incorporate various metals dispersed at the atomic level throughout the zeolite. These cations are strongly associated with the lattice and possess coordination sites potentially active for catalytic reactions. The cations are introducted into the zeolite through ion exchange using the solution of the metal salt, amine complex, or the liquid compound of the metal in an inert atmosphere. Since the transition metal ion solutions are normally acidic, partial exchange of protons of the framework may occur. The excess transition metal may also be preciptated due to a basic reaction with the zeolite (110). To avoid complications, the exchange should to be carried out using a very dilute solution of less than 0.05N

with the suspended solids at less than 5%. Ambient temperature is suitable for adequate exchange. The ion exchange condition has a pronounced effect on the extent of ion-exchange and the location of ions in the zeolite skeleton as well as subsequent reduction behavior and dispersion level of metals on the zeolites. The preparation of metal-containing zeolites includes both the loading of metal in or on the zeolite and the subsequent treatments governing the final disperson of the metal. Ion exchange conditions and the subsequent reduction treatments may change the catalytic properties fundamentally (111-112).

The interaction between the dipoles of water molecules and the charges on the zeolite framework usually causes the cavities and intracrystalline channel systems of the zeolite to be filled with water. In the hydrated state, the zeolite is regarded as a polyanionic framework surrounding a solution of positive ions in water. The water molecules can usually be removed reversibly without destruction of the framework. A typical dehydration procedure consists of subjecting the zeolites to an elevated temperature of 350°C under vacuum of 10^{-5}mm-Hg. The intracrystalline channels are then vacant except for the remaining inorganic cations and the solid structure possesses highly absorbant properties. In a dehydrated state the cavities can be filled rapidly with gas or vapors. The sorptive properties of the zeolites play a key role in various catalytic applications. Studies on the pore systems and the relation of pore structure to absorption properties indicate that the mechanism of adsorption in such micropores occurs via enchanced adsorption forces in narrow pores and the increased inter-molecular forces which are pressure dependent (113).

The zeolite lattice displays the characteristics of a very strong electrolyte. The strength of the electrolytic property of the structure depends on the degree of ionic character of linkages between the lattice atoms. The ionic character of the crystal is mainly controlled by the alumina content of zeolite. The corresponding crystal field dominates the intracrystalline pore system of the zeolite. Since the intrapore surface of the zeolite is fully surrounded by the crystal lattice, both the surface atoms and the molecules adsorbed within the zeolite crystal are influenced by the zeolite crystal field. The crystal field present in the zeolite is known to be responsible for its high affinity for occluded alkaline salts (114), its high polarization and the ionization power of occluded atoms or molecules (115).

The affinity of zeolites for ionic species is best shown by the frequently observed ionization of water molecules by cation hydrolysis (116). The polarization of absorbed water molecules in a zeolite followed by the thermal ionization of water molecules catallized by exchanged bi-or multi valent metal cations is believed to be responsible for the formation of two distinct hydroxyl groups. One of them, $M^{+}(OH)$, is attached to the zeolite cations and the other is formed by the interaction of protons from the ionization of water with framework's oxygen. The hydroxyl group with very acidic hydrogens has been well recognized as the source of acidic catalytic activity in zeolite. The catalytically effective acid sites in bi-or multi-valent cation Y zeolite are the acidic hydroxyls linked to the framework. The tendency for cation hydrolysis increases with the Si/Al ratio of the zeolite framework. At higher Si/Al ratio the distance between the anion sites (AlO_2) is increased and the electrostatic shielding of the highly charged cations is ineffective (117).

2. METAL-SUPPORT INTERACTION AND REDOX BEHAVIOR OF THE TRANSITION METALS IN ZEOLITES.

Small metallic particles dispersed on high surface area supports are of industrial importance in heterogeneous processes. Small particles are demanded because of their structural and chemical importance as well as the obvious economy of metal utilization. Changes in size can alter the distribution of exposed faces, surface irregularities, and edges; thus the number of available structural ensembles on the surface and the degree of coordinative unsaturation of individual surface atoms are directly related to the particular size of the particle involved. For many reactions the dependency of the activity of the supported catalyst on the metal particle size is now well established. Direct information on the chemical nature and microstructure of such well dispersed catalysts however is limted due to the complexity of the system and the practical difficulties involved in generating and stabilizing, as well as characterizing, such particles of small size and low concentration. The demand for improved catalyst systems requires careful examination of variables which control the particle size and reduction behavior of supported catalysts during preparation and subsequent treatments.

Information concerning the nature of the interaction of the metallic component with the carrier and the solid solvent effect of the carrier matrix is essential for synthesizing small metallic particles. One of the main effects influencing the formation of highly dispersed, zero valent metal entities on the surface of the carrier is the strength of metal-support interaction. If the interaction is too strong, reduction of metal ions to the metallic state usually can not be achieved.

On the other hand, if the metal-support interaction is too weak, large metallic particles are formed with the tendency to agglomerate. To obtain highly dispersed zero valent metal particles on the surface of the carrier an optimum strength of metal-support interaction is needed. The effect of support can be due to the electron transfer from the metal to the acid sites of the zeolite which promotes the electron deficiency in the valence bond (124-127) and/or can be due to solid solvent effects of the matrix which include the effects of the electrostatic field of the zeolite framework.

Zeolite supported metal catalysts exhibit a different reduction behavior when compared to conventional metal catalysts. Reduction may be hindered or promoted depending on the nature of the metal-support involved (112, 118, 120). It has been established that very small zeolite encaged metal particles have unusual electronic properties (121-122). Since the electronic structure of transition metals tends to change as the number of atoms involved in the particle decreases (123), different reduction behavior of metals in a dispersed state can be associated with an intrinsic change of electronic properties with particle size. In addition to intrinsic size effects, the electronic structure of the cluster can be altered by the environment; i.e., the effect of support. The order of reducibility of transition metals on zeolites does not follow the ionization potential of the metal (112), thus the properties of transition metals on zeolites more closely resemble those of ions in solution rather than those of the isolated metal ions.

The understanding of the kinetics and mechanism of reduction of transition metals on zeolites is particularly valuable in the prepara-

tion of these catalysts. The reduction scheme of metal ions on zeolite is generally achieved by using hydrogen (112). It is known that the oxygens of the lattice participate in the redox phenomena of transition metals by accepting protons and forming hydroxyl groups (126). The reduction of some transition metal cations or complexes on zeolites to the metallic state can be accomplished by vacuo-thermal dehydration pretreatment. Partial or complete thermal decomposition reduction of Cu^{2+}, Cr^{3+}, Ni^{2+}, and Ag^{+} cations in zeolites has been reported (112, 120). In most cases, the $M^{+}(OH)$ and zeolite O-H species have been detected as the reduction intermediate and have been confirmed by experimental evidence. Since the reduction processes involve the formation of the hydroxyl group, the precipitation of hydroxides will be more prevalent in the zeolites with lower Si/Al ratios, when stronger alkaline properties allow a greater reaction between framework and protons. This may explain the observation of metallic Cu in X type zeolite under mild conditions (128), and the formation of metallic iron in X type zeolite (129). It has also been suggested that the ease of reduction is dependent on the location of the ions in the zeolite (120, 130). The reduction process is believed to be diffusion controlled when the reduction of supercage ions is assumed to take place first, followed by the migration of sodalite ions into the supercage, and subsequent reduction. The ions remaining in the hexagonal prism are not easily reduced. Correlations have been observed between standard electrode potential and the reducibility of transition metal ions in zeolites (112). The order of reducibility of the ions follows the electrochemical potentials. The ease of reduction of Pd^{2+}/Pd^{0} is in agreement with the position of this element in the electrochemical series (+.83V). The reduction of Ni or

Cu (smaller standard electrode potentials) is achieved at higher temperature. No reduction has been observed for ferrous ions in Y zeolite which is in agreement with its small standard electrode potential (-.41V).

In general, noble metals on zeolite are reducible by hydrogen to the metallic state, but treatment conditions must be optimized to obtain the highest dispersion. Thermal decomposition of the $Pt(NH_3)_4^{2+}$ complexe on zeolite results in the formation of a hydride species, $Pt^+(H)$, when the hydride can be reduced with hydrogen to metallic Pt. The influence of treatment conditions on reduction behavior and metal dispersion of this catalyst have been extensively studied (112, 122). When the $Pt(NH_3)_4^{2+}$ complex is reduced with hydrogen without previous decomposition pretreatment, a neutral hydride is formed. Its decomposition leads to agglomeration of the platinum. Activation by flowing O_2 or air prior to hydrogen reduction is an essential treatment to obtain the highest dispersion of Pt.

The redox behavior of palladium on zeolite is very similar to that of platinum. In the course of the thermal decomposition of $Pd(NH_3)_4^{2+}$, the oxidation pretreatment in air or oxygen is needed to avoid palladium agglomeration (112, 122). After calcination of the amine complex, Pd^{2+} ions are formed which can be easily reduced to dispersed metallic Pd even at room temperature (131).

The chemistry of transition metals in zeolites has attracted considerable attention because these systems have potential both in fundamental and applied chemistry. The reduction-oxidation and hydration-dehydration of Ru and Fe and their bimetallic mixtures supported on Y zeolite will be described in detail in subsequent chapters.

CHAPTER II

IRON EXCHANGED Y-ZEOLITE

INTRODUCTION

There is significant current interest in developing methods for preparing small, stable iron particles. Such particles have special surface structures and electronic properties and their high surface areas are of particular interest in catalytic processes. Iron is an active and selective catalyst for a number of reactions, but it plays a big role in two important industrial processes, the production of ammonia and Fischer-Tropsch synthesis, where it has been used as porous iron prepared by the reduction of iron oxide. While dispersed small metallic particles prepared on the surface of a support normally result in higher activity and improved selectivity, there is considerable evidence in the literature that iron compounds introduced onto the support are difficult to reduce to the metallic state. The formation of fine, zero valent iron particles on the surface of a support is influenced by two effects which act in opposite directions; i.e. the extent and strength of metal-support interaction, and the degree of loading. A strong interaction between metal and support usually prevents the reduction of iron particles to the metallic state. On the other hand, in the presence of a weak metal-support interaction, large metallic particles may be formed due to migration, which in turn further accelerates the reduction. Reduction also proceeds at high metal load-

ings or when large precursor particles have been reduced, leading again to large metallic particles. Thus, full reduction of large metallic particles can be achieved in the presence of weak metal-support interaction or by high metal loading. To obtain highly dispersed zero valent iron particles on the surface of a carrier, optimum strength metal-support interactions and degree of loading is needed.

One method of characterizing iron containing particles is Mossbauer spectroscopy. This technique has been used to study the chemical states of iron on the surface of Al_2O_3 supports during various reduction-oxidation treatments. Ferric ions in low concentration (0.1%) were unaffected by hydrogen at room temperature and reduced only to the ferrous state in H_2 at temperatures up to 700°C. Thus, at low metal loading, the reduction of Fe^{3+} on the surface of Al_2O_3 does not go beyond the Fe^{2+} state even at high temperature. The Al_2O_3 support strongly bonds the ferric ions in empty octahedral positions of the support and prevents migration on the surface. At high metal loadings when the iron concentration exceeds the amount needed to fill these empty sites, large metallic iron particles are detected after treatment. No change occurres in the Mossbauer spectrum upon exposure of the catalyst to oxygen at room temperature (132-134). The result of an earlier investigation dealing with iron on the surface of the same carrier indicates the formation of very fine Fe^{3+} particles during the oxidation treatment (135). The fine particles have been detected by means of an asymmetric doublet spectrum. The asymmetric character of the doublet is the result of the anisotoropy of the amplitude of thermal vibration of iron atoms on the surface of the particles. With fine particles (less than 100 A°), the ratio of the number of atoms on the

surface to those in the bulk is high enough to distinguish surface atoms in the total Mossbauer spectrum.

SiO_2 supports provide a weaker interaction between the support and the iron particles than the corresponding Al_2O_3 supports. Thus reduction to the metallic state should be possible at lower metal loading on SiO_2. However, several Mossbauer studies have shown that Fe on the surface of SiO_2 at loadings less than 1% is generally difficult to reduce to the metallic state. Reduction can be achieved however for loadings of about 3% where agglomeration occurs to form larger particles (136-141).

Reduction can also be accomplished if large precursor particles, such as α-Fe_2O_3 are being reduced. However, Al_2O_3 and SiO_2 supported α-Fe_2O_3 may behave differently than the unsupported oxide. The Temperature Programmed Reduction (TPR) profile for Fe_2O_3/SiO_2 consisted of two peaks at about 300°C and 450°C where the corresponding Fe_2O_3/Al_2O_3 reduction commenced above 400°C and proceeded to about 700°C (120, 142). This TPR study clearly demonstrates the existence of a stronger interaction between α-Fe_2O_3 with the surface of Al_2O_3 than the corresponding interaction on the surface of SiO_2. Mossbauer studies of the same materials, prepared by the impregnation of supports with iron compound solutions and subsequent oxidation treatment, resulted in the formation of bulk α-Fe_2O_3 and iron oxide in the superparamagnetic state. After reduction, large metallic particles were detected as the result of the reduction of α-Fe_2O_3, while the superparamagnetic fraction was reduced only to the ferrous state (138).

Factors which influence the overall dispersion of the metal ions are mainly those associated with the extent of metal-support interac-

tion. One of the factors which affects the interaction is the acidity of the impregnating solution. Impregnation at lower pH values results in a weaker interaction between a silica gel surface and ferric ions, as indicated by a low intensity Mossbauer spectrum. The spectrum at low temperature exhibited hyperfine splitting. By increasing the pH value during impregnation, the interaction increased and no hyperfine splitting was observed at low temperature, indicating a smaller particle distribution on the surface (137). The precipitation of ferric oxyhydrate molecules (as the result of hydrolysis of the ferric nitrate solution) is assumed to be occurring on the surface at higher pH values during the impregnation process (22).

The nature of the starting material is found to play an important role in the reduction and dispersion behavior of iron metal on the surface of the carrier (148-149). The result of these investigations implies that decomposition of the precursor structure occurs before a distribution of iron particles can be attained. Those precursors which decompose slowly lead to smaller dispersed particles. Very small and stable metallic particles were detected on the surface of MgO supportes (145-148). The reduced particles consisted of metallic iron and some Fe^{2+} clusters. The clusters of Fe^{2+} apparently isolate the metallic iron particles. It is suggested that MgO is not an inert carrier for metallic iron and that chemical interaction is essential for stabilization of small metallic particles.

The Mossbauer spectroscopy of ferrous and ferric ion-exchanged zeolite A (150-154), X (129) and Y (155-160) has been reported as a function of hydration-dehydration and/or oxidation-reduction treatments. Type A, X and Y zeolites are basically similar. All contain the soda-

lite cage as their basic structure unit and internal site for cations. In zeolite A the six four-membered rings of sodalite are joined to neighboring sodalite cages to give an octahedral array, while in the X and Y zeolites the four six-membered rings are joined by oxygen bridges to give a tetrahedral array forming a hexagonal prism between the sodalite cages. Thus the hexagonal prism cages in X and Y zeolite, which are the major internal sites for cations, do not exist in A zeolite. Zeolite X and Y have the same structure. X has a lower Si/Al ratio and consequently, a lower acidic property than Y zeolite. The Y zeolite has received the most attention because of its great importance in absorption and catalysis. Ferric and ferrous exchanged Y zeolite in a dehydration pretreatment step exhibited a Mossbauer spectrum which was composed of two superimposed doublets. One set of signals was assigned to ferrous ions in an octahedral coordination site in an oxygen ligand environment in the hexagonal prism (site I) (159-160). This doublet was not observed for ferric exchanged A zeolite, a zeolite which does not contain hexagonal prism structural units (152). This assignment has also recently been confirmed by X-ray powder examination of the location and coordination environment of cations in Y zeolite (156). The Mossbauer spectrum of dehydrated material also displays a second quadrupole doublet which was originally assigned to ferrous ions in four fold coordination sites near the hexagonal windows having three Fe-OAl bonds and one Fe-OH or Fe-O-Fe bond (160). The second doublet has also been tentatively assigned to the precipitated iron oxide or hydroxides. On the basis of an X-ray crystal structure examination, this doublet has now been assigned to the three coordinated ferrous ions at site I' (156). The reduction of ferrous or ferric ion exchanged Na-Y has been

carried out in flowing hydrogen at temperatures up to 700°C. Although ferric ion could be reduced to ferrous, further reduction to metallic iron has not been observed. The reduction of ferric exchanged Ca-X type zeolite to metallic iron by hydrogen at 360°C has been reported (129). This different reduction behavior of ferric ion is attributed to the difference in acidity of X and Y type zeolites. Lower Si/Al ratios, consquently lower acidic properties, of X type zeolites seem to promote the reduction behavior of iron.

The above background information indicates the difficulty in preparing catalytically active, highly dispersed metallic iron particles on a particular support. The thrust of our work in this area was to explore possible new ways to accomplish this task. Our approach was to modify the acidity of Na-Y zeolite by ion exchanging the Na^+ with NH_4^+ ion. Upon heating this material, de-ammoniation should produce a species such as H^+-Y forming a bifunctional catalyst with acidic properties different from those of Na-Y zeolite. Furthermore, the product of de-ammoniation, NH_3, might mix with hydrogen under reduction conditions and the use of an ammonia/hydrogen mixture as the reductant might facilitate the reduction processes. Also Fe^{2+}, but not Fe^{3+}, strongly coordinates with NH_3 ligands (161). This could lead to a reduction in the strength of the Fe^{2+} interaction with the zeolite framework which would promote the reduction of the initial iron species. Thus, this portion of the study was undertaken to charaterize the chemical states and the reducibility of ferric ions supported on NH_4-Y zeolite. The behavior of this bifunctional catalyst during hydration-dehydration and oxidation-reduction treatments was assessed by Mossbauer spectroscopy.

EXPERIMENTAL

A Na-Y zeolite (SK-40 Linde company), was ion exchanged with fresh portions of 10% ammonium sulfate solution. Chemical analysis confirmed almost 90% replacement of Na^+ by NH_4^+. The sample of iron supported NH_4-Y zeolite was prepared by ion exchange using ferric nitrate solution under N_2 atmosphere at ambient temperature. The concentration of the solution was adjusted to produce an exchange of 30% of NH_4^+ by iron. The exchange levels were determined by analyzing for Na ions in the solution after ion exchange by the uranyl acetate method (206). The resulting weight precent of metal in the zeolite was approximately 2.5% iron. The exchanged sample was thoroughly washed with distilled water to remove excess salts and dried under vacuum overnight at ambient temperature. The X-ray powder diffraction pattern did not reveal any decomposition or reformation of the zeolite's crystal lattice during the ion exchange process. A catalyst pellet was made by taking 150mg of sample and pressing at 1000psi into a 1.25cm diameter wafer. The finished wafer was placed in the reaction cell. The cell was arranged so that the catalyst pellet could be lowered into position between the windows of the reactor for spectroscopic examination and pulled upward into a heated section for various treatments. Mylar windows were used for Mossbauer spectroscopy measurements and NaCl windows were used for I.R. examination. This allowed in situ spectra to be obtained for catalyst treatments up to 500°C. A gas vacuum rack system provided a means for pumping down the reactor vessel as well as filling it with oxygen-free, moisture-free gas, Fig.10. The vacuum in the system was monitored by mean of a T.C. vacuum gauge connected to a manifold with a glass to metal joint.

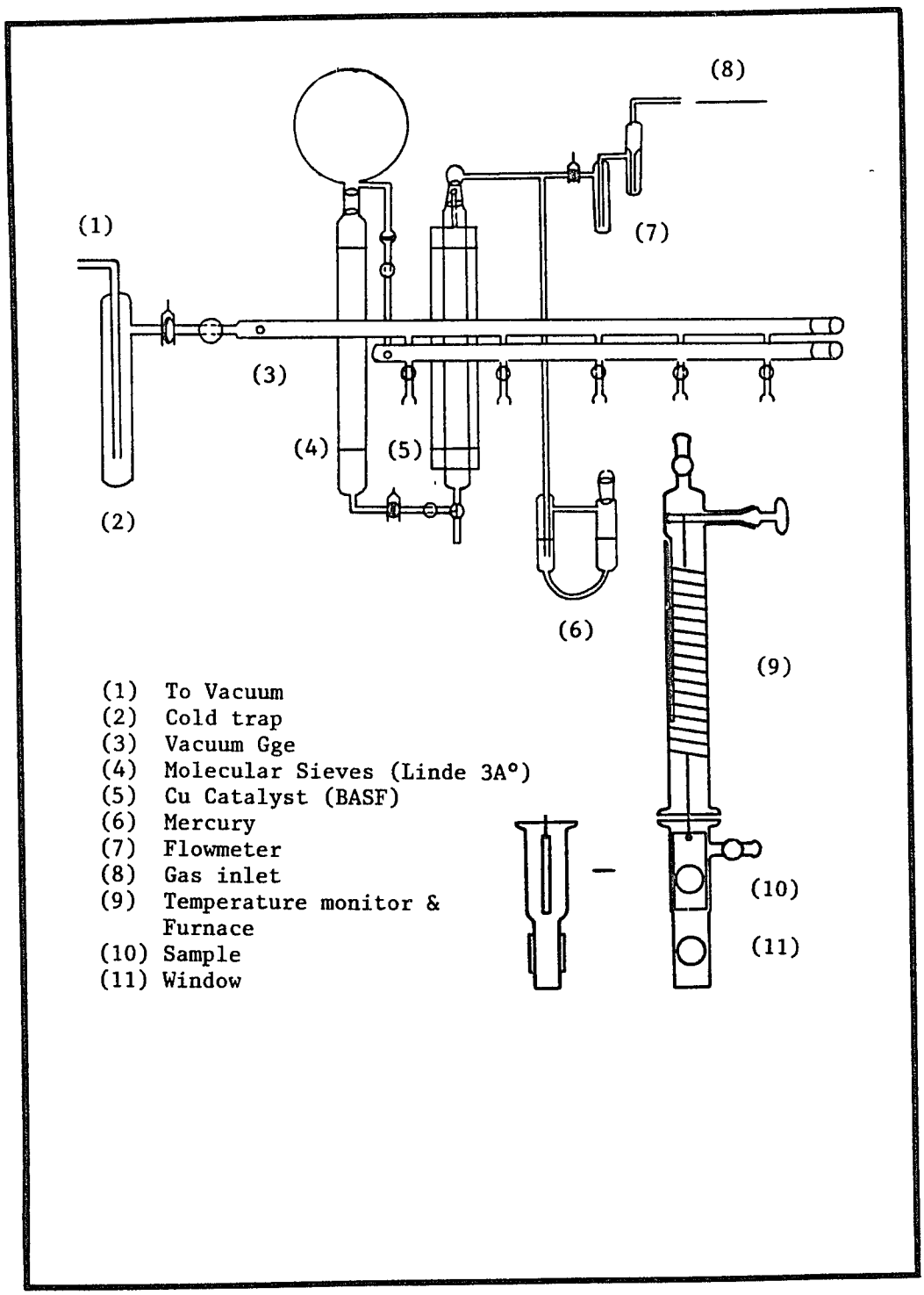

Figure 10. Reaction cell and gas vacuum rack system.

^{57}Fe Mossbauer spectra were obtained on a constant acceleration, Austin Science Associates spectrometer which provided the Doppler velocity modulation to a 50 mCi ^{57}Co source in a rhodium host lattice. The source was purchased from Spire corporation, Bedford, Mass. A full description of the spectrometer is presented in a previous chapter. The data were accumulated in a signal averager and data reduction was carried out by a conventional least squares Lorentzian line shape program on an Interdata 32/8 computer. A modified standard Mossbauer fitting program written originally by Stone (162) was used to define values of peak positions, full width at half maximum, peak intensities peak areas, isomer shifts in mmsec^{-1}, quadrupole splitting in mmsec^{-1} and standard deviations. The experimental points and the calculated least square curves were plotted by a Tectronix interactive digital plotter 4662. All velocities are reported relative to the center of the split spectrum of an iron foil standard at room temperature.

RESULTS AND DISCUSSION

The Mossbauer spectrum of the fully hydrated Fe^{3+},NH_4-Y zeolite, containing 2.7% iron, showed a doublet of relatively high signal intensity at room temperature, Fig.11a, (I.S. = 0.37 mm s^{-1}, and Q.S. = 0.78 mm s^{-1}). The parameters indicate that the iron is present as high spin ferric ions. The comparison of the isomer shift with comparable values for ferric ions in different coordination sites (67), suggests that the Fe^{3+} ions are octahedrally coordinated. The most probable environment for the ferric ions in the zeolite are the oxygens of the framework and/or water molecules. In zeolite Y the ratio of Si/Al is about 2.4 and there is a considerable negative charge density on the framework, thus the cations have a tendency to interact more strongly

with the framework. Additional support for this conclusion is provided by liquid nitrogen temperature examination of the sample where the Mossbauer signals showed a small enhancement in intensity over those observed at room temperature. The broad line of the ferric doublet is interpreted as resulting from variations in the electric field gradient tensor at different cationic sites which indicates a distribution of iron environment.

A catalyst pellet made from the initial sample was placed in the Mossbauer cell and evacuated to 10^{-5}torr pressure for 24 hours at room temperature. The sample was then subjected to a final temperature of 350°C which was increased in one stage during a 30 minute period. The cell was evacuated at this temperature for 4 hours, to the final pressure of 10^{-5}torr, and the Mossbauer spectrum recorded (Fig.11b). The results are not significantly different from those obtained for ferric or ferrous exchanged Na-Y zeolite (155-160), and Ca-X zeolite (129). Dehydration up to 500°C did not change the characteristic spectrum significantly. Only a small increase in the area of the two inner peaks was observed; thus, the 350°C temperature condition for the dehydration process is sufficient for the removal of the majority of water molecules. The total area of spectrum 11b, the dehydrated sample, is at least 70% larger than that obtained for the original sample. The area under the Mossbauer peaks is gradually enhanced during the step wise dehydration process of A zeolite (150-151), L-zeolite (165) or Na-Y zeolite (160). The difference is attributed to the removal of water molecules causing localization of ions originally solvated with subsequent formation and/or increased bonding between the metal ions and the zeolite framework. The best fit to this spectrum consists of at least

two superimposed doublets, one outer doublet; (I.S. = 1.2 mms^{-1} and Q.S. = 2.3 mms^{-1}) and one inner doublet; (I.S. = 0.9 mms^{-1} and Q.S. = 0.7 mms^{-1}). The values indicate that the dehydration process reduces most of the ions to the ferrous state. The reduction mechanism may involve the cation hydrolysis processes, described in the previous chapter, p. 40-41. As the result of this reduction scheme, $Fe(OH)^{+}$ species must have been formed. The isomer shift value for Fe^{2+} in tetrahedral coordination in $FeAlO_4$ (164), and in the mineral staurolite (67) is very close to the value deduced for the inner doublet. The inner doublet therefore has been assigned to ferrous ions tetrahedrally coordinated to three oxygens of aluminum and to a hydroxyl group. The outer, intense quadrupole lines are characteristic of ferrous ion in an octahedral ligand environment. This symmetry is provided by site I of the zeolite framework, located at the hexagonal prism window between the sodalite cages. Good evidence for this assignment is provided by the dehydration study performed on ferric exchanged A zeolite which does not contain hexagonal prisms and does not exhibit the outer doublet described above.

The exposure of the dehydrated sample to air at room temperature for 24 hours did oxidize a major portion of the ions to the ferric state, (spectrum 11c). Oxidation of ferrous ions in the presence of water should form $Fe(OH)^{2+}$ groups. The strong tendency of ferric ions to hydrolyze (166), can lead to structures such as $Fe(OH)_2^{+}$. Thus the final spectrum can contain peaks representative of $Fe(OH)^{2+}$, $Fe(OH)_2^{+}$ and some unreduced Fe^{2+} species. The subsequent treatment in air at 200°C for 2 hours, converts all of the iron to the ferric state (spectrum 11d) which produces a spectrum indistinguishable from that observed for the

freshly hydrated starting material. Line width examination of the spectrum indicated that the environment of the iron species has become more uniform and symmetrical during the oxidation process.

A portion of the dehydrated sample(11b) was exposed to hydrogen at room temperature (Fig.11e), and subsequently reduced at 400°C for 4 hours (Fig.11f). The reduction process has changed the shape of the Mossbauer spectrum, indicating further distribution of the iron species but no reduction of the ferrous ions to the metallic state. Furthermore, a major portion of the ferrous spcies can be converted to the ferric state by oxidation at room temperature (Fig.11g). This result is indicative of a reversible oxidation-reduction cycle, where ferrous and ferric state are interconvertible. X-ray powder diffraction profiles of the sample after two repeated oxidation-reduction cycles at 400°C showed some decomposition of the zeolite lattice, as evidenced by a decrease in the peak intensities and an increase in the peak width and profile background.

In a separate experiment, the reduction of the dehydrated ferric or ferrous species exchanged into Y-zeolite was carried out by hydrogen treatment at higher temperatures and for longer periods of time than previously described. Again the reduction did not proceed beyond the ferrous state. No evidence for reduction to the metallic state was found. Upon exposure of these samples to air, in some instances, no Mossbauer spectrum was observed at room temperature. This feature is similar to the disappearance of the resonance when ferric Dowex 50 resin is hydrated (167). In this case, the disappearance of the resonance effect has been attributed to the solvation of ions (168). In the case of Y zeolite, there is a high affinity for water molecules, causing a

strong interaction between water molecules present in air and the zeolitic cations and/or framework; consequently the metal-support interaction is weakened and metal cations become solvated and mobile in the intracrystalline fluid. The solvation of iron has usually been observed when the starting materials contain ferric, rather than ferrous cations (to keep the ferrous in +2 oxidation state during the preparation, the exchange solution should be slightly acidic). This effect can probably be attributed to the stronger interaction between the zeolite and the ferrous, rather than ferric, ions during the preparation stage. In the broader sense, one can speculate that the nature of the iron-zeolite interaction involves the electron transfer from the metal to the acid sites of zeolite. The extent of such phenomena is pronounced for the ferrous cation, consequently the strong metal-support interaction prevents solvation. The solvation effect probably differenciates between ferrous and ferric exchanged Y-zeolite systems. Other oxidation-reduction properties of the two systems are very similar. The same solvation effect was observed when a hot reduced sample was suddenly air exposed. The solvation phenomena is also sensitive to the nature of the second metal in the system as will be discussed in a subsequent chapter.

In spite of different approaches taken to modify the reduction behavior of iron and to overcome the difficulties in preparing highly dispersed metallic iron particles on the zeolite, the result of this work has so far shed no new light on this problem. The thrust of our work in this area is to explore possible new ways to accomplish this task.

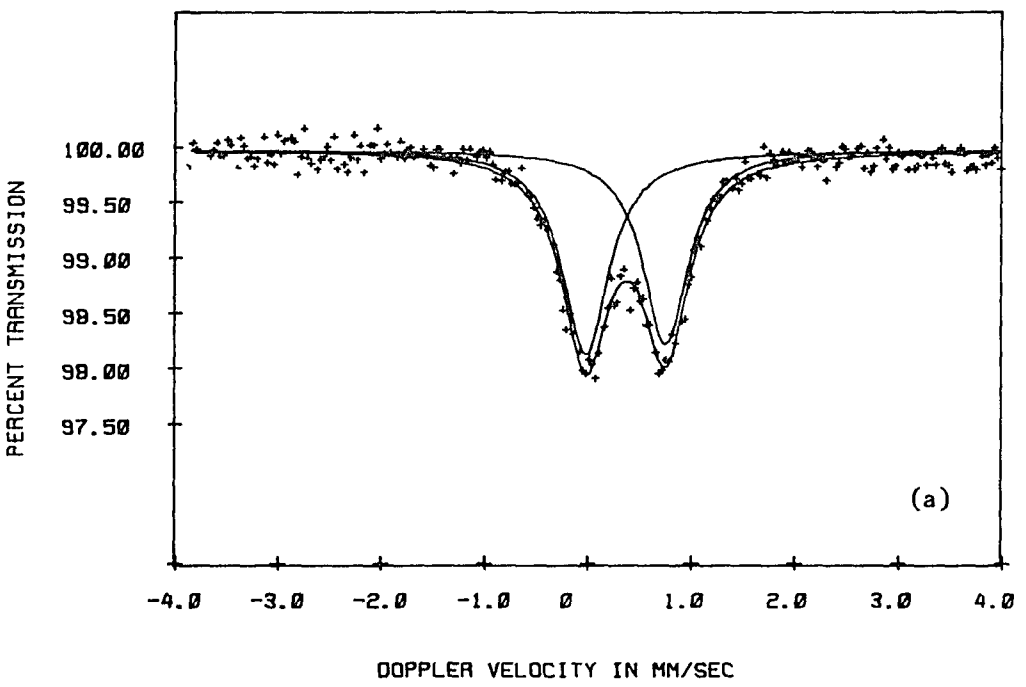

Figure 11. ^{57}Fe Mossbauer spectra at room temperature of ferric exchanged NH_4-Y zeolite: (a) catalyst as initially prepared.

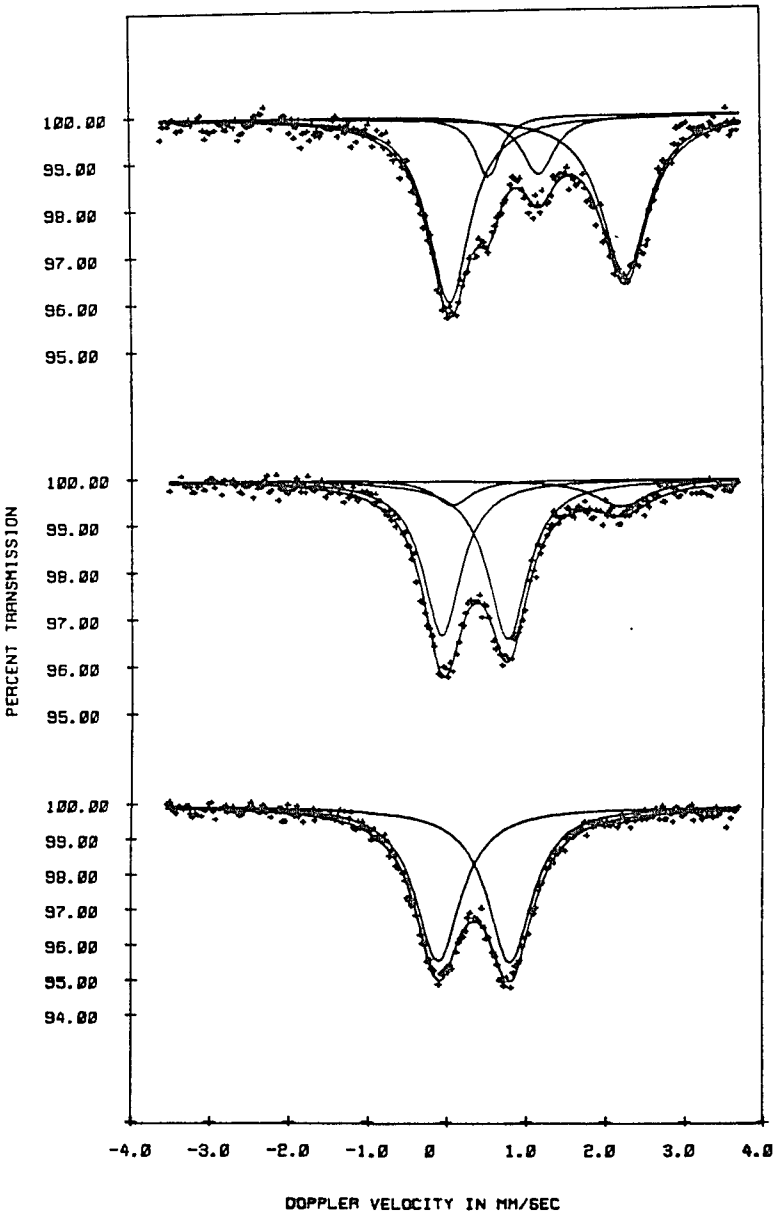

Figure 11. (Cont's)
(b) Evacuated 4 Hr. @ 623°K. (c) Exposed to air > 24 Hr. @ room temperature. (d) oxidized in air 2 Hr. @ 573°K.

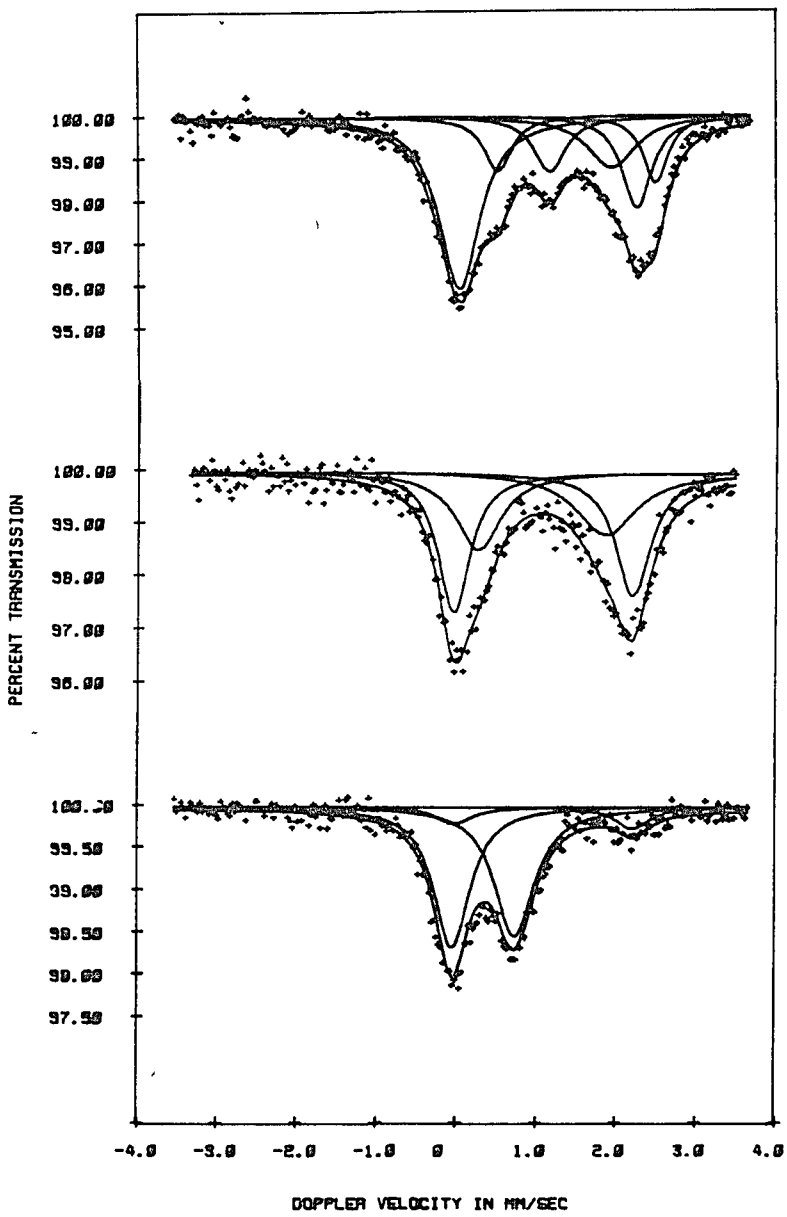

(e)

(f)

(g)

Figure 11. (Cont's)
(e) A portion of dehydrated sample b is reduced 2 Hr., H_2 @ room temperature. (f) Reduced 4 Hr., H_2 @ 673°K. (g) Exposed to air > 24 Hrs. @ room temperature.

CHAPTER III

RUTHENIUM AND IRON-RUTHENIUM EXCHANGED Y-ZEOLITES

INTRODUCTION

The modification of supported iron catalysts in the presence of other transition metals has been previously established. There is evidence that the presence of noble metals promotes the formation of an iron species different from that in the iron only systems. In the presence of Pt or Pd a remarkable chemical change in the nature of the iron has been observed. The accelerated reduction process for iron in the presence of transition metals leads to bimetallic formation. It has been proven that the addition of Pt to iron on the surface of SiO_2 and Al_2O_3 has induced the formation of a bimetallic catalyst after reduction (132-134, 197-199). The bimetallic formation is pronounced at high metal loadings and especially when the catalyst is rich in the noble metal. Where the Fe/Pt concentration ratio is about one, some unreduced iron is left in the system. At higher concentration (~15 wt%), in addition to PtFe and Fe^{2+}, large ferromagnetic iron particles are also formed. The nature of the accelerated reduction process at the surface of the bimetallic clusters is involved in hydrogen atom spillover which is caused by the dissociation of molecular hydrogen on the adjacent Pd or Pt atoms. When iron is surrounded by noble metals, the iron-oxygen bond is apparently weakened, and the adsorbed oxygen is titrated by the spillover of hydrogen.

In contrast, the addition of ruthenium to iron did not appear to influence significantly the reduction behavior of iron (200). At high concentrations however, a Fe-Ru interaction has been observed (48). It was also observed that in the presence of iron at very low concentration, the iron can not be reduced; yet the presence of the iron caused the dispersion of ruthenium on the surface of the carrier (22). This effect was rationalized in terms of a strong bond between iron and oxygen leading to the formation of iron oxide which prevents the agglomerization of ruthenium particles. The thrust of the work outlined below was to investigate the characteristics of this bimetallic system more fully, particularly in Y-Zeolite. However, to provide appropriate comparisons, it was necessary to examine the zeolite system with ruthenium only. In the following sections, the behavior of ruthenium on the surfaces of different supports will be reviewed.

Among various transition metals used in catalytic processes, a unique and versatile chemical reaction is demonstrated by the ruthenium nucleus. Due to its rich chemistry and ease in oxidation/reduction in a variety of oxidation states, it can catalyze a wide range of reactions, i.e. pronounced selectivity for the reduction of nitrogen oxide to nitrogen in exhaust gases (169-170), high activity for methanation of carbon monoxide (171-172), utility in the Fischer-Tropsch synthesis of hydrocarbons (1-2), activity in the water gas shift reaction (173-175), catalytic activity in photochemical and solar conversion reactions (3-4), and activity for the hydrogenation of benzene (176) and several other feedstocks. Also ruthenium oxide is currently of interest as an oxide for chlorine production in the chloro-alkai industry and metallic

ruthenium is being utilized as a promoter for Pt in the electrooxidation of methanol in fuel cells (177-179).

The oxidation-reduction behavior of unsupported ruthenium catalysts has been extensively studied by means of Temperature Programmed Reduction (TPR). This technique consists of increasing the temperature of a partially oxidized catalyst at a low uniform rate and measuring the rate of hydrogen consumption. TPR curves of RuO_2 reveal a maximum rate of reduction at 200°C with reduction complete at 270°C. When a freshly formed surface of ruthenium was exposed to oxygen at room temperature, it was covered by a film of RuO_2 (180-181). The reduction of ruthenium oxide at 170°C with a H_2 consumption equivalent to the reduction of Ru^{4+} to Ru^0 has also been reported (182).

Silica supported Ru is oxidized more easiy than the unsupported metal because of the smaller metal particle size (180). Ru/SiO_2 prepared by the reduction of $RuCl_3/SiO_2$ undergoes surface oxidation followed by bulk oxidation upon air exposure of the sample at room temperature. The oxidation-reduction behavior of $RuCl_3 \cdot 1\text{-}3\ H_2O$ impregnated on Al_2O_3 and SiO_2 has been studied by Mossbauer spectroscopy (183). The data indicate that ruthenium trichloride undergoes a chemical change when impregnated on an alumina support but not when supported on silica, indicating that Ru may be coordinated to the Al_2O_3 support. Upon calcination of both samples in flowing air at 400°C, RuO_2 particles were formed. Ruthenium metal was detected as the result of the subsequent reduction of these same samples in flowing hydrogen at 400°C. No observable Mossbauer spectrum could be seen for the reduced ruthenium on SiO_2 although clearly defined spectra were observed for the reduced ruthenium on Al_2O_3. This effect can be attributed to the

existence of much smaller metallic particles or for a much weaker support interaction for silica as compared with Al_2O_3.

Because of their catalytic potential for many selected reactions, the zeolite supported ruthenium catalysts have been studied extensively. The investigation usually consists of a preparation step utilizing ion exchange loading of the zeolite with an appropriate ruthenium complex cation followed by the characterization of sequential chemical products formed during decomposition, oxidation-reduction and/or reaction treatments. Several ruthenium amine complexes have been used for ion exchange including: $[Ru(NH_3)_5\ NO]^{2+}$ (186), $[Ru(NH_3)_5\ N_2]^{2+}$ (186-188), $[Ru(NH_3)_6]^{2+}$ (189), $[Ru(en)_3]^{2+}$ (186), $[Ru(NH_3)_6]^{3+}$ (189-193). Also complexes such as $[Ru(bpy)]^{2+}$ (194), and $[Ru(H_2O)_6]^{3+}$ (195) have been used.

The $[Ru(NH_3)_5\ N_2]^{2+}$ complex exchanged Y-zeolite has been studied by Mossbauer spectroscopy (187-188). In this system the metal ion complex was distorted by its attachment to the zeolite and exhibited a spectrum having a large quadrupole splitting as compared with initial bulk material. The exchanged material completely turned a wine red color when exposed to air at room temperature. Based on extensive I.R. and U.V. visible spectral characterization of this material, an oxygen-bridged ruthenium trimer, $[Ru(NH_3)_5\text{-}O\text{-}Ru(NH_3)_4\text{-}O\text{-}Ru(NH_3)_5]^{6+}$, "ruthenium red" was postulated (187). The oxidation state of ruthenium was increased from (II) in the starting material to a mixture of III and IV in ruthenium red. The mechanism of formation and the assignment of "ruthenium red" as the compound in the zeolite formed as the product of air oxidation of dinitrogen ruthenium however, is a matter of controversy in the literature. The hydroysis of $[Ru(NH_3)_5N_2]^{2+}$-Y in air to

the purple complex $[Ru(NH_3)_5\ OH]^{2+}$-Y has also been proposed, (186-196). The conversion was thought to occur according to the following reaction:

$$[Ru^{II}(NH_3)_5\ N_2]^{2+} + H_2O \rightarrow [Ru^{III}(NH_3)_5\ OH]^{2+} + NH_4^+ + \text{other products.} \quad [5]$$

Where the H_2O came from hydrates in the zeolite . The formation of $[Ru^{III}(NH_3)_5\ OH]^{2+}$ could however be an intermediate which is further oxidized to ruthenium red, according to the following reactions (191).

$$[Ru(NH_3)_5\ OH]^{2+} + H_2O \rightarrow \text{trans} - [Ru^{IV}(NH_3)_4\ (OH)_2]^{2+} + NH_4^+ \quad [6]$$

$$2[Ru^{III}(NH_3)_5\ OH]^{2+} + \text{trans} - [Ru^{IV}(NH_3)_4\ (OH)_2]^{2+} \rightarrow \quad [7]$$

$$[Ru^{III}(NH_3)_5\text{ -O- }Ru^{IV}(NH_3)_4\text{ -O- }Ru^{III}(NH_3)_5]^{6+} + 2H_2O.$$

The $[Ru(NH_3)_6]^{3+}$ complex exchanged in Y zeolite has also been reported to undergo a slow reaction with zeolite hydrates to form a deep wine red complex. ESCA examination of this material, exhibited a nitrogen 1s peak which was composed of two components (190). One was assigned to the coordinated NH_3 and a weak shoulder was found to correspond to the binding energy of nitrogen in NH_4-Y zeolite. The following hydrolysis is proposed:

$$[Ru(NH_3)_6]^{3+} + H_2O \rightarrow [Ru(NH_3)_5\ OH]^{2+} + NH_4^+ \quad [8]$$

followed subsequently by equation [6] and [7]. These hydrolysis reactions were found to proceed faster on more basic X-type zeolite (191). The "ruthenium-red" complex is held easily in the zeolite supercage, and is thermally unstable (190). Vacuum thermal decomposition at temperatures as low as 112°C resulting in partial or complete reduction of

ruthenium to the metallic state has been reported. Nitrogen gas has been detected in the decomposition product, (193) leading to the proposal that NH_3 ligands decompose into N_2 and H_2. The labile H_2 is then available for the reduction of ruthenium cations. By monitoring the amount of hydrogen uptake in the subsequent reduction step, it has been calculated that up to 80% of the ruthenium ions have been reduced to the metallic state during the dehydration step. The results of an X-ray structural determination and the examination of power diffraction patterns for ruthenium(III)hexamine on Y zeolite have identified the atomically dispersed Ru inside the sodalite cages formed either by vacuum thermal decomposition treatment or by heating under hydrolyzing condition where a $H_2O + H_2$ mixture is present (192). Under oxidation conditions the migration of particles to the surface was observed (190). The high temperature thermal activation of the supported transition metals in O_2 prior to the reduction step, usually helped to achieve high metal dispersion. In the case of ruthenium, however, this approach is not feasible because the metal in the oxide form sinters easily into large RuO_2 particles. An optimum strength of interaction between the metal and the support in the calcination step is needed to obtain the highest dispersion (22). The weak ruthenium-support interaction in the calcined state, is due to the very low bond strength of the metal to support oxygens as in RuO_2 compared with oxides of other transition metals. It has been suggested (190) that ruthenium clusters may be oxidized at ambient temperature and retained in a dispersed state if the oxygen is added slowly in order to prevent a thermal excursion.

The influence of certain preparation conditions on metal dispersion has been investigated. A higher degree of dispersion and a more uni-

form distribution is achieved by impregnating the support with an acidic ruthenium precursor solution. A calcination treatment prior to the reduction step increases the particle size and larger Ru metal particles are detected (183). Repeated oxygen-hydrogen treatments disintegrate the ruthenium particles and the activity of the catalysts is enhanced (185).

After a study phase in our laboratory dealing with attempts to generate and study Ru(II) trapped in the Y zeolite matrix, this second phase was undertaken to extend the investigation to Ru(III) species, and to exploit the ^{99}Ru Mossbauer effect as a tool for obtaining direct spectroscopic evidence of the oxidation state of ruthenium species during dehydration and oxidation-reduction treatments.

Studies were also conducted to evaluate the affect of the addition of ruthenium to iron zeolite systems to look for enhanced reducibility of iron. Evaluation of these systems can be accomplished by combining ^{99}Ru and ^{57}Fe Mossbauer data. The use of this "double-labelled" bi-metallic system characterization provides a unique tool for the determination of the overall chemical properties of the mixed metal catalyst system.

EXPERIMENTAL

MATERIAL AND CATALYST PREPARATION

Hexammine ruthenium(II) chloride, $[Ru(NH_3)_6]Cl_2$, was prepared by the method of Fergusson and Love (202). $RuCl_3 \cdot 1\text{-}3\ H_2O$ (Engelhard Ind.) was thermally activated by the addition of concentrated hydrochloric acid and evaporation to dryness over a steam bath. The resulting metal chloride was added to concentrated ammonia hydroxide and reduced by the addition of excess zinc dust (Mallinckrodt, analytical reagent grade),

and boiled until a change in the color of the solution was evident. The solution was immediately filtered and a small portions of ammonium chloride reagent was added to the yellow filtrate until crystallization of the product, $[Ru(NH_3)_6Cl_2$, commenced. Crystallization was complete upon ice cooling of the solution. The product was subsequently filtered and washed with small portions of cold ammonium hydroxide, followed by cold ethanol washings, and stored over P_2O_5 in the desiccator under vacuum. The hexammine ruthenium(III) chloride was obtained by the oxidation of the ruthenium(II) complex (203). The identity of the product was verified by I.R. examination (204-205).

$[Ru(NH_3)_6]^{3+}$ exchanged Y-zeolite was prepared by standard ion exchange techniques using Na-Y (SK-40) from the Linde Company. The exchange solution was $3x10^{-3}$ M l^{-1} $[Ru(NH_3)_6]Cl_3$, and the volume of the solution was adjusted so that 30% of the Na^+ ions were replaced by the ruthenium complex. The exchange was performed overnight under nitrogen atmosphere at ambient temperature.

The $[Ru(NH_3)_6^{3+}, Fe^{3+}]$ - Y catalyst was prepared by a sequential ion exchange technique in which the $[Ru(NH_3)_6]^{3+}$ ions were exchanged first. The resulting catalyst was filtered under N_2 atmosphere and subsequently dispersed in oxygen-free water containing $Fe(NO_3)_3$. The solution concentrations were adjusted so 30% of the Na^+ ions were replaced by each cation.

The $[Ru(NH_3)_6^{2+}, Fe^{2+}]$ - Y zeolite bimetallic catalyst was prepared by a sequential ion exchange method using solutions containing $[Ru(NH_3)_6]Cl_2$ and $FeCl_2$. The solution concentrations were adjusted so that 30% of the Na^+ ions were exchanged by either Fe^{2+} or $[Ru(NH_3)_6]^{2+}$ cations. To maintain the iron in the (II) oxidation state during the

exchange process, the exchange, filtrations and washings were performed under N_2 atmosphere. The exchange reaction was allowed to proceed over night.

The filtrates were washed throughly with oxygen free, distilled water and then dried overnight under vacuum at ambient temperature and stored over P_2O_5 in the desiccator under vacuum. The exchange levels were determined by analyzing for Na ions in the solution after ion exchange by uranyl acetate methods (206). The resulting weight percent of metal in the zeolite was determined to be approximately 5% for Ru and 2.5% for Fe.

To make the results comparable, the treatment conditions for the dehydration and oxidation-reduction of the exchanged materials were maintained as reported in the previous chapter. The initial catalysts (INIT.), were reduced by evacuation of the sample to 10^{-5}torr with subsequent heat treatment to 400°C under flowing hydrogen for 2 hours (REDU.). The oxidation was carried out by exposing the samples to air at room temperature (EXPO.). In some cases, high temperature oxidation in air was also performed (OXID.).

^{99}Ru MOSSBAUER SPECTROSCOPY.

The Mossbauer effect in ruthenium was first reported by Kistner for the 90 Kev transition in ^{99}Rh (207-208). The chemical exploitation of the effect was begun by Good and co-workers (209-213) and by Mossbauer and co-workers (214). The effect has been successfully applied to a variety of chemical compounds containing ruthenium in oxidation states II through VIII and to some mixed oxidation, binuclear compounds. The chemical shift and quadrupole splitting parameters and their interpretation in terms of structure and bonding provide a unique probe of the

divers chemistry of ruthenium. In general, the isomer shift increases with the ruthenium oxidation state as observed for a large variety of ruthenium compounds (210, 214). The values of the isomer shifts have largely been attributed to the shielding of s electrons by different 4d configurations, which are localized at the nucleus and occupy t_{2g} orbitals in octahedral and 2e orbitals in tetrahedral complexes. Using the established correlation between the isomer shift and the oxidation state, the observed values can easily be used to identify the chemical state of the ruthenium nucleus, while the symmetry and chemical environment of the nucleus can be defined by the interpretation of the observed quadrupole splitting value.

A typical quadrupole split spectrum consists of a partially resolved doublet. Each component of the doublet contains three unresolved lines (only simple quadrupole splitting of the excited I=3/2 state is predominate because the nuclear quadrupole moment of the excited state Q_I=3/2 is 3 times larger than the nuclear quadrupole moment of the ground state, Q_I=5/2), (212). Thus, the simple extraction of the Ru Mossbauer parameters usually consists of an isomer shift value which is reported as the center of a doublet and a quadrupole splitting value for the apparent doublet. These simple extractions, however, are not entirely accurate and studies have been carried out for more rigorous extraction of the hylerfine parameters for mixed nuclei transition levels (212, 215). A fully resolved 18 line magnetic hyperfine pattern for the transition between the I=3/2 excited state and I=5/2 ground state of the ruthenium nucleus has been obtained for an absorber of enriched ^{99}Ru dissolved in iron (208).

The instrumentation utilized for ^{99}Ru Mossbauer work is the same as that used for the observation of ^{57}Fe spectra, with the exception of the detector and temperature control units. The half life of the excited states of both isotopes are of the same order of magnitude, ($2x10^{-8}$sec for ^{99}Ru and $9.8x10^{-8}$sec. in the case of the ^{57}Fe isotope), and the Doppler velocity required to shift the gamma ray energy by one line width is essentially the same. Thus, the same velocity drive systems used in iron Mossbauer study have been quite applicable to ruthenium work. The detector used in this work was a NaI(Tl) scintillation crystal from Harshaw chemical Company. The source consisted of 8mCi of 16 day ^{99}Ru in a host lattice of ruthenium metal prepared by New England Nuclear, Corp. A detailed description of the Kontes-Martin low temperature glass dewar system has been given in an earlier publication from this laboratory (183, 208).

The conventional transmission experiments were carried out with both source and absorber at liquid helium temperature. For an appreciable resonance effect to be observed in the ^{99}Ru nucleus, the following experimental conditions must be provided: intense source (the half life of ^{99}Ru precursor is only 16 days), liquid helium cooling of both source and absorber, and a large absorber cross section. The 90Kev gamma was identified and isolated by the usual pulse-height analysis techniques. The experiments were continued long enough to produce spectra with good signal to noise ratios. Data reduction was carried out in the same manner as described for ^{57}Fe Mossbauer work. Isomer shift values are all reported with respect to ruthenium metal.

RESULTS AND DISCUSSION

The original zeolite Y exchanged ruthenium(III) hexamine, $[Ru(NH_3)_6^{3+}$-Y] was pale yellow. The characteristic symmetrical deformation of coordinated NH_3 in this sample was observed as a displaced strong I.R. hand at 1316cm^{-1} having a shoulder at 1340cm^{-1} (Fig.12a). The NH_3 symmetric deformation mode for the $Ru(NH_3)_6Cl_3$ solid state material is split into a number of bands. Three such bands are detected: a strong band at 1315cm^{-1} and two shoulders at 1338cm^{-1} and 1360cm^{-1} - in good agreement with the literature values (204-205). The above data reveal that upon ion exchanging the ruthenium hexamine cation into the zeolite, the symmetric deformation of coordinated NH_3 is lowered; this effect can be due to the interactions between hydrogens of the ammine and oxygens of the framework. The very strong, broad absorption band at 1620cm^{-1} has been assigned to the degenerate $\sigma(NH_3)$ mode in conjuction with the absorbed water in the zeolite which has a bending vibration in this region (216) Fig.12a. The ruthenium-nitrogen stretching vibrations are expected to occur in the 450cm^{-1} region and coincide with the vibrations of the zeolite framework, so that no conclusions can be drawn about any change in the frequency of the band as the result of an ion exchange process.

The ruthenium complex exchanged Y zeolite is unstable and the yellow color changes to a wine-red, when it is left in the air. The reaction leading to the characteristic color proceeded slowly at room temperature and the change of the color was evident after 4 weeks. The reaction could be accelerated by room temperature evacuation of the sample. Review of the literature regarding the assignment of chemical species to the characteristic red colored material indicates that the

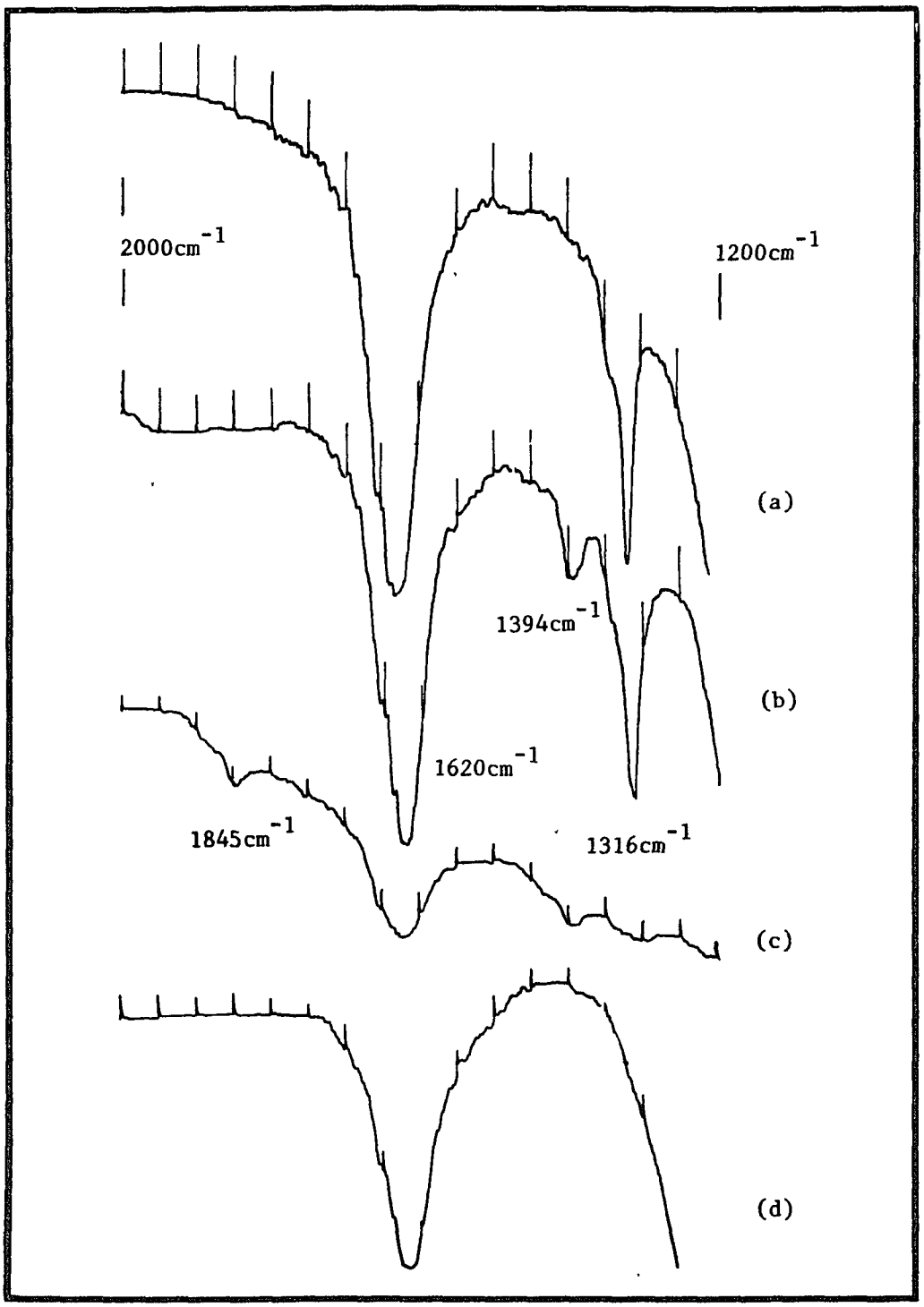

Figure 12. Infrared spectra of ruthenium hexamine(III) exchanged Na-Y zeolite system as a function of treatments.

reaction is a basic hydrolysis process. Since $Ru(NH_3)_6^{3+}$ is relatively stable at atmospheric conditions both in the solid state and in aqueous solution, the zeolitic framework must act as a catalyst in the process, leading to the characteristic red complex formation. A series of sequential reactions can be proposed. First, due to the strong electrolytic properties of the zeolite, the polarization and the ionization of water molecules takes place. This reaction is catalized by ruthenium, leading to the dissociation of NH_3 from the complex and the production of $[Ru(NH_3)_5\ OH]^{2+}$ entities. The protons from the ionization of water interact with the oxygens of the zeolite, creating Bronsted acid sites. The hydrolysis reaction apparently proceeds faster on an X type zeolite than on a Y zeolite (191). The more basic property of X zeolite allows a greater tendency for interaction with protons, consequently the hydrolysis is promoted. The I.R. spectrum for the red sample as depicted in Fig.12b indicates the appearance of a new band at $1394cm^{-1}$. The bands in this region are ascribed to the NH_4^+ species, which are produced as the result of the interaction of the liable NH_3 with the Bronsted sites in the zeolite. As this interaction proceeds, the extent of association of the ruthenium complex with the framework decreases. The red color $[Ru(NH_3)_5\ OH]^2$ complexes are reported to be intermediates to the more stable, oxygen-bridged complexes (Ru-red) via equation [6] and [7]. These deformations lead to the final dissociation of the complex from the framework. No analyzable peaks could be detected in the ^{99}Ru Mossbauer examination of this sample. The absence of an observable spectrum is most probably the result of a small nuclear recoil free fraction for the ruthenium complex and/or the small concentration of ruthenium (90 mg cm^{-2}) in the sample. The subsequent thermal

dehydration of the same sample however, provided a sample that exhibited relatively intense Mossbauer lines. Thus, the absence of an observable spectrum for the ruthenium-red material indicates that the complex must have been loosely held in the zeolite skeleton, and that there is no significant surface interaction of the zeolite with the ruthenium. In this state, the complex is probably located in the interfluid of the supercage, the only site which can possibly accommodate such a large particle. Nevertheless, the previous ^{99}Ru Mossbauer investigation in this laboratory, dealing with ruthenium(II) pentamine dinitrogen exchanged into Y-zeolite, (having the same characteristic red color), exhibited a spectrum which is characterized as ruthenium in the mixed 3 and 4 oxidation states, in good agreement with the chemical state of ruthenium in the Ru-red moieties (217). The contradictory Mossbauer results for presumably the same materials can possibly be due to the difference in the surface interaction of the zeolite and the ruthenium moiety. The extent of the removal of water molecules from the intra-channels of the zeolite during the drying procedure could be the determining step. Dehydration may bring about closer association of the complexes with each other and with the framework and consequently, lead to a higher recoil-free fraction.

To examine the effect of the oxidation treatment, the red sample was left exposed to air at room temperature for several months. The I.R. spectrum for the brownish, dark purple sample, Fig.12b indicates that the relative concentration of NH_4^+ in the system (band at 1324cm^{-1}) has been increased and a new band has appeared at 1845cm^{-1}. The new band has been attributed to υ(NO), which is postulated to be formed upon air oxidation of ammine complexes (191, 187). To investigate further

the nature of the oxidation process, in a separate experiment, a portion of the freshly formed ruthenium-red sample was deoxygenated and sealed and stored for over two years under an inert atmosphere. The original red wine color was preserved and the I.R. spectra of this sample did not have the band due to (NO) formation. This indicates that the formation of the N-O bond in air is solely due to the interaction of ammonia with oxygen, where neither water molecules nor the zeolitic oxygens are taking any part in the oxidation process.

The Mossbauer spectrum for the red sample, degassed to 10^{-5}torr and dehydrated at 400°C for 1/2 hour, exhibited an asymmetric doublet, Fig.13a. There is no doubt that the majority of the ruthenium species have been reduced to the metallic state as is evident by an intense singlet peak (I.S. = -0.01 mm s^{-1}) in the middle of the spectrum. The small isomer shift is indicative of weak metal-support interaction. The nature of the species leading to the appearance of the shoulder peak in spectrum 13a is less certain. However, since this peak disappears in subsequent treatments in H_2, Fig.13b, it must have been due to the existence of ruthenium in a high oxidation state. This peak can be analyzed in terms of being half of a doublet spectrum, superimposed on the central singlet, having the parameters (I.S. = -0.19 mm s^{-1} and Q.S. = 0.37 mm s^{-1}). Comparison of the isomer shift value with those reported for ruthenium compounds in different oxidation states (210) would indicate an average +2 oxidation state for these compounds. Elliott and Lunsford (172), have reported an average oxidation of +2 for ruthenium on zeolite following dehydration at 400°C. EPR results indicates the presence of residual Ru^{3+} in addition to ruthenium metal during dehydration at 300°C (173). Probably there are several ammonia

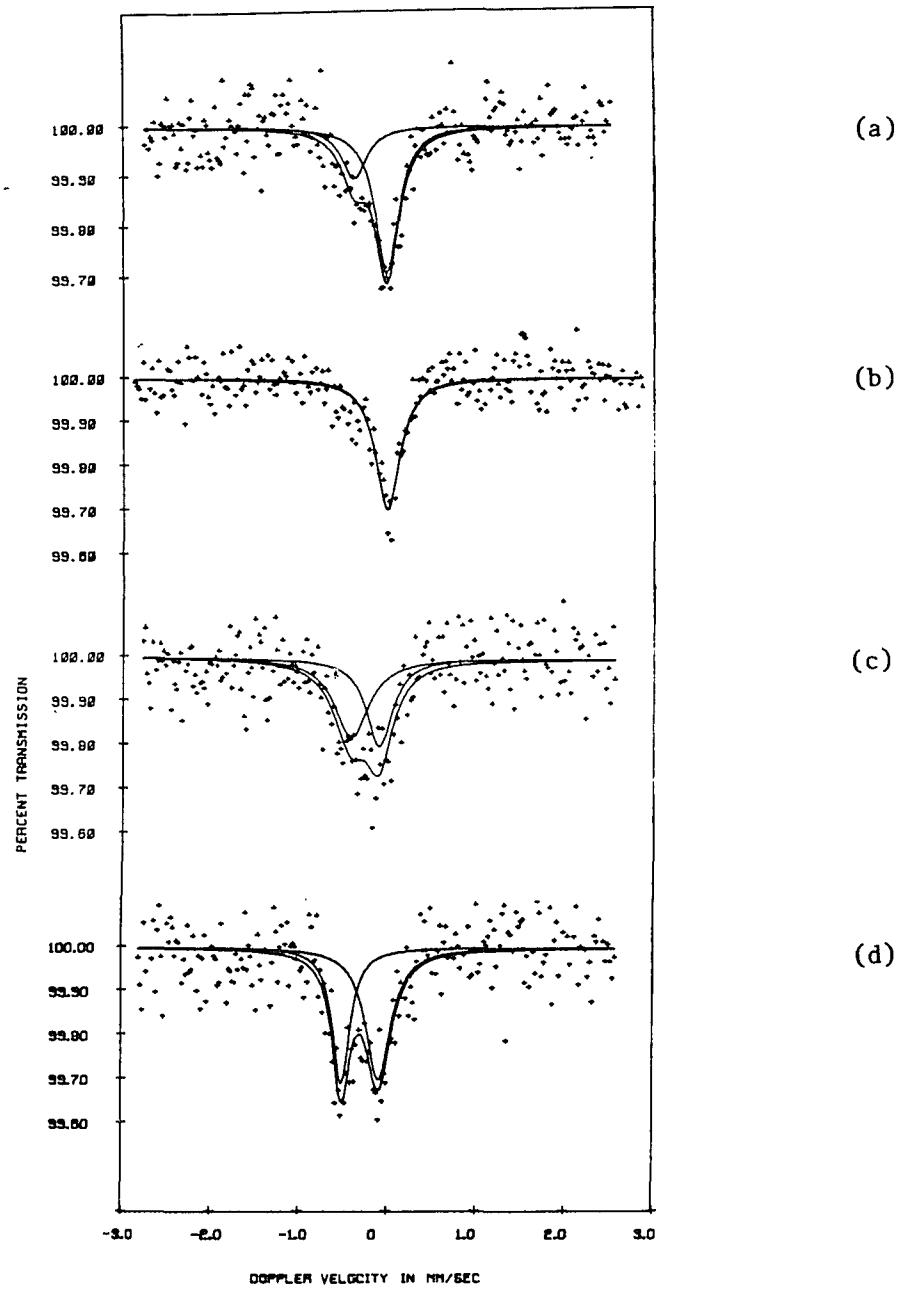

Figure 13. ^{99}Ru Mossbauer spectra at 4.2°K of ruthenium hexamine(III) exchanged Na-Y zeolite system as a function of treatments.
(a) Evacuated ½ Hr. @ 673°K. (b) Reduced 2 Hr., H_2 @ 673°K.
(c) Exposed to air > 24 Hr. @ room temperature.
(d) Oxidized in air 2 Hr. @ 673°K.

complexes in which different numbers of coordinated ammonia molecules are present.

When the dehydrated sample was reduced at 400°C in H_2 for 2 hr., the recorded Mossbauer spectrum, Fig.13b, (I.S. = 0.005 mm s^{-1}), indicated that all of the ruthenium was reduced to the metallic state. The broad line widths of this spectrum compared with the corresponding signal for bulk ruthenium metal, must have resulted from Ru atoms in dissimilar sites, where each different location imposes its particular electronic and geometric requirements on the ruthenium nucleus; thus the particules must exist in the dispersed state. As the result of exposure of the sample to air at room temperature, RuO_2 is formed, Fig.13c, (I.S. = -0.26 mm s^{-1} and Q.S. = -0.32 mm s^{-1}). Again, the broad line width for this sample, compared with the line width of RuO_2 bulk material, indicates that the RuO_2 exists in a dispersed state. The I.R. spectrum for this sample, Fig.12d, did not exhibit any peaks due to the existence of NH_3, NH_4^+ or NO in the sample following these treatments. The subsequent oxidation treatment in air at higher temperature (400°C for 2 hrs.), Fig.13d, (I.S. = -0.29 mm s^{-1} and Q.S. = -0.42 mm s^{-1}), was not expected to change the oxidation state of the ruthenium. The narrow peak parameters are characteristic of bulk RuO_2, which indicates that the thermal oxidation at elevated temperatures results in the migration of RuO_2 to the external surface with the formation of large particles.

IRON-RUTHENIUM SUPPORTED Y-ZEOLITE SYSTEMS

Respective ^{99}Ru and ^{57}Fe Mossbauer spectra of the initial samples and the sequentially reduced and oxidized materials are represented in Fig.14-15. The Mossbauer parameters and corresponding chemical assign-

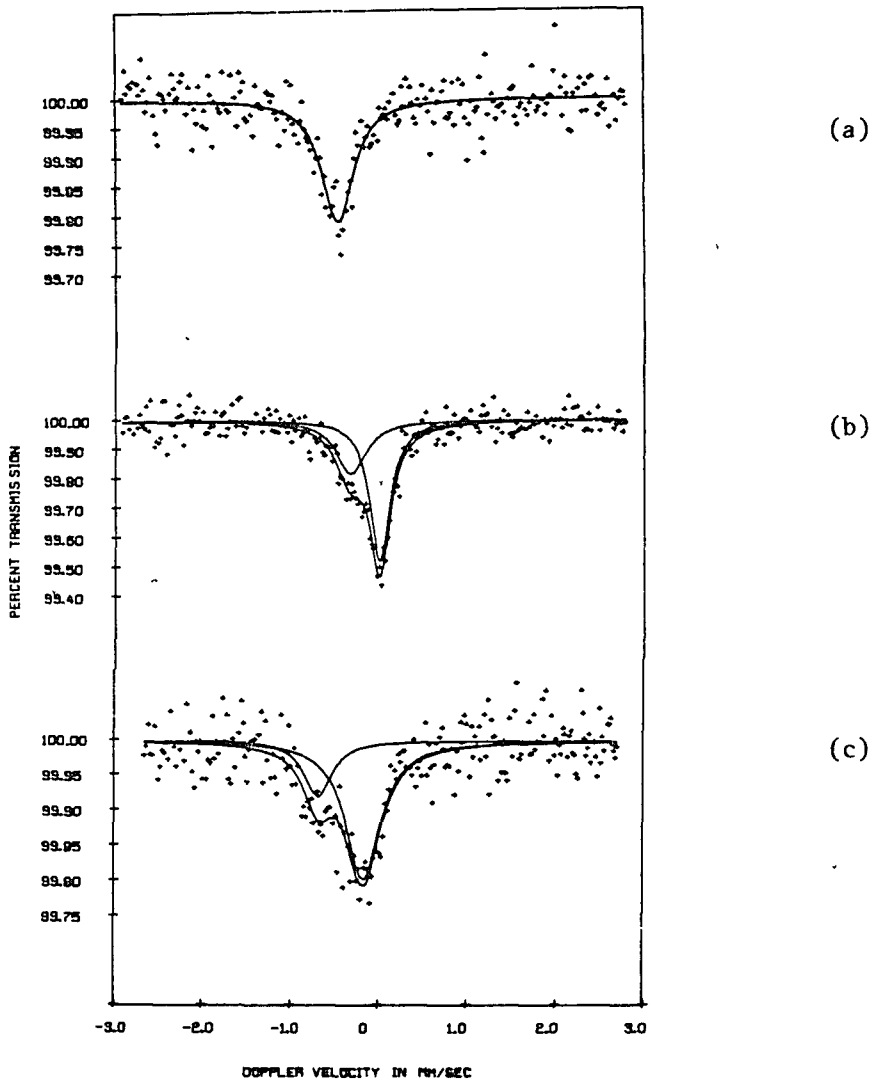

Figure 14. ^{99}Ru Mossbauer spectra at 4.2°K of ruthenium hexamine(III) and ferric exchanged Na-Y zeolite system as a function of treatments. (a) Catalyst as initially prepared. (b) Reduced 2 Hr., H_2 @ 673°K. (c) Exposed to air > 24 Hr. @ room temperature.

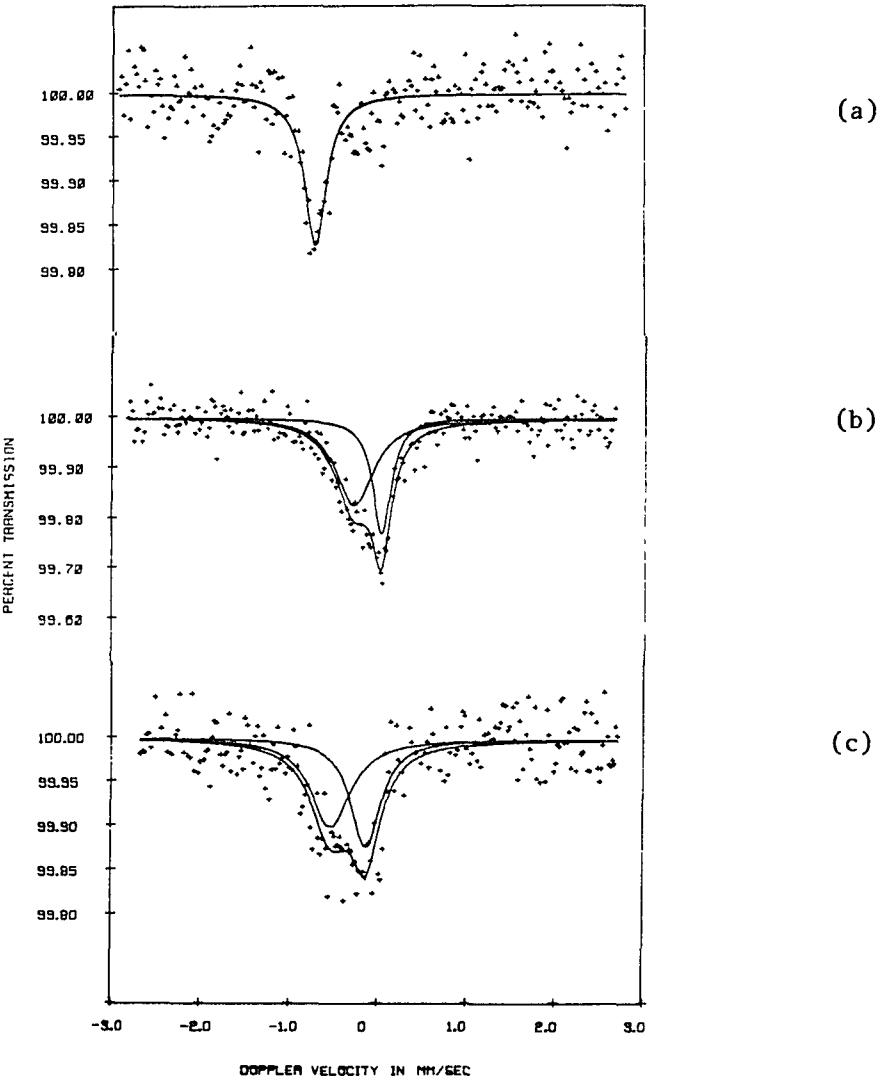

Figure 15. ^{99}Ru Mossbauer spectra at 4.2°K of ruthenium hexamine(II) and ferrous exchanged Na-Y zeolite system as a function of treatments. (a) Catalyst as initially prepared. (b) Reduced 2 Hr., H_2 @ 673°K. (c) Exposed to air > 24 Hr. @ room temperature.

ments are also given in Table 1. The ^{99}Ru results are very similar for both $[Ru(NH_3)_6^{3+}, Fe^{3+}]$ - Y and $[Ru(NH_3)_6^{2+}, Fe^{2+}]$ - Y systems. The spectra of the initial compounds represent ruthenium in +3 and +2 oxidation states respectively. One of the major differences between the bimetallic and the ruthenium only systems was that the formation of the "ruthenium-red" species is hindered. Even after a period of a year the formation of the characteristic red color was not evident. Since the formation of the ruthenium red involves the hydrolysis reactions, the interpretation is that any cation which favorably competes to draw the water into its coordination sphere suppresses the formation of ruthenium red. The strong bond between iron and oxygen may be responsible for the strong association of this cation with the intrachannel water molecules. The material in the reduced state exhibited a ^{99}Ru asymmetrical doublet spectrum, Fig.14b and 15b. The intense peak near zero velocity corresponds to ruthenium metal plus the other half of the quadrupole splitting doublet due to a second kind of ruthenium, which was originally assigned to the oxide form (189). Under reduction conditions however, the only oxygens present in the system are those belonging to the framework and those associated with the hydroxyl group. Thus, the chemical species leading to the doublet in question can be a result of the coordination of ruthenium with oxygens of the framework and/or the association with hydroxyl groups. The second interpretation is parallel to the observed effect of thermal ionization of water in zeolite by transition elements which leads to the formation of $M(OH)^+$ species as described on page 40-41 of Chapter I. An alternative interpretation of the observed asymmetric doublet spectrum for the reduced material involves the assignment of the whole spectrum to ruthenium metal in a very dispersed

state. Where the particles are very small, the surface to bulk atomic ratio is high and an asymmetric doublet is expected for ruthenium atoms at the surface. This is the so-called Gol'danskii-Karyagin effect and is frequently seen in the case of fine iron particles as described previously in Chapter I. In the presence of iron, even at lower concentrations, the dispersion of ruthenium is observed (22). This interpretation is supported by considering the values for the isomer shift and quadrupole splitting (I.S. = -0.15 mm s^{-1} and Q.S. = 0.30 mm s^{-1}) of the doublet which are at variance with the corresponding values for RuO_2 (I.S. = -0.23 mm s^{-1} and Q.S. = 0.51 mm s^{-1}). Thus, the assignment to the oxide form of ruthenium is less certain. Additional support for the existence of very fine metallic particles in the reduced state is provided by the room temperature oxidizability of this material, Fig.14c and 15c. The ^{99}Ru parameters for the oxidized sample are close to those of dispersed RuO_2 clusters Table 1. Since the isomer shift value for ruthenium increases with oxidation state, the lower isomer shift value for this doublet compared to the corresponding value for RuO_2 can be attributed to the presence of ruthenium in an oxidation state lower than +4, probably in association with lower numbers of oxygen. In the case of iron exchanged zeolite, the existence of oxygen bridged iron species has also been theorized (160). The existence of such a species in the case of ruthenium is probably limited due to the lower strength of the ruthenium-oxygen bond as compared to the corrresponding bond in the case of iron. The ^{57}Fe Mossbauer parameters for these materials indicate a reversible oxidation-reduction process between Fe^{3+} and Fe^{2+} states, identical to the iron only system on zeolite (Chapter I). There is some evidence however, that the reduction of Fe^{3+} to Fe^{2+} may be enhanced by

the presence of ruthenium, but reduction to the metallic state was not observed. This latter effect is attributed to the strong iron-zeolite interaction due to strong iron-oxygen bonding.

The results of the Mossbauer investigation of the bimetallic iron and ruthenium exchanged on Y zeolite is interesting in that we see no evidence of the Fe-Ru bulk alloy observed by Vannice (201) for sequentially impregnated ruthenium and iron on silica. In our system the nearly independent behavior of iron in the zeolite is expected because of low concentration of the metals in the large surface area of the zeolite. The fact that the metals are introduced by the ion exchange technique leads to a system dispersed at the atomic level in different locations throughout the framework. At high metal loading accomplished by the impregnation technique a closer interaction between iron and ruthenium would be expected. When the composition is shifted to a ruthenium rich catalyst, hydrogen spillover should increase, producing a pronounced effect on the reduction behavior of iron.

Table 1. The ^{99}Ru and ^{57}Fe Mossbauer parameters of bimetallic catalyst on Y-Zeolite

SYSTEM	ISOTOPE	SAMPLE	#PEAKS AND POSITIONS		I.S.*	Q.S.*	ASSIGNMENTS	SPECTRUM
$[Ru(NH_3)_6]^{3+}$,Fe^{3+} ON Y-ZEOLITE	^{99}Ru	INIT.	Singlet	-0.48±0.01	-0.48	-	Ru^{3+}	14a
		REDU.	Asymm.	-0.01±0.01	0.0	-	Ru^0	14b
			Doublet	-0.30±0.05	-0.15	-0.31	Ru-O	
		EXPO.	Asymm.	-0.16±0.02	-0.16	-	Ru^0, Ru-O	14c
			Doublet	-0.6810.04	-0.42	0.52	RuO_2	
	^{57}Fe	INIT.	Doublet	-0.09±0.02 -0.80±0.02	0.35	0.89	Fe^{3+}	(189)
		REDU.	Doublet	0.01±0.01 2.35±0.01	1.17	2.36	Fe^{2+}	(189)
		EXPO.	Doublet	-0.08±0.02 0.73±0.02	0.33	0.81	Fe^{3+}	(189)
$[Ru(NH_3)_6]^{2+}$,Fe^{2+} ON Y-ZEOLITE	^{99}Ru	INIT.	Singlet	-0.71±0.01	-0.71	-	Ru^{2+}	15a
		REDU.	Asymm.	0.01±0.0	0.0	-	Ru^0	15b
			Doublet	-0.25±0.05	-0.13	-0.26	Ru-O	
		EXPO.	Asymm.	-0.12±0.14	-0.1	-	Ru, Ru-O	15c
			Doublet	-0.51±0.07	-0.32	-0.40	RuO_2	

Table 2 (cont's.). The ^{99}Ru and ^{57}Fe Mossbauer parameters of bimetallic catalyst on Y-Zeolite

SYSTEM	ISOTOPE	SAMPLE	#PEAKS AND POSITIONS		I.S.*	Q.S.*	ASSIGNMENTS	SPECTRUM
$[Ru(NH_3)_6]^{2+}$,Fe^{2+} ON Y-ZEOLITE	^{57}Fe	INIT.	Doublet	0.02±0.01 0.73±0.01	0.38	0.71	Fe^{3+}	(189)
		REDU.	Doublet	0.15±0.01 2.19±0.02	1.17	2.1	Fe^{2+}	(189)
		EXPO.	Doublet	-0.01±0.01 0.77±0.01	0.34	0.78	Fe^{3+}	(189)

REFERENCE PARAMETERS

						REFERENCE
Ru (metal)	^{99}Ru	Singlet	0.00	0.00	-	Standard
RuO_2 (bulk)		Symmetric Doublet	-0.02±0.01 -0.49±0.01	-0.23	0.51	(217)
$Ru(NH_3)_6Cl_3$		Singlet	-0.49±0.01	-0.49	-	(214)
$Ru(NH_3)_6Cl_2$		Singlet	-0.92	-0.92	-	(210)

*The Isomer Shift (I.S., mm s^{-1}), and Quadrupole Splitting (Q.S., mm s^{-1}) valves are reported relative to zero velocity for iron and ruthenium metal standards.

CHAPTER IV

IRON-RUTHENIUM CLUSTERS ON Y-ZEOLITE

The cation exchange ability of zeolites offers significant opportunities for the preparation of novel supported catalytic metal systems. However, as seen in the previous chapter the exchange method of preparation has not been successful in producing a supported metallic iron catalyst after reduction of the iron-zeolite system. Thus, alternative preparation techniques must be employed. There is a number of methods by which the supported bimetallic catalyst can be prepared. For example, the high surface area of the zeolite can be impregnated with an aqueous solution containing the appropriate concentration of salts of a single metal, or two metals if a bimetallic sytem is desired. This method is not expected to be effectve for the production of dispersed metallic iron as indicated by the Mossbauer and ESCA results of the system containing 1.5 atm. % Fe and 3 atm. % Ru (51). Also, the impregnation method is very difficult to reproduce and specimens from the same preparation can be different. Another approach, the precipitation procedure, is expected to be less reproducible than the iron exchange method, but careful variable control can yield uniform catalysts. In an attempt to reduce the iron in combination with ruthenium or by itself on the surface of a the zeolite, several experiments were carried out. Some of these attempts and their results will be described below.

The strong association of iron with the zeolite framework is the main cause of the inefficient reduction behavior of the element when it

is ion exchanged into a zeolite. The fact that cations can be exchanged reversibly into a zeolite without destroying the aluminosilicate framework, provided the idea for back exchanging the iron cations from the framework by NaCl solution as indicated below:

$$NaCl + Fe - Y \rightarrow Na - Y + Fe(Cl) \qquad [9]$$

The cations of the added salt would be expected to penetrate the crystal lattice and exchange with the iron cations. This approach has apparently not been previously reported. The presence of a guest salt in the zeolite leads to the simple concept that the occluded salt will reduce undesirable strong iron - zeolite interaction and consequently promote the reduction of iron. To keep the iron trapped in the zeolite crystals, the salt molecules were introduced from salt solution by impregnation.

The procedure required the determination of the incipient wetness volume of the zeolite material. This is easily accomplished by the titration of zeolite with water and the determination of the volume of water which can be contained within the framework. The catalyst material is then prepared by the addition of the same volume of 2 M NaCl salt solution. The water is then removed by heat treatment at 200°C to cause the occlusion of the salt molecules into the small pores of the zeolite. The sample is subsequently reduced in flowing hydrogen at 400°C for 6 hours. A broad asymmetric doublet is observed in the Mossbauer spectrum with parameters characteristic of Fe^{2+}. The spectrum does not confirm the presence of metallic iron. The extremely broad lines of the doublet indicate that the Fe^{2+} ions are randomly distributed throughout the zeolite. The quadruple splitting of the Fe^{2+}

doublet indicates that the local environments of the iron cations are diverse. The broad line widths can be attributed to the existence of iron atoms at dissimilar sites, where each location imposes its particular electronic environment on the iron nucleus. The presence of Na^+ ions in the system has promoted the rearrangement of the iron species. The result of this experiment can be further modified by the application of higher impregnation temperature for the inclusion of the guest salt cation.

Another unconventional preparation procedure was attemped to obtain bimetallic iron and ruthenium clusters in a Y-zeolite. This approach, referred to as the homogeneous-deposition method, consists of the preparation of a homogeneous mixture of ruthenium hexamine and iron nitrate solutions. The concentration of the solution was 0.5 M in each metal compound. The Na-Y zeolite powder was added to the solution under constant mechanical stirring. The volume of solution and the amount of zeolite were adjusted so the system contained 10 weight % of each metal component. The mixture was stirred constantly at room temperature to allow the diffusion of the metal compounds into the pore systems of the zeolite. The process was continued until evaporation of the solvent occurred. The sample subsequently dried at 110°C. The reduction process was carried out in flowing hydrogen at 400°C for 6 hours.

The Fe Mossbauer spectra of the reduced and air exposed materials, Fig.16, exhibited an asymmetric quadrupole doublet. The spectrum is consistent with the presence of iron metal in a very dispersed state. Where the particles are very small, the surface to bulk atomic ratio is high and an asymmetric doublet is expected for the iron atoms at the surface. This is the so called Gol'danskii Karyagin effect and is

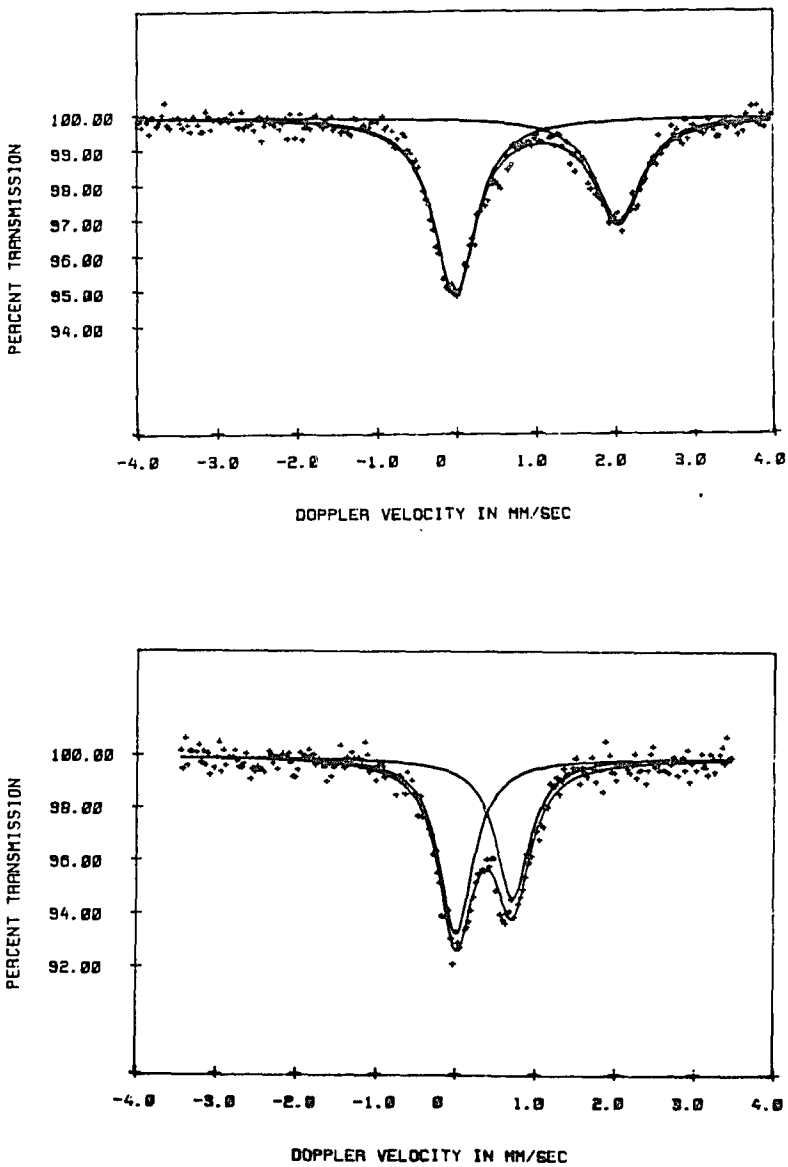

Figure 16. ^{57}Fe Mossbauer spectra of iron-ruthenium clusters on Na-Y zeolite. (a) Reduced 6 Hr., H_2 @ 673°K (Room temperature spectra). (b) Exposed to air $\geq$ 24 Hr., @ room temperature (Liquid Nitrogen temperature spectra).

frequently seen in the case of small iron particles (the principles of the effect have already been described in chapter I). The effect is temperature dependent, i.e. at low temperatures the anisotropic vibration of surface atoms is expected to vanish, leading to a more symmetrical quadrupole doublet spectrum (135). Liquid nitrogen examination of the exposed sample, Fig.1b6, did not reveal any change in the asymmetrical nature of the doublet. Therefore, the assignment of the asymmetric doublet to small metallic iron particles is probably not appropriate. An alternative interpetation involves the assignment of the spectra to two forms of iron where the first iron species gives rise to a symmetric, quadrupole split, two peak spectral component. Half of this doublet could be hidden in the peak in the central region of the spectrum. To determine the actual parameters for this doublet, the intensity of the hidden peak was constrained via the regular Mossbauer spectral program to the value calculated for the visible half of doublet. The Mossbauer parameters for this doublet (I.S. = 1.0 mm s^{-1} and Q.S = 2.1 mm s^{-1}) identify this species as iron in an oxidation state of +2. The second form of iron is responsible for the singlet peak (I.S. = 0.03 mm s^{-1}) in the central region of the spectrum and is assigned to the ε-phase of iron (see details in Chapter V). The ε-phase is the high pressure phase of iron and the only known stable form at normal pressure is when it is associated with the hcp ruthenium lattice in an iron-ruthenium alloy. The value of the isomer shift is consistent with the corresponding parameter for the Fe-Ru alloy (48). The concept of alloy formation between iron and ruthenium will be described and demonstrated in the next chapter.

The postulation of the existance of both Fe^{2+} and Fe-Ru on the surface involves the assignment of Fe^{2+} species to those iron cations which are ion exchanged during the catalyst preparation and are strongly held by interaction with the zeolite framework. The Fe-O zeolite interaction tends to cluster the Fe^{2+} species thereby isolating the resulting metallic iron particles which are formed on further reduction. The same behavior has been observed for MgO supported iron catalysts (145-148). One can postulate that a thick film deposit is formed on the surface of the zeolite during the preparative procedures. Upon reduction, the layers break up into iron (iron-ruthenium) crystallites separated by zeolite and supported on unreduced iron oxide islands. The clustering would lead to metallic iron. The extent of reduction in this sample is about 30% of the total iron in the system as approximated by considering the relative intensities of the Mossbauer peaks and assuming that both species have the same recoil-free fraction. The extent of reduction may actually be higher than 30% because a higher recoil-free fraction is expected for Fe^{2+} particles since they are strongly held by the zeolite surface.

These results are a preliminary indication that the classic problem of reduction of iron in the Y-zeolite system is solvable. Careful examination of the variables is needed to develop a reproducible method for controlling the amount of iron reduced and the degree of dispersion. For example, an increasing concentration of the impregnation solution will increase metal deposition probably leading to a decreased dispersion. Several other parameters can have significant effects. The ruthenium/iron concentration ratio may determine the degree of reduction. The initial pH of the impregnating solution may control the metal

dispersion. The effect of reduction time, temperature and hydrogen flow rate may have an impact on crystallite size distribution as well as the extent of reduction. Passivation, calcination, and dehydration may affect the resulting crystal size distribution. Thus to achieve the ultimate goal of predictable reduction behavior, it will be necessary to understand and optimize these many experimental conditions.

CHAPTER V

IRON-RUTHENIUM ALLOYS

INTRODUCTION

A clear understanding of the nature of the interaction between ruthenium and iron can be provided by studying them in the absence of complications caused by support effects. Information on the solid state and surface properties of possible alloys can be used to determine the electronic and structural nature of the interaction between the two metals. The results can provide the necessary data for constructing and evaluating theoretical models of the electronic structure of these alloys at the atomic leve.

Iron has three allotropes: α-phase, body centered cubic (bcc); γ-phase, face centered cubic (fcc); and ε-phase, hexagonal close packed (hcp). The α-phase is stable at room temperature under atmospheric pressure, the γ-phase is formed at high temperatures and the ε-phase is the high pressure phase (218). A great deal of interest has been exhibited in the magnetic properties of different forms of iron with considerable attention directed to the magnetization of the bcc α-phase. This phase is ferromagnetic with an internal magnetic field of 330 KG at 0°K, a magnetic moment of 2.22 μ_B, and a Curie temperature of 1043°K (219). The γ-phase of iron is antiferromagnetic with a Neel temperature of 8°K, a magnetic moment of 0.7 μ_B (220), and an internal magnetic field of 24 KG (221). The hcp ε-phase of iron is an interesting

material which is only stable under pressures $\geq$ 130 Kbar and is paramagnetic at room temperature (222). High pressure, low temperature Mossbauer studies of the ε-phase have revealed little sign of any magnetic ordering down to 2.2°K (218). This phase has been shown to be stabilized under atmospheric pressure by the addition of hcp ruthenium. The Mossbauer effect has been utilized to determine the magnetic properties of the alloyed iron (219, 223-225) which exhibited a Neel temperature of 100°K and an internal magnetic field of 16 KG. α and ε phases of iron were found to coexist over a large range of pressures. The transformation to ε-phase began at pressures as low as 50 Kbar (226). At pressures above 165 Kbar only the ε-phase was detected. On depressurizing, the ε→α transformation began at a pressure of 81 Kbar with complete conversion to α-phase at 45 Kbar. These results are indictive of a martensitic transformation (218).

Most of the work involving the Ru-Fe alloys originated due to the practical difficulties involved in stablizing pure iron in the ε-phase. The iron-ruthenium alloy which stabilizes the ε-phase at atmospheric pressure provides an alternative method of studying this phase. Ruthenium forms a solid solution with iron: above 24.5 mole% Ru, Fe is substituted into the hcp Ru lattice; between 24.5 and 4.5 mole% Ru, a two phase region exists. When the Ru concentration is below 4.5 mole%, Ru is substituted into the bcc iron lattice (219, 223-225).

In alloys, regular solution theory (227) predicts the enrichment of the surface with the more volatile constituent, provided sufficient annealing allows the attainment of microstructure equilibrium. This segregation phenomenon arises because the free energy of the system is reduced by positioning the element with the smaller heat of sublimation

(weaker bonds) at locations with fewer neighbors. In the case of a highly dispersed catalyst, where the microclusters are very small and a large percentage of the atoms are on the surface, segregation of the more volatile component to surface sites with low coordination numbers is expected (228). X-ray photoelectron spectroscopy (XSP) has been used to provide a quantitive analysis of the average composition of the surface in an Fe-Ru alloy system. The alloy was prepared by mixing a 1:1 ratio of $RuCl_3 \cdot 1\text{-}3\ H_2O$ with $Fe(NO_3)_3$ in solution. After drying, the fresh catalyst contained mixed oxides of Fe and Ru with both Fe^{2+} and Fe^{3+} species. After reduction in flowing hydrogen at 400°C, metallic Fe and Ru as well as Fe-Ru clusters were detected. XPS quantitative analysis of the first several surface layers indicated enrichment of the surface region in Fe. Greater enrichment has been detected in the uppermost layer using secondary ion mass spectroscopy (229-230). These results were expected due to the lower bond enthalpy for iron compared with that of ruthenium. For example, the activation energy values for ammonia synthesis on the surface of an Fe-Ru catalyst are closer to that of Fe than Ru. Thus, the surface of the bimetallic material must be occupied largely by iron atoms (231).

The lattice parameters of Fe-Ru alloys have been shown to be different from those of the pure metallic constituents. A solid catalyst prepared from an equimolar mixture of $RuCl_3$ and $FeCl_3$ produces the hcp structure as identified by X-ray diffraction and the lattice constants were detected to be smaller in both the a and c axis then pure hcp ruthenium (245). The effect of Ru addition on lattice parameters of bcc iron has also been reported. A solution of up to about 10 atom% Ru vacuum melted in high purity α-Fe was hot-rolled at 1100°C to a thin

plate, austenitized at 1000°C in an evacuated silica capsule and water quenched. The lattice parameters of the resulting bcc Fe-Ru alloy, measured by X-ray diffraction were found to be larger than those of pure bcc iron and could be correlated to a linear function of ruthenium concentration (232).

^{57}Fe Mossbauer analysis of the hyperfine fields of ferromagnetic iron has been accompanied by studies of the exchange interaction and the change and distribution of spin-density in alloy systems. Various transition metals, including ruthenium, have been introduced into the bcc α-phase iron lattice and changes in magnetic splitting structure as a function of solute concentration have been observed. Data for these alloys consist of the superposition of a number of six-line hyperfine spectra whose amplitude, position and overall splittings are related to the environment and atomic arrangement within the alloy. The hyperfine field value reduces by an amount proportional to the number of near neighbor impurities (nn) and next nearest neighbors (nnn). The reduction is largely independent of the nature of the impurity atom with the proportionality constant being different for nn and nnn occupancy but independent of concentration. Although the cubic symmetry of the iron atoms is destroyed by nn solute atoms, no quadrupole addmixture to the magnetic hyperfine splitting of Fe atoms is predicted. The largest isomer shift due to nn impurity atoms is less that 0.8 mm sec^{-1}, corresponding to a change in the d electron density of less than 1/20 of a d electron. The corresponding change in hyperfine interaction amounts to 26 KG (233).

It has been recognized that the anions associated with the metal ion in the initial salt mix can influence the final reduction product.

The initial work in this laboratory on the unsupported Ru-Fe system indicated that a mixture of ruthenium trichloride trihydrate and hydrated ferrous sulfate produce a hydrogen "reduced" product containing a complex mixture of Ru metal, RuO_2 and γ-Fe_2O_3 (234). This result was in contrast to the conclusions drawn from surface analysis techniques on a similar system where the reduced product from an initial mixture of hydrated ruthenium trichloride and hydrated ferric nitrate was described as "metallic" (230). A related study using the same initial chloride-nitrate salt mixture impregnated on silica, indicates that bimetallic clusters of Ru-Fe were the products of hydrogen reduction (48). These anion effects on the solid state chemistry of salt mixtures are of vital importance to catalytic chemists who must produce uniform materials of known characterization.

This portion of our study was undertaken to evaluate the chemical differences of the solid state reactions which take place during preparation of bimetallic Ru-Fe catalysts from a variety of starting materials. It was hoped that the investigation would provide the information necessary to design uniform materials of known characteristics and afford the opportunity to compare the properties of first and second row transition metals in a variety of environments (235). In this section, the results of an ^{57}Fe Mossbauer survey are reported for the products formed when ruthenium trichloride trihydrate is mixed with a variety of iron salts or oxides and for the products of the subsequent oxidation-reduction of these materials.

EXPERIMENTAL

MATERIALS AND CATALYST PREPARATION

Ruthenium trichloride trihydrate was purchased from Engelhard Industries. Hydrated ferric chloride was obtained from Mallinckrodt Chemical Works. Hydrated ferric nitrate and ferrous sulfate were purchased from Fischer Scientific Company. α-Fe_2O_3 was obtained from Matheson Coleman Company. All were reagent grade and used as received.

1:2 molar ratio mixtures of $RuCl_3 \cdot 1\text{-}3\ H_2O$ and the iron salts were slurried with distilled water. A few grains of ascorbic acid were added and the mixture was evaporated to dryness in a steam bath. These initial samples were designated as Fe-Ru (chloride-chloride), Fe-Ru (nitrate-chloride), and Fe-Ru (sulfate-chloride). Each sample was then heated under a vacuum of 10^{-5}torr to 400°C for one half hour and subsequently reduced in flowing hydrogen at 400°C for 4 hours. The resulting samples were designated Fe-Ru (REDU.). A portion of each reduced sample was exposed to air at room temperature for a minimum of 24 hours to form samples designated Fe-Ru (EXPO.). The air exposed samples were heated in air at 400°C for 4 hours and labeled Fe-Ru (CALC.). A 1:1 molar ratio mixture of $RuCl_3 \cdot 3H_2O$ and iron oxide (α-Fe_2O_3) was also prepared and treated as described. The catalyst treatments were carried out in the same apparatus as previously described. For all above catalyst systems the metal composition in the solid solution is 33 atom % ruthenium and 67 atom % iron.

X-RAY PHOTOELECTRON SPECTROSCOPY

The intrinsic surface nature of XPS makes it extremely useful in the field of heterogeneous catalyst evaluation. The application of the technique has been reviewed extensively (236-238). It is sensitive to

nearly all elements and qualitative, as well as quantitative, analyses of surface regions several atoms thick is possible. XPS is essentially a semi-surface technique with several aspects of the measurements related directly to the surface properties.

The XPS spectrum is obtained by the analysis of the kinetic energy of photoelectrons ejected from the surface of the sample material during bombardment by X-rays. The primary process consists of the impingement of (1-3 Kev) X-ray incident photons and the detection of the energy of the electrons emmitted from the core levels of an atom. The detected energy is essentially the difference between the energy of the incident photon and the specific binding energy of the atom, therefore the binding energy of the core electrons can be extracted. A plot of the number of the electrons detected versus the electron binding energy produces the photoelectronic spectrum. Qualitative analysis is straightforward and is accomplished by comparison of observed binding energies which reflect the chemistry of the atoms under study, with binding energies of known materials. Correlations between chemical shifts and calcuated charges on atoms have also been made.

The intensity of an XPS peak is proportional to the atomic concentration of the elements, the cross section for photoelectron emission and the depth of the escape paths of the electrons. The depth from which an electron can escape without energy lost caused by inelastic collisions is called the escape depth (10-100°A). The inelastic scattering of the photoelectrons contributes to "tailing" and, in general to background signal. "Tailing" appears on the higher binding energy side of the peak. The escape depth depends on both the atomic number of the material and the kinetic energy of the electrons, and becomes an impor-

tant factor in the interpretation of the chemical composition of heterogenous samples and in the differentiation between solid solution and surface segregation of particular species; i.e. the relative atomic concentration of iron and ruthenium in the surface region can be evaluated by using the spectral area of the most intense lines, $2p_{3/2}$ for iron $3d_{5/2}$ for ruthenium, corrected for the mean free paths of the electrons

$$\frac{N_{Fe}}{N_{Ru}} = \frac{I_{Fe\ 2p_{3/2}}}{I_{Ru\ 3d_{5/2}}} \cdot \frac{\sigma_{Ru}}{\sigma_{Fe}} \qquad [10]$$

The cross section (σ) for the photoelectron emission for the ruthenium $3d_{5/2}$ electron is 7.51 and for iron $2p_{3/2}$ electron is 10.54 (246).

The x-ray photoelectron spectra were obtained on a Perkin Elmer-Physical Electronics, PHI model 548 ESCA/Auger spectrometer, using monochromatic Mg Kα X-ray photons. A detailed description of the spectrometer and the techniques used have previously been published (51). The sample material was pressed into pellets for mounting in the spectrometer and were treated <u>in situ</u> using a PHI model 2100 sample introducer and an optional PHI model 02-120 hot/cold specimen transport probe. Specific conditions for each sample are described in the text. The binding energies are corrected by taking advantage of the carbon 1s peak as a reference line. In this case the surface carbon which is present on almost all samples produces a carbon peak that is incidental to the sample composition (binding energy of the carbon 1s peak was taken to be 284.6 ev according to reference 239).

X-RAY DIFFRACTION

X-ray powder diffraction data were obtained using a Phillip's diffractrometer equipped with an XRG-3000 X-ray generator and an APD-3500 data controller and processor. The 2θ scan range was from 2 to 60 degrees in increments of 0.02. Counting time was fixed at one second for each step.

RESULTS AND DISCUSSION

Fe-Ru ALLOY (CHLORIDE-CHLORIDE) SYSTEM

Respective ^{57}Fe Mossbauer spectrums for the initial sample and the subsequently reduced, exposed, and oxidized materials are represented in Fig.17 for the chloride-chloride system. The Mossbauer parameters and the correponding chemical assignments are provided in Table 2. The data indicate the presence of both Fe^{2+} and Fe^{3+} species in the initial compound. The six-line magnetically split spectra of α-Fe is clearly visible in the reduced sample, Fig.17b. In addition a single line in the middle of the spectrum is also evident. The central peak could represent a fraction of iron in a dispersed state < 15°A in the superparamagnetic phase, or it could be a signal associated with the ε-phase of iron. As indicated earlier, ε-phase is a high pressure phase of iron and is stable at atmospheric pressure only when it is associated with the hcp ruthenium lattice. The substitution of iron into the hcp ruthenium structure takes place when the solid solution contains more than 24.5 mole present ruthenium (22). This condition is satisfied by our sample composition. Theoretical calculations predicted a ferro or antiferromagnetic ordering for hcp iron alloy with ruthenium (219) and a single Mossbauer line is detected at room temperature (223). The isomer shift value for the Fe-Ru alloy varies slightly with composition, i.e.

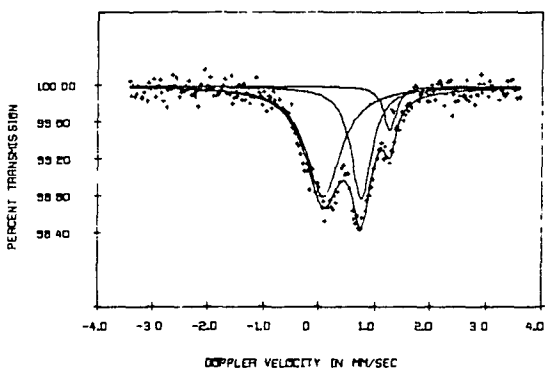

a: (INITIAL)

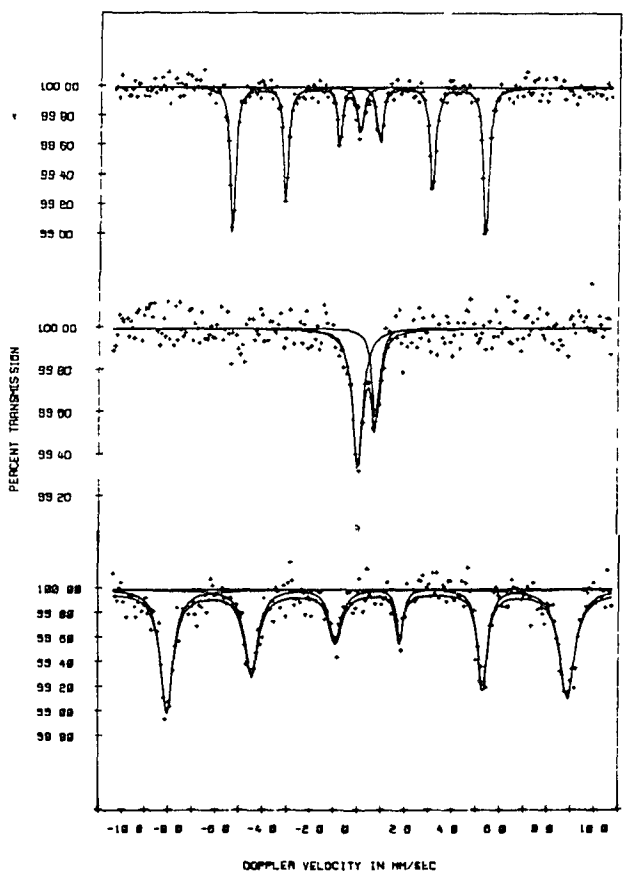

b: (REDUCED)

c: (EXPOSED)

d: (CALCINED)

Figure 17. ^{57}Fe Mossbauer spectra at 83°K of iron-ruthenium alloy (CHLORIDE-CHLORIDE) system as a function of treatments.

in the range of 0.0-0.06 mm s^{-1} with respect to α-Fe as a standard. The single line in the middle of the spectrum is defined by the Mossbauer parameters: I.S. = 0.05 mm s^{-1} and linewidth = 0.34 mm s^{-1}. These parameters are consistent with the conclusion that a portion of the sample has been converted to ε-phase iron in the form of an Fe-Ru alloy.

The enrichment of the surface of Fe-Ru alloys with iron has been observed and is expected due to the lower bond enthalpy for Fe than for Ru (229-230). Our interpretation is that the iron enrichment on the surface in the reduced material is responsible for the observed six line Mossbauer spectra. Chemical evidence for the existence of very small metallic particles and a subsequently high surface area is exhibited by the highly exothermic reaction which takes place when the sample is exposed to air; in some instances the sample actually flames. On air exposure, the six line pattern due to magnetically split α-Fe vanishes, and two peaks due to superparamagnetic α-Fe_2O_3 become evident, Fig.17c. The fraction of iron in the ε-phase in the form of Fe-Ru seems not to be affected, which indicates that this species exists within the particles. The superparamagnetic relaxation time varies with the temperature and also depends on the volume of the particles. At room temperature the critical particle diameter for the onset of superparamagnetic behavior in α-Fe is less than 15°A (139) and for α-Fe_2O_3 is 135°A (79). Although it is not possible to completely characterize the particle size of the microcrystallites in a solid state mixture by the Mossbauer effect, some further information can be gained by determining the spectra at different temperatures. To elucidate the nature of the transformation of this hyperfine field of iron upon air oxidation and the corresponding particle size involved, a separate experiment was performed where a

reduced sample was oxidized via a slow leak of air through the reactor for a few minutes at room temperature. Spectra 18a was observed for this product. The experiment repeated at liquid nitrogen temperature produced the spectrum shown in Fig.18b. The six line magnetic splitting was barely apparent at room temperature but well developed at 83°K. The temperature dependency of the hyperfine field would imply that the average effective size of iron particles in this stage of treatment is in the range of the critical diameter for onset of superparamagnetic behavior. The isomer shift and quadrupole splitting values for the doublets in the central region of the spectrum are typical for highly dispersed Fe_2O_3. The magnetic behavior of these particles is not affected by lowering the temperature to 83°K which indicates that the particle size of Fe_2O_3 is less than 100A° (79).

The product after high temperature oxidation treatment in air shows the characteristic six-line magnetic spectrum of bulk α-Fe_2O_3 (Fig.17d). The broad line width of this spectrum could be attributed to one or more of the following effects, i.e., the magnetic sites have a large line width because the magnetic field is very sensitive to any local perturbations or local perturbation due to the presence of ruthenium impurities in the α-Fe_2O_3 crystal lattice. Another possible origin for the observed broad magnetic lines can be thought of in terms of the superparamagnetic relaxation time and its volume dependency. When the relaxation time is close to the nuclear Larmor precession time, spectra with broadened lines are expected, which implies that the average particle size of α-Fe_2O_3 is in the range of the critical diameter for onset of superparamagnetic behavior; i.e. in the order of 135A°. This interpetation is consistent with our previous particle size predictions and

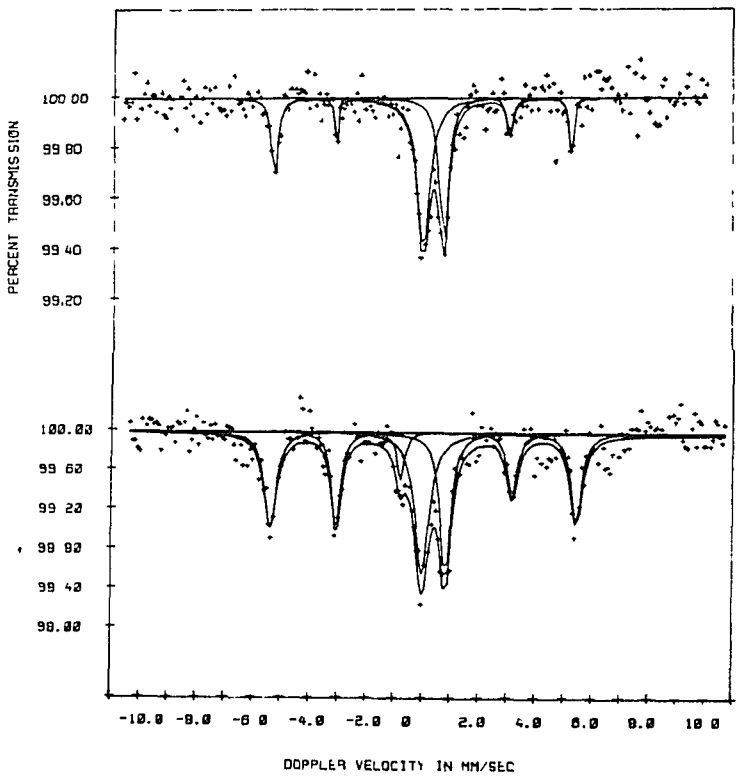

Figure 18. ^{57}Fe Mossbauer spectra of partially exposed iron-ruthenium alloy (CHLORIDE-CHLORIDE) system as a function of temperature. (a) Room temperature spectra. (b) Liquid Nitrogen spectra.

indicates that particle sintering has taken place during the high temperature oxidation.

Fe-Ru ALLOY (NITRATE-CHLORIDE) SYSTEM

The nitrate system behaves very similarly to that of the chloride materials except that the quality of the spectra is poor and some unidentified residue remains in both the reduced and calcined samples. The iron nitrate is expected to undergo decomposition when heated. The evolved gases which may be trapped in the sample or significantly smaller particles could be the cause of the low recoil fraction observed for these materials. The variation in the line width for the magnetic peaks and the poor signal to noise ratio for the superparamagnetic α-Fe_2O_3 spectrum in the exposed case are both indicative of the existence of anisotropic particles. The fact that the oxidation is essentially complete when the sample is exposed to air at room temperature clearly demonstrates the high surface area of the iron metal component in the reduced state (235).

Fe-Ru ALLOY (SULFATE-CHLORIDE) SYSTEM

The Fe-Ru sulfate sample has been reported to behave quite differently (234) as compared to nitrate or chloride systems. This portion of the study was undertaken to remove any ambiguity about the chemical differences which exist between these materials and to elucidate the role of sulfate ions in the system by an interpretation of the Mossbauer results.

The Mossbauer representation of the initial compound, Fig.19a, shows the existence of two quadrupole doublets. The more intense outer doublet has been assigned to iron in the (II) oxidation state. The

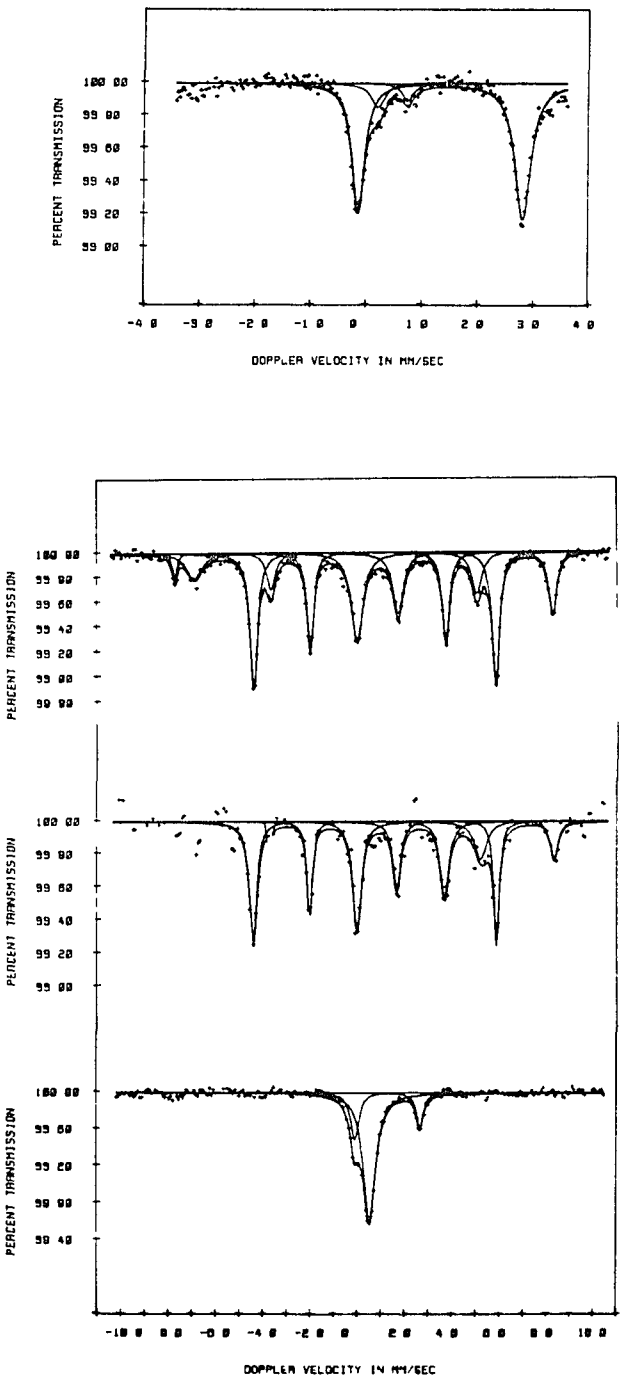

a: (INITIAL)

b: (REDUCED)

c: (EXPOSED)

d: (CALCINED)

Figure 19. ^{57}Fe Mossbauer spectra at 83°K of iron-ruthenium alloy (SULFATE-CHLORIDE) system as a function of treatments.

presence of the second doublet, which is characteristic of iron III, indicates that a portion of the iron has been oxidized. Earlier work on the effect of γ radiolysis on iron II sulfate hydrated material has indicated that iron II is oxidized to iron III by oxidizing radicals, mainly OH, which originate from the radiolysis of water (102). Thus, gamma radiolysis of iron II sulfate during the Mossbauer experiment could be the cause of the oxidation of this compound to hydroxy iron II sulfate.

The room temperature Mossbauer spectrum for the reduced sample is shown in Fig.19b. This spectrum consists of the overlap of three, six-peak patterns. The comparison of this spectrum with the typical spectrum of Fe_3O_4, Fig.20a (263), clearly demonstrates the existence of the magnetite species in the reduced sample. Magnetite, Fe_3O_4, crystallizes in the inverse spinel structure. Tetrahedral sites of the structure (site A) are occupied by Fe^{3+} ions, where the octahedral sites are occupied by both Fe^{3+} and Fe^{2+} ions coordinated to oxygen. Above a characteristic transition temperature, $T_v \cong 120°K$, each site exhibits its own six peak pattern Mossbauer spectra. Below this temperature, it has been found that the lines of the B site spectrum are broadened due to electron hopping between Fe^{2+} and Fe^{3+} ions. The Mossbauer demonstration of the transition is provided in Fig.20. A closer look at the previously reported Mossbauer results for the same material (234), also identifies the Fe_3O_4 species as the more likely species responsible for the observed six peak pattern obtained at liquid nitrogen temperature. This pattern has previously been assigned to γ-Fe_2O_3. The structure of this phase may be regarded as a cubic close packed array of oxide ions with the Fe^{3+} ions distributed randomly over both the octahedral and

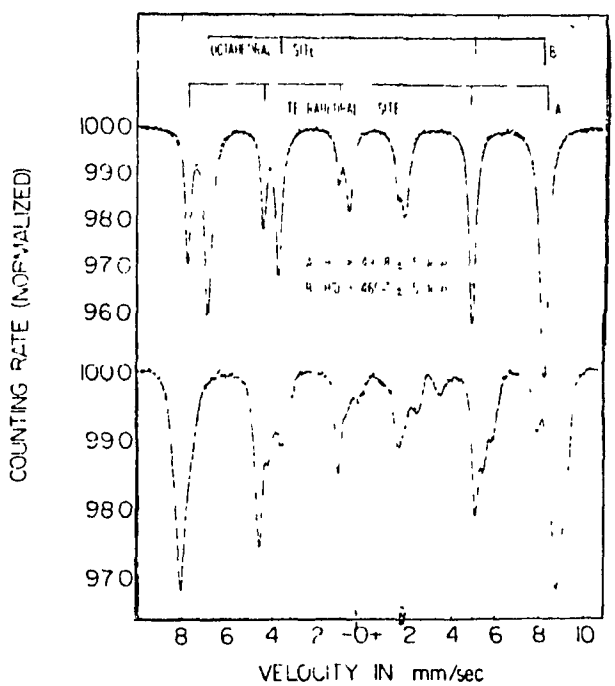

Figure 20. Typical ^{57}Fe Mossbauer spectra of Fe_3O_4 as a function of temperature. (a) Room temperature spectra. (b) Liquid Nitrogen spectra. Figure according to Kundig (163).

tetrahedral sites (244). This phase can be obtained easily by oxidation of Fe_3O_4. No explanation for the possible origin of the excess oxygen in the system has been given.

The evidence for the existence of the magnetite in the reduced sample and the mechanism for the formation of such species in the system is ambiguous. One possible explanation indicates that the oxidation of iron in the presence of a limited amount of oxygen leads to the formation of non stoichiometric iron monoxide (wastite phase), which is unstable, tending to disproportionate finally into iron and magnetite (240). This mechanism would explain the existence of magnetite in our system, but the question of the oxygen source remains. The fact that these species are not present in the other samples which do not contain sulfate ions, clearly demonstrates that the sulfate ions are responsible for the processes leading to the formation of magnetite type species. The retained sulfate ions in the structure could provide a cubic close-packed array of oxide ions in which the divalent iron cations with coordination number 4 are in tetrahedral interstices and the trivalant iron cations with coordination number 6 are located in the octahedral interstices. Recently the inclusion of SO_4^{2-} in the structure of α-Fe_2O_3 has also been observed (241). Iron sulfate is stable up to 570°C without any decomposition or phase change (242). The assignments suggested above are substantiated by the ESCA data which exhibited two sulfur peaks for the reduced sample (234). The more intense six line pattern in Fig.19b, is assigned to iron associated with sulfur in the form of FeS. The isomer shift and internal magnetic field results are very close to those reported for FeS (243), table 2-3. Additional evidence for the presence of sulfur in the structure is provided by the resis-

tance of the sample to oxidation. The explosure of the material to air induced no significant chemical changes at room temperature in contrast to the behavior of the chloride or the nitrate systems. High temperature oxidation produced species characterized by a central, near zero velocity, Mossbauer peak. In addition, a less intense quadrupole doublet was also observed, Fig.19d. The isomer shift value of the control peak was very close to that reported for bulk Fe-Ru alloy. The doublet can be assigned to superparamagentic iron in association with oxygen or sulfur. It seems likely that the high temperature oxidation treatment of the compound leads to the titration of sulfur by oxygen with the sequential formation of Fe-Ru species.

Fe-Ru ALLOY (OXIDE-CHLORIDE) SYSTEM

The character of the ruthenium salt is not expected to change the oxidation state or the crystalline structure of α-Fe_2O_3 during the initial preparation treatment when the salt is mixed with α-Fe_2O_3. This conclusion is verified by the Mossbauer spectrum shown in Fig.21a. The initial material was subsequently subjected to a thermal vacuum treatment at 400°C for 3 hours. The representative XPS survey scan binding energy for the ruthenium $3d_{5/2}$, $3d_{3/2}$ and the iron $2p_{3/2}$, $2p_{1/2}$ electrons are represented in Fig.23-24, respectively. The ruthenium $3d_{3/2}$ peak coincides with the carbon 1s peak which has a binding energy of 284.6ev (239). The ruthenium $3d_{3/2}$ transition is expected to be 4.1ev higher in energy than the ruthenium $3d_{5/2}$ electrons. Since the value of Ru $3d_{3/2}$ / Ru $3d_{5/2}$ intensity ratio is equal to 1.5 (239), the intensity and the position of Ru $3d_{3/2}$ peak is adjusted so that the contribution of the carbon 1s electrons to the total spectrum can be extracted. The binding energies and corresponding chemical shifts are evaluated based

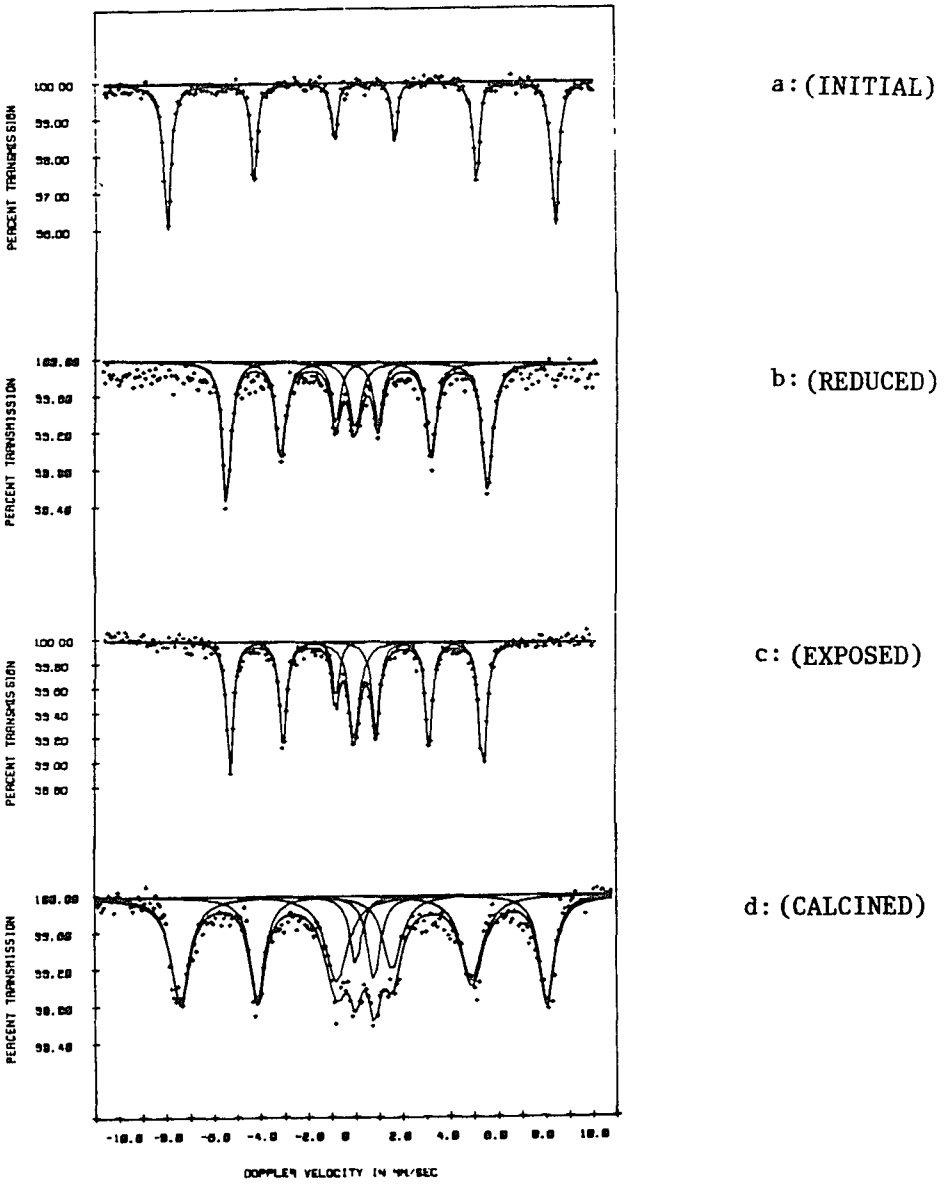

Figure 21. ^{57}Fe Mossbauer spectra at 83°K of iron-ruthenium alloy (OXIDE-CHLORIDE) system as a function of treatments

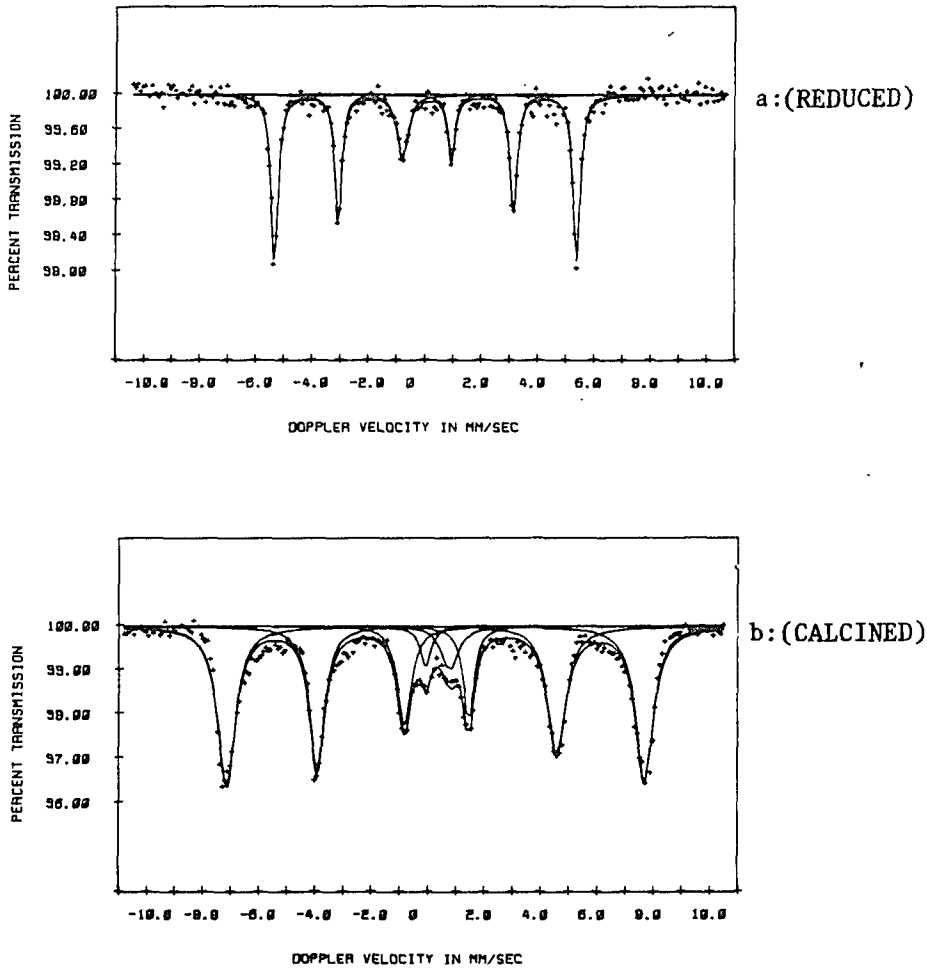

Figure 22. ^{57}Fe Mossbauer spectra at 83°K of α-Fe_2O_3 as a function of treatments.

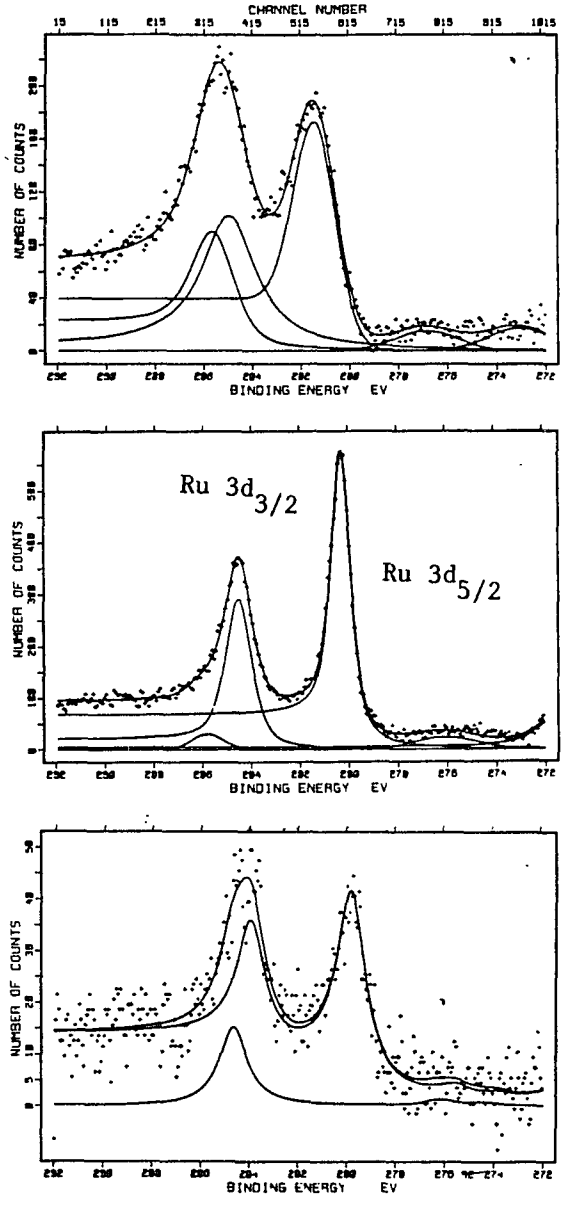

(a) Catalyst as initially prepared, evacuated 3 Hr. @ 673°K.

(b) Reduced 4 Hr. H_2 @ 673°K.

(c) Exposed > 24 Hr. air @ R.T.

Figure 23. XPS spectra of Ru $3d_{3/2}$, Ru $3d_{5/2}$ and C 1s peaks of iron-ruthenium alloy (OXIDE-CHLORIDE) system as a function of treatments.

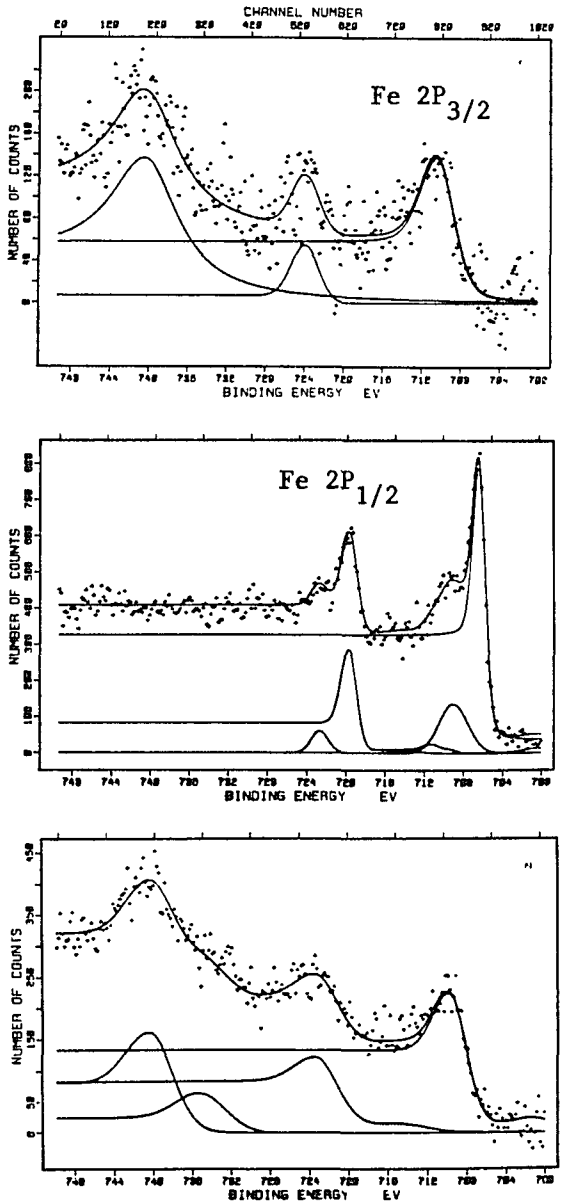

(a) Catalyst as initially prepared, evacuated 3 Hr. @ 673°K.

(b) Reduced 4 Hr. H_2 @ 673°K.

(c) Exposed > 24 Hr. air @ R.T.

Figure 24. XPS spectra of Fe $2P_{1/2}$ and Fe $2P_{3/2}$ peaks of iron-ruthenium alloy (OXIDE-CHLORIDE) system as a function of treatments.

on the carbon binding energy of 284.6ev as a reference. The ruthenium $3d_{5/2}$ peak is characterized by a full width at half maximum of 2.1ev and a binding energy of 281.1ev which identifies ruthenium in the metallic state. The value of 280.0ev for ruthenium metal has been reported (230). The value of 710.1ev binding energy for iron $2P_{3/2}$ electrons was observed, Fig.21a. This value is consistent with an assignment of iron in the +2 oxidation state (247). The peak at 723.3ev corresponds to the reported binding energy of iron $2P_{1/2}$ electrons. The band at 740.1ev is due to oxygen is the system. This band disappears and two new bands appear at 719.80ev and 706.5ev as the result of subsequent reduction of the sample in flowing hydrogen at 400°C for 4 hours, Fig.24b. These two bands are due to the iron $2P_{1/2}$ and $2P_{3/2}$ electrons in the metallic state, which indicates that the oxygens are titrated by hydrogen and consequently, the iron has been reduced. The value of 707.2ev for iron metal has been previously reported (230). Although the oxidation state of ruthenium was not expected to change since it already existed in the metallic state, a 0.8ev shift for the ruthenium $3d_{3/2}$ and $3d_{5/2}$ peaks was observed. This may be the result of the interaction of ruthenium in the Fe-Ru alloy formation.

The relative concentrations of iron and ruthenium in the few top surface layers of the catalyst are calculated using the spectral area of the most intense lines, $2p_{3/2}$ for iron and $3d_{5/2}$ for ruthenium. The mean free paths of the electrons were correlated as follows. The mean free path in this region of the spectrum varies as the square root of the kinetic energy (248). To account for the fact that the higher energy ruthenium electrons (Kinetic energy 1207ev) can escape from deeper within the sample than the iron electrons (Kinetic energy 780ev),

the intensity of the iron $2p_{3/2}$ line is multiplied by $(1207/780)^{\frac{1}{2}}$. The corrected intensities have then been subjected to equation [10], and the corresponding relative concentrations calculated. Within these normalizations the iron to ruthenium concentration ratio of 2.2 was detected for the reduced sample which indicates a 68% iron enrichment in the surface region, in good agreement with the predictions made previously for the chloride system by interpretations of the Mossbauer results. The value of the concentration ratio was reduced after exposing the sample to air, dropping to 50 atm% Ru ad 50 atm% Fe composition in the surface region which may indicate the reveral of segregation phenomenon under oxidation condition.

The Mossbauer spectral examination of the reduced material, Fig.21b, identified the iron as the metallic state as is evident by the magnetically split six line pattern characteristic of α-Fe. However, there is a The central line near zero velocity in this system. To elucidate the nature of the species leading to the characteristic singlet line, in a separate experiment a sample of bulk α-Fe_2O_3 was reduced under the same conditions as those for the bimetallic catalyst, Fig.22a. The central line was not observed. This is clear evidence that the ruthenium is responsible for the formation of an iron species different from that of the iron only system and which can be attributed to Fe-Ru formation.

Oxidation of the material at room temperature converts some fraction of the α-Fe to superparamagnetic iron oxide as evidenced by the appearance of a doublet in the center of the Mossbauer spectrum, Fig.21c. This conversion was observed for both iron only, and iron-ruthenium catalysts, which indicates that the formation of the super-

paramagentic iron oxide is independent of the presence of ruthenium and primarily involves the species located on the surface of the catalyst. Thermal oxidation of the material at 400°C (Fig.21d and 22b) increased the intensity of the superparamagnetic iron oxide fraction and converted the rest of the iron in the system to α-Fe_2O_3.

The X-ray diffraction pattern of the exposed material identified the ruthenium and iron in the metallic states. The representative peak for hcp ruthenium was detected at a higher diffraction angle, which indicates the existence of a smaller crystal lattice (273). This effect is a consequence of the substitution of iron in the hcp structure of ruthenium. A lattice parameter calculation identified the lattice constants (a = 2.681, c/a = 1.583) which were smaller in both a and c axis than the hcp ruthenium (a = 2.706 A°, c/a = 1.582), indicating Fe-Ru formation.

These results indicate the possible interactions of iron and ruthenium when they are admixed to form bimetallic catalysts. The concepts of surface segregation and the Fe-Ru alloy formation are particularly important as they indicate the possibility of new types of metallic species which may actually be formed on and/or in the catalyst as a function of catalyst preparation and environment.

Table 2. ^{57}Fe Mossbauer parameters of bimetallic iron-ruthenium alloy system

SYSTEM	TREATMENT	# PEAKS		I.S.*	Q.S.*	Hm**	ASSIGNMENT	SPECTRUM
Fe-Ru (Chloride-Chloride)	INIT.	A	2	0.35	0.70	-	Fe^{3+}	17a
		B	2	0.60	1.30	-	Fe^{3+}	
	REDU.	A	6	0.03	-	331	bcc-Fe	17c
		B	1	0.05	-	-	hcp-Fe (Fe-Ru)	
	EXPO.	A	2	0.38	0.77	-	Superparamag. Fe_2O_3	16c
		B	1	0.03	-	-	hcp-Fe (Fe-Ru)	
	CALC.	A	6	0.43	-	523	α-Fe_2O_3	17d
Fe-Ru (Nitrate-Chloride)	INIT.	A	2	0.36	0.71	-	bcc-Fe	(235)
	REDU.	A	6	0.03	-	331	bcc-Fe	(235)
		B	1	0.00	-	-	hcp-Fe (Fe-Ru)	
	EXPO.	A	2	0.41	0.76	-	Superparamag. Fe_2O_3	(235)
		B	1	0.00	-	-	hcp-Fe (Fe-Ru)	
	CALC.	A	6	0.86	-	513	α-Fe_2O_3	(235)

Table 2 (cont't). ^{57}Fe Mossbauer parameters of bimetallic iron-ruthenum alloy systems

SYSTEM	TREATMENT	# PEAKS		I.S.*	Q.S.*	Hm**	ASSIGNMENT	SPECTRUM
Fe-Ru (SULFATE-CHLORIDE)	INIT.	A	2	0.39	.67	-	Fe^{3+}	19a
		B	2	1.32	3.04	-	Fe^{2+}	
	REDU.	A	6	0.36	-	493.3	Fe_3O_4	17b
		B	6	0.76	-	472.2		
		C	6	0.74	-	315.0	FeS	
	EXPO.	A	6	THE SAME AS REDUCED SAMPLE			Fe_3O_4 or γ-Fe_2O_3	19c
		B	6					
		C	6				FeS	
	CALC.	A	2	1.37	2.07		Fe^{2+}	19d
		B	1	0.35	-	-	hcp-Fe (Fe-Ru)	
Fe-Ru (OXIDE-Chloride)	INIT.	A	6	0.61	-	532.6	α-Fe_2O_3	21a
	REDU.	A	6	0.07	-	330.4	bcc-Fe	21b
		B	1	0.00	-	-	hcp-Fe (Fe-Ru)	
	EXPO.	A	6	0.04	337.2	-	bcc-Fe	21c
		B	1	0.00	-	-	hcp-Fe (Fe-Ru)	
	CALC.	A	6	0.31		526-0	Superparamag. Fe_2O_3	21d
		B	2	0.37	0.95	-	α-Fe_2O_3	

Table 3. ^{57}Fe Mossbauer Reference Parameters

MATERIAL	SOURCE	TEMP.	# PEAKS	I.S.*	Q.S.*	Hm**	REFERENCE
bcc-Fe	^{57}Co in Rd	R.T.	6	0.0	0.0	330.0	Standard
α-Fe_2O_3	^{57}Co in Rd	R.T.	6	0.40	0.38 (Δ_{12}-Δ_{56})	517.0	This work
α-Fe_2O_3	^{57}Co in Rd	473°K	6	0.39	0.39 (Δ_{12}-Δ_{56})	508.0	This work, Fig.6
α-Fe_2O_3	^{57}Co in Rd	L-N_2	6	0.39	-0.73 (Δ_{12}-Δ_{56})	536.8	This work, Fig.6
Fe_3O_4	-	R.T.	6(Th.) 6(Oct.)	0.04 0.67	- -	491.8 460.7	(163) (163)
Fe_3O_4	^{57}Co in SS	L-N_2	6	0.65	-	510.0	(184)
γ-Fe_2O_3	^{57}Co in SS	R.T.	6	0.50	-	505.0	(184)
γ-Fe_2O_3	^{57}Co in SS	L-N_2	6	0.40	-	515.0	(184)
FeS	^{57}Co in Cu	R.T.	6	0.73	0.07	312.0	(243)

*Isomer shift (I.S., mm s^{-1}), and Quadrupole splitting (Q.S., mm s^{-1}) valves are reported relative to the center of splitting of lines of an iron foil standard at room temperature.

**Internal magnetic field (Hm, KG) is calculated based on 330KG field of iron standard equivalent to 10.6 mm s^{-1} (184), and 517 KG internal field of α-Fe_2O_3 equivalent to 16.7mm s^{1}.

CHAPTER VI

IRON AND RUTHENIUM CYANIDE COMPLEXES IN ZEOLITES

INTRODUCTION

The chemistry of transition metal complexes in zeolites has important implications both in fundamental and applied catalysis (119). The synthesis of well defined, active complexes within the large cavities of zeolites can provide systems which will allow more meaningful catalytic mechanisms to be deduced from reaction parameters. Possible correlations between activity and well defined structure may lead to a better understanding of the nature of active sites in catalytic reactions.

Recently, a new class of materials has been designed by utilizing a zeolite to trap soluble transition metal complexes. It has been shown that the chemistry of the transition metal ions or complexes in zeolites are generally similar to the analogous materials in solution (118). The close similarity between exchanged zeolities and homogeneous catalysts has been illustrated by many studies. Dimerization of ethylene is known to be catalyzed by rhodium complexes in solution. Later it was found that ethylene is selectively dimerized over rhodium exchanged Y-zeolite (249-250). It has also been shown that the activity of the soluble catalyst was retained in many cases when bonded to the solid carrier. The observed activation energy of methanol carbonylation on Rh-X zeolite was identical to that previously measured in the homogeneous analog. A high conversion of 1-hexene to aldehydes was observed when it was reacted with CO + H_2 over rhodium exchanged Y-zeolite, similar to the

reaction observed in homogeneous catalysis. Similarly, an iridium based homogeneous catalyst and an iridium exchanged zeolite showed identical catalytic properties for methanol carbonylation (251). In these systems similar kinetic properties were observed for both the liquid phase using iridium complexes and for the vapor phase reaction on Ir-Y zeolite. There is sufficient data available to demonstrate that, for many systems, a large number of reactions catalyzed by a metal complex in solution can be carried out in the gas phase by analogous zeolite exchanged metal ions or complexes. The exploitation of such behavior is of obvious importance in the attempts to heterogenize homogeneous catalytic systems.

The solid solvent effect of the zeolite matrix for synthesizing and/or immobilizing transition metal complexes within the framework offers may opportunities. Immobilization of the complexes in the cavities is expected since they are held strongly by ionic forces within the zeolite. The strong electrostatic interaction between the active entity and the support minimizes activity loss via leaching processes. The immobilization of the clusters on a carrier increases their stability toward aggregation (118). For example, the restricted motion of $Ru(bpy)^{2+}$ on Y-zeolite is expected to exclude collisional deactivation of the complex during the solar conversion of water (194).

The traditional and popular approach to the introduction of transition metal complexes into zeolites utilizes an ion exchange process. This method is generally limited to cationic complexes since the zeolite structure is anionic. In some cases the transition metal complexes are two large to enter the zeolite cavities through the small cage openings,

but small enough to fit the dimension of the cavity. In some of these cases attempts have been made to synthesize the metal complex directly within the zeolite cavity. There is evidence, that some fully coordinated complexes can be syntheszed from ligands which are introduced via the gas or liquid phase. For example, divalent Co^{2+} cations were dispersed by ion exchange into a Y-type zeolite followed by dehydration. In the presence of an excess amount of methylisocyanide, EPR signals indicated the formation of the hexacoordinated complex. Partial desorption of methylisocyanide at 100°C gave a complex which had magnetic parameters very close to the pentacyano complex in water. It is assumed that the unoccupied sixth coordination site is the interactive metal-zeolite site and is unaccesible for other ligands (119, 253). When Y-zeolite was exchanged with cobalt(II) ammine and contacted with molecular oxygen, the oxygen bridge was formed, similar to analogous adducts formed in solution. Ligand exchange reactions can also take place within the zeolite cavities, i.e. $Ru(bpy)_3^{+2}$ complexes have been synthesized within Y-zeolite by allowing bipyridine to react with the $Ru(NH_3)_6$-Y form of the zeolite (194). The formation of polynuclear transition element complexes within the large cavity of certain zeolites has also been observed. For example, a rhodium exchanged zeolite was reacted with CO + H_2 under a pressure of 80 atmosphere and it was suggested that $Rh_6(CO)_{16}$ clusters were formed and entrapped within the zeolite cavity (251). The same reaction at atmospheric pressure led almost exclusively to the formation of the $Rh(CO)_2$ complex (254).

A new preparative method has been developed based on the reaction of a metal exchanged cation with a metal-containing coordination complex anion (255). Ferric exchanged zeolite was found to react with the

$[Fe(CN)_6]^{4-}$ anion to subsequently form the $Fe_4[Fe(CN)_6]_3$ complex. The same method can be used for the preparation of bimetallic or polymetallic catalysts. Ferric exchanged zeolites can react with the $[Ru(CN_6]^{4-}$ anion which leads to the formation of the $Fe_4[Ru(CN)_6]_3$ complex in the zeolite.

Several mixed iron cyanide polynuclear complexes can easily be prepared by the interaction between the high spin iron cations (Fe^{3+} or Fe^{2+}) and the low spin cyanide anions $[(Fe(CN)_6]^{4-}$ or $[Fe(CN)_6]^{3-}$). The lack of consistancy between experimental conditions during the preparation of these compounds may cause different products to be formed. Some irrelevant data has been introduced into the literature since the discovery of these materials. The source of difficulty is that most of these compounds are easily interconvertible and all have closely related structures. The starting materials are also easily convertible to each other, i.e. the potential energy for Fe^{2+}/Fe^{3+} is -0.71 V and for $[Fe(CN)_6^{4-}/[Fe(CN)_6]^{3-}$ is -0.36 V. The exchange of electrons between ferricyanide and ferrocyanide anions has been observed in neutral, acidic and alkaline solutions (256). Using Mossbauer spectroscopy, it has been demonstrated that Prussian Blue, prepared by mixing the solutions containing ferric and ferrocyanide ions, and Turnbull's Blue, prepared by mixing solutions containing ferrous and ferricyanide ions, give similar compounds (257). The internal redox phenomenon involves the transfer of one electron from the ferrous ion to ferricyanide (258). The nature of the anion associated with the high spin iron and also the nature of the cation in association with the low spin iron cyanide in the starting material may influence the resulting product. The sequence

of the addition of the two components to each other can lead to different product formation. For example, "soluble" Prussian Blue, $KFe[Fe(CN)_6]$, is prepared by the addition of aqueous $FeCl_3$ to aqueous $K_4Fe(CN)_6$. "Insoluble" Prussian Blue, $Fe_4[Fe(CN)_6]_3$, can be made by the drop wise addition of aqueous $K_4Fe(CN)_6$ to $FeCl_3$ solution (259). To avoid complications, all preparative procedures should be described properly and great caution should be taken in the formulation of these materials.

Mixed valence compounds of iron are common and a variety of species have been prepared and characterized. The first known coordination complex was Prussian Blue, $Fe_4[Fe(CN)_6]_3 \cdot 14\ H_2O$. It was prepared in 1704 by the German artist Diesbach and is considered one of the most classical inorganic compounds (252). This compound crystallizes as a microcrystalline powder which may be readily peptized to form a colloidal dispersion (263). The structure is face centered cubic with high spin Fe^{3+} and low spin Fe(II) ions at the corners of the lattice and cyanide ions bridging the irons along the cube. Prussian Blue crystals are not a definite hydrate (264) and are zeolitic with channel diameters of 3.2 A° (265). The cages normally contain water, 30-40% by weight (266) and the centers of the cubes are filled with charge - compensating potassium cations where necessary (260). The formulation $KFe^{3+}FeII(CN)_6$ has been proposed for the "soluble" form of Prussian Blue where potassium cations in the structure surround the iron tetrahedrally (263). The crystal structure of "soluble" and "insoluble" forms of Prussian Blue are closely related to one another (267), the differentiation between the two forms stems from the ease which each can be peptized to form a colloidal dispersion (260).

For many years, workers have attempted to determine which iron ion valence resides where in Prussian Blue material. At the present time, Prussian Blue is considered as the ferric salt of ferrocyanic acid, where the high spin Fe^{3+} ions are coordinated to the nitrogen by ionic force, and the low spin Fe(II) species are coordinated by covalent linkages to the carbon end of the cyanide bridge. This formulation is supported by the results of Mossbauer studies which demonstrate the existence of high spin Fe^{3+} ion in octahedral coordination, and low spin Fe(II) in the form of $[Fe(CN)_6]^{4-}$ (261). The H.S. Fe^{3+} - L.S. Fe(II) distance is 5.1°A as deduced from X-ray diffraction patterns (267). A single crystal of Prussian Blue has been grown by the diffusion of aerial oxygen and water vapor into a solution of $FeCl_2$ and $K_4Fe(CN)_6$ in 10 M HCl (262). The H.S.Fe^{3+}-H.S.Fe^{3+} distance in the face cubic structure was measured to be 10.18°A.

The molecular orbital representation of the low spin iron(II) cyanide anion, in the absence of π bonding, is constructed from the metal 3d electrons including a t_{2g}^6 configuration and a cyanide ligand electron donation from σ orbitals (a_{1g}, e_g, t_{1u}). The overlap of iron $3d_z2$, $3d_{x^2-y^2}$, 4s and 4p with appropriate σ orbitals of the cyanide ligands populate the molecular orbitals. In hybridized terms, the σ bonds are formed by overlaps between d^2sp^3 hybrids of iron atoms with the σ orbitals of the cyanide ligands. The π character of the bond is constructed by the overlap of t_{2g}^6 electrons of the metal and empty antibonding π^* of ligands. The bonding is charge transfer in nature and results in the donation of charge from the metal to the ligand. The cyanide ligand is a good σ donor but a poor acceptor. The isomer shift in this compound is very close to that of iron metal, which indicates

that the 3d electrons are delocalized. The donation of electrons from the metal to the ligand stabilizes the t_{2g}^6 level and reduces the shielding of 3s electrons which results in a small isomer shift value. Since the t_{2g}^6 shell has cubic symmetry and is diamagnetic, any variation in the isomer shift and quadrupole splitting for low spin octahedral complexes must be related to the variation in the nature of the ligand and the metal-ligand interaction. In contrast, in the case of low spin iron III cyanide complexes, the isomer shift is remarkably insensitive to variations in ligand properties. In these compounds, the isomer shift and quadrupole splitting are not readily rationalized because of the difficulty in estimating the relative magnitude of the contribution from covalency and t_{2g}^5 shell symmetry (63. 268-269).

Prussian Blue and many of its analogs are characterized by strong absorption bonds in the visible region of spectrum. In these compounds the presence of two ions of the same or similar metal atoms in the crystal, in different oxidation states leads to a deep color which is unrelated to the color of the ions taken separately (263). The intensity of the blue dye, Prussian Blue, for a long time was explained by the popular concept of the resonance between H.S. Fe^{2+}, L.S. Fe(III)$\leftrightarrow$ H.S. Fe^{3+}, L.S. Fe(II). This concept however is not consistant with recent Mossbauer data. The absorption bands are charge transfer in nature. A strong band occurs at 14,100 cm^{-1}, assigned to a L.S. Fe(II)$\rightarrow$ H.S. Fe^{3+} charge transfer from t_{2g}^6 configuration of L.S. Fe(II) to t_{2g}^3 of H.S. Fe^{3+}. A second weaker transition occurs at 25,000 cm^{-1}, assigned to the transition from t_{2g}^6 of Fe(II) to e_g^2 of Fe^{3+}. The same interpretation also accounts for the charge transfer band in ferric ruthenocyanide (Ruthenium Purple) at 17,400 cm^{-1} (263).

This portion of the present study was conducted to confirm the formation of the mixed spin iron cyanide complexes in zeolites by means of Mossbauer spectroscopy and to extend the investigation to synthesizing polynuclear mixed iron and ruthenium cyanide complexes in zeolites. An attempt was made to synthesize these complexes in single crystals of X type zeolites.

Since the formation of mixed iron cyanide complexes in zeolites involves the iron cations ionically bonded to the zeolite framework, the dissociation of iron from the framework is expected. This provides potentially attractive opportunities to achieve the full reduction of iron and the formation of dispersed Fe-Ru clusters in a zeolite. The model catalysts prepared here were characterized during dehydration-hydration and oxidation-reduction treatments.

EXPERIMENTAL

The sample of ferric exchanged Na-Y zeolite was prepared by a ion exchange technique using iron nitrate solution. The concentration of the exchange solution was adjusted so that 30% of the Na^+ cations would be exchanged by iron. The exchange was carried out under N_2 atmosphere at ambient temperature for 24 hours. The exchanged sample was thoroughly washed with distilled water and dried under vacuum at room temperature. The exchange level was determined by counting the Na^+ ions in the solution after the ion exchange, by chemical uranyl acetate methods (206). The resulting weight percent of metal in the zeolite was approximately 2.5% iron. Mossbauer spectral examination confirmed the existence of iron in the ferric state. The Fe^{3+}-Y zeolite was reacted by the addition of 1 weight % $K_4[Fe(CN)_6]$ solution for 3 hours under nitrogen atmosphere. The volume of solution was adjusted based on the

amount of iron in the system according to the following stoichometric reaction:

$$4\ Fe^{3+}\ (\text{on Y-zeolite}) + 3K_4[Fe(CN)_6] \rightarrow \quad [11]$$
$$(\text{Dark Blue})\ Fe_4[Fe(CN)_6]_3 + 12\ K^+\ (\text{on Y-zeolite})$$

The resulting sample was filtered and washed with distilled water. The dark blue power was designated as $Fe_4[Fe(CN)_6]_3$ - Y zeolite.

The $Fe_4[Ru(CN)_6]_3$ - Y zeolite was prepared by the same method using 1 weight % $K_4[Ru(CN)_6]$ solution according to the following steiochometric reaction:

$$4\ Fe^{3+}\ (\text{on Y-zeolite}) + 3K_4[Ru(CN)_6] \rightarrow \quad [12]$$
$$(\text{Purple})\ Fe_4[Ru(CN)_6]_3 + 12\ K^+(\text{on Y-zeolite})$$

To make the results comparable, the treatment conditions for the dehydration-hydration, oxidation-reduction of the material were constant employing apparatus and techniques described previously. All velocities are reported relative to the center of splitting of lines of an iron foil standard at room temperature.

RESULTS AND DISCUSSION

$Fe_4[Fe(CN)_6]_3$ ON Y-ZEOLITE

The crystal structures of both Prussian Blue and aluminosilicate Y-zeolite are preserved during the preparation of the catalyst, as revealed by X-ray powder diffraction as shown in Fig.25. The Mossbauer spectra of the sample identifies two distinct kinds of iron ions in the catalyst Fig. 26a. The right side peaks are halves of two doublets associated with two different high spin ferric ions, and the single peak in the central region is due to low spin ferrous species. The Mössbauer

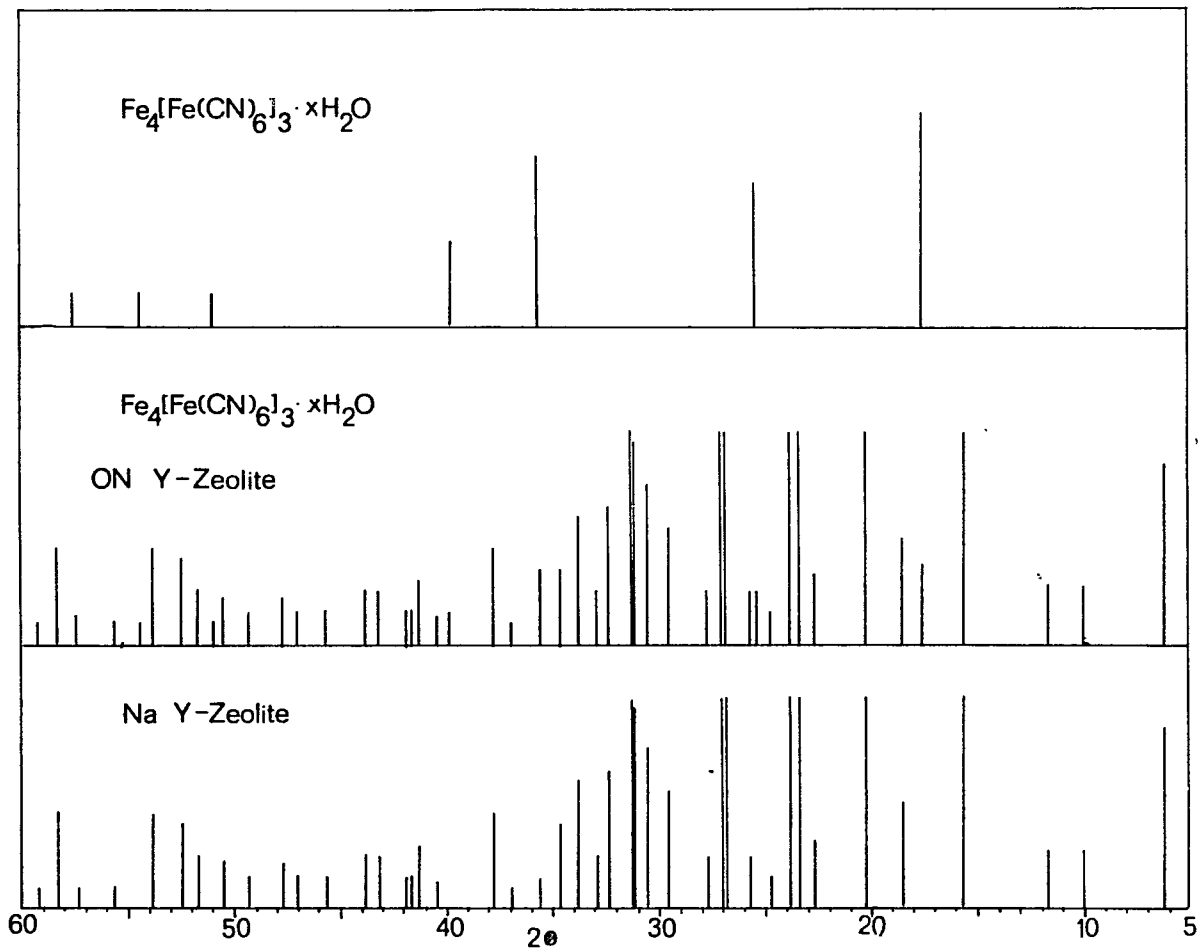

Figure 25. X-ray powder diffraction pattern for Na-Y zeolite, Prussian Blue, and Prussian Blue on Y-zeolite.

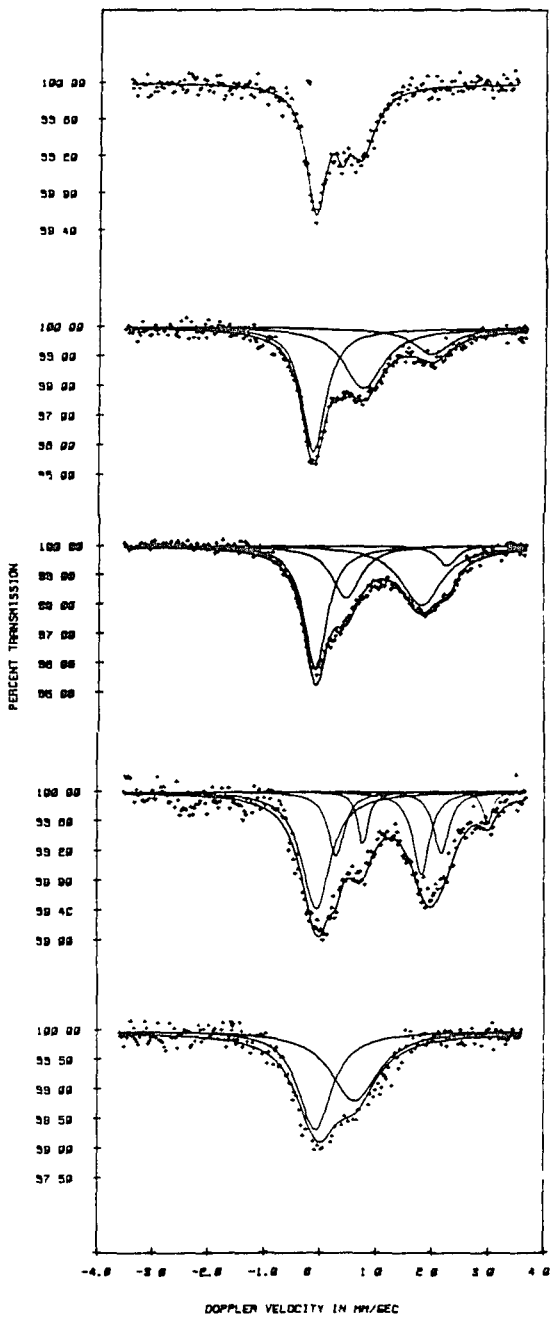

(a) Catalyst as initially prepared, Prussian Blue on Y-zeolite

(b) Dehydrated 1 Hr. 10^{-5}torr @ 473°K.

(c) Dehydrated 1 Hr. 10^{-5}torr @ 573°K.

(d) Dehydrated 4 Hr. 10^{-5}torr @ 727°K.

(e) Exposed > 24 Hr. air @ R.T.

Figure 26. ^{57}Fe Mossbauer spectra of Prussian Blue on Y-zeolite at room temperature as a function of dehydration-hydration treatments.

parameters for the outer doublet (I.S. = 0.30 mm s^{-1} and Q.S. = 0.83 mm s^{-1}) are very close to values found for ferric ion originally exchanged in the zeolite, which clearly indicates that some of the ferric ions do not react with the ferrocyanide anion during the preparation. This is not unexpected since the diffusion of complex anions to the cavities will be slow due to the repulsion of the negatively charged oxygens of the zeolite. The K^+ cations however are expected to penetrate rapidly. The mechanism for the formation of Prussian Blue on Y zeolite therefore may first involve the back ion exchange of ferric cations from the framework by potassium cations, and then the mobilization of ferric cations towards the reactive ferrocyanide anion with the subsequent formation of the complex outside the cavity. To explore this possibility, in a separate experiment a sample containing Prussian Blue was prepared using single crystals of X-type zeolite (single crystal growth description and transmission electron microscopy projection of X type zeolite are given in P. 38 of chapter I and shown in Fig.9). The transmission electron microscopy clearly showed the existance of Prussian Blue deposits on the surface of the crystal. Also some cracks in the zeolite crystals were evident. The latter effect could have been due to the fragile nature of the single crystals grown in our laboratory and may not be representative of commercially made polycrystalline Y-zeolite.

The Mossbauer parameters for the inner ferric doublet in Fig.26a, (I.S. = 0.11 mm s^{-1} and Q.S. = 0.46 mm s^{-1}) are close to those observed for ferric ions in Prussian Blue. The singlet peak is assigned to low spin ferrous, (I.S. = -0.20 mm s^{-1}), from the ferrocyanide entities in the Prussian blue crystals. The sample was arbitrarily designated as

$Fe_3[Fe(CN)_6]_4$ on Y zeolite although the possibility of $KFe^{3+}FeII(CN)_6$ on Y zeolite can not be excluded.

While performing this experiment, it was not known that the Prussian Blue material was located mainly outside the zeolite cavities. An extensive investigation of this material was performed under dehydration-hydration and oxidation-reduction conditions in the hope of establishing a well dispersed metallic system throughout the zeolite. Some highlights of the results are given in the following sections.

In the process of the thermal vacuum dehydration treatments of ferric ferrocyanide material on Y-zeolite, Mossbauer spectra representations indicate significant changes in the oxidation states of iron, Fig.26b-d. The conversion of H.S. Fe^{3+} to H.S. Fe^{2+} is apparent. There are at least three H.S. Fe^{2+} sites in the sample dehydrated at 450°C, Fig.26d. The L.S. Fe(II) to L.S. Fe(III) conversion is also evidenced by a doublet in the middle of the spectrum. The valency reversal mechanism of the type H.S. Fe^{3+}, L.S. Fe(II) H.S. Fe^{2+}, L.S. Fe(III) appears as previously observed by Collins and co-workers who studied Prussian Blue during pyrolysis at 570°C (258). The proposed mechanism is supported by studies dealing with the effect of external pressure on the high spin and low spin ferric ions. It has been shown that at an external pressure of 145 Kbar, much of the H.S. Fe^{3+} is reduced to H.S. Fe^{2+}. At an external pressure of 4 Kbar, the L.S. Fe(II) showed partial conversion to L.S. Fe(II) (271). The effect of dehydration is to remove the entrapped water molecules from the Prussian Blue, consequently, the internal pressure of the crystal is reduced. It has also been postulated that the dominant mode of valency reversal on pyrolysis can be due to cyanide rotation (266). The possible mechanism for a CN^- flip can be

the formation of CN bridged intermediates which involve the bimolecular formation of a cyanide bridged activated complex, following by generation of an isocyanide species which undergoes a unimolecular rearrangement. Such a mechanism, or even a simple terminal cyanide linkage isomerization, in polynuclear crystals of Prussian Blue should be considered less likely. It seems reasonable to assume that the cyanide ligands remain firmly attached to the iron ion with which they are associated in Prussian Blue and do not flip within the crystal upon dehydration treatment. There are at least three H.S. Fe^{2+} sites in the samples dehydrated at 450°C, Fig.26d. At first it appeared that dissimilar Fe^{2+} sites may be due to the influence of the zeolite lattice. The fact that Prussian Blue in the absence of support has been shown to exhibit a similar behavior during pyrolysis (258, 266), argues against the zeolite influence and suggests that a major structural change takes place. The dissimilar Fe^{2+} sites have been designated as α, β and γ (266) and no explanation for their nature has been provided.

It is tempting to propose that upon dehydration, as the water molecules are removed from the Prussian Blue crystal cages, that shrinkage in the lattice takes place and the potassium ions become closely associated with the negatively charged ferrocyanide anions. It has been stated (271), that iron has an increased affinity for electrons with increasing compression. Considering these factors, the internal redox may involve the transfer of one electron from L.S. $Fe(CN)_4^{4-}$ to H.S. Fe^{3+}. The CN^- could serve as an electron transport. Under these circumstances the lattice may aquire K^+ ions from the solution to maintain electrical neutrality resulting in the formation of

$(K\ Fe^{2+}FeIII(CN)_6)_x$. Many of the cubic cyanide polymers contain additional cations, e.g. potassium, which occupy positions in the octant (269). Such a formulation requires a close association of potassium with the lattice. This effect is probably accomplished during dehydration treatment. It is known that the free cation does have little effect on the Mossbauer spectrum of low spin complexes, but such an arrangement would undoubtedly cause some electron anisotropy in the region of the spin free iron cation, especially when the octants are occupied in random fashion. This mechanism may very well explain the apparent dissimilar Fe^{2+} sites in the Mossbauer spectrum.

Prussian Blue can be reconstituted during the exposure of the dehydrated material to air, Fig.26e. The oxidation of H.S. Fe^{2+} to H.S. Fe^{3+} is evident. The conversions of L.S. Fe(II) to L.S. Fe(II) is not apparent because of the overlap of the Mossbauer lines. The color of an exposed sample was blue with shades of green, which revealed the existence of proportions of hexacyanoferrate in the II and III states. Prussian green, formulated as $Fe^{3+}FeIII(CN)_6$, is the most oxidized member of the series of mixed spin iron cyanides (272). The reluctance of CN^- to form strong π-bonds is reflected in the comparative instability of its complexes with metals in low oxidation states. The C-N stretching frequencies of various ferricyanides fall at 2150 cm^{-1} (260). Prussian blue was essentially reconstituted as was evident by the intense blue color and the I.R. examination which showed the C-N stretch in the region of 2080cm^{-1}, characteristic of the Prussian Blue compound.

The stepwise reduction-oxidation treatment of the dehydrated material is represented in Fig.27. The six line Mossbauer spectrum (Fig.27a) revealed the presence of particles of α-Fe on the zeolite

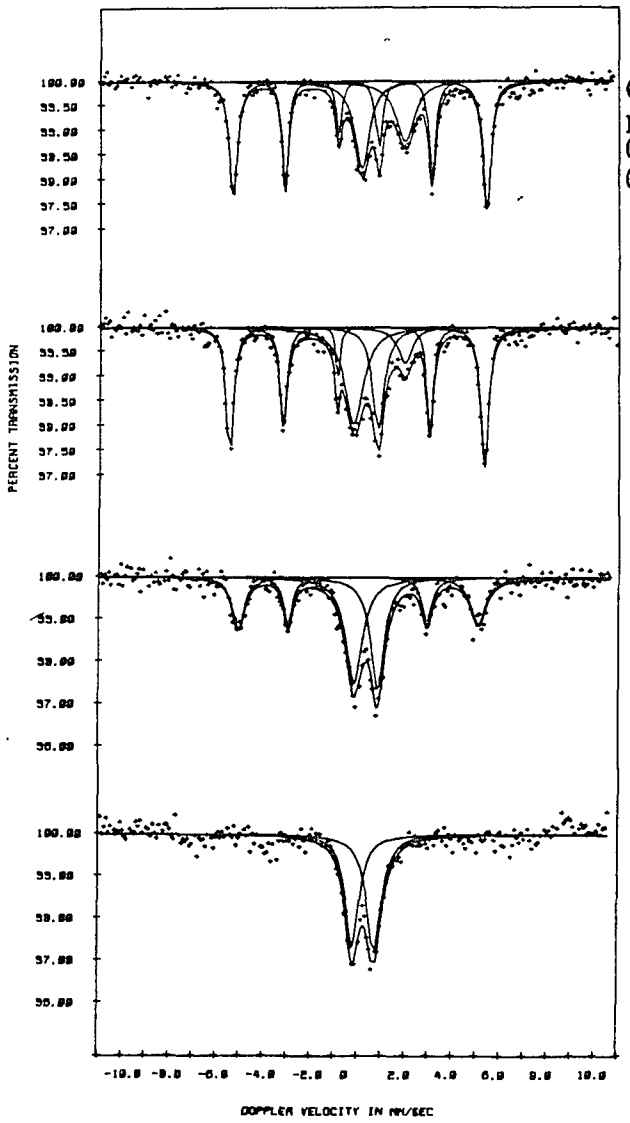

Figure 27. ^{57}Fe Mossbauer spectra of Prussian Blue on Y-zeolite at room temperature as a function of reduction-oxidation treatments.

crystals. The metallic particles must be 15A° to exhibit a magnetically split behavior, (139) thus, they must exist outside of the zeolite cavities. The oxidation of the material in air converts the metallic particles to superparamagnetic iron oxide, Fig.27g. The critical diameters for oxides in superparamagnetic state is < 135A° (79).

We propose a modified preparation procedure as follows. First, to synthesize the complex inside the cages, the anion solution should be introduced to throughly dried Fe^{3+}-Y zeolite by incipient wetness impregnation techniques. The catalyst material should then be thermally activated to achieve the transfer of the reactive anion through the zeolite windows. The amount of anion added should be minimized to promote the formation of "soluble" Prussian Blue, which is a microcrystalline entity, and to avoid the peptization to "insoluble" colloidal dispersion.

$Fe_4[Ru(CN)_6]_3$ ON Y-ZEOLITE

Ferric ruthenocyanide has the same basic structure as Prussian Blue, Fig.35. The ruthenium analog is known to be isomorphous with Prussian Blue. The I.R. transmission properties of this material are shown in Fig.28. In the spectrum the band in the region of 2080cm^{-1} is the C-N stretching frequency characteristic of $Fe(CN)_6^{4-}$ and $Ru(CN)_6^{4-}$ (263, 268). The band at 1630 cm^{-1} is due to physically retained water (255). The metal-carbon vibration frequency at 585cm^{-1} for $K_4Fe(CN)_6$ and at 546cm^{-1} for $K_4Ru(CN)_6$ is reported (272). These bands are shifted to higher frequencies for Prussian Blue and Ruthenium Purple material.

The ^{57}Fe Mossbauer representation of the ferric ruthenocyanide polymer complex reveals the presence of high spin Fe^{3+} cations, Fig.29a. A larger quadrupole splitting value for the ferric doublet was detected

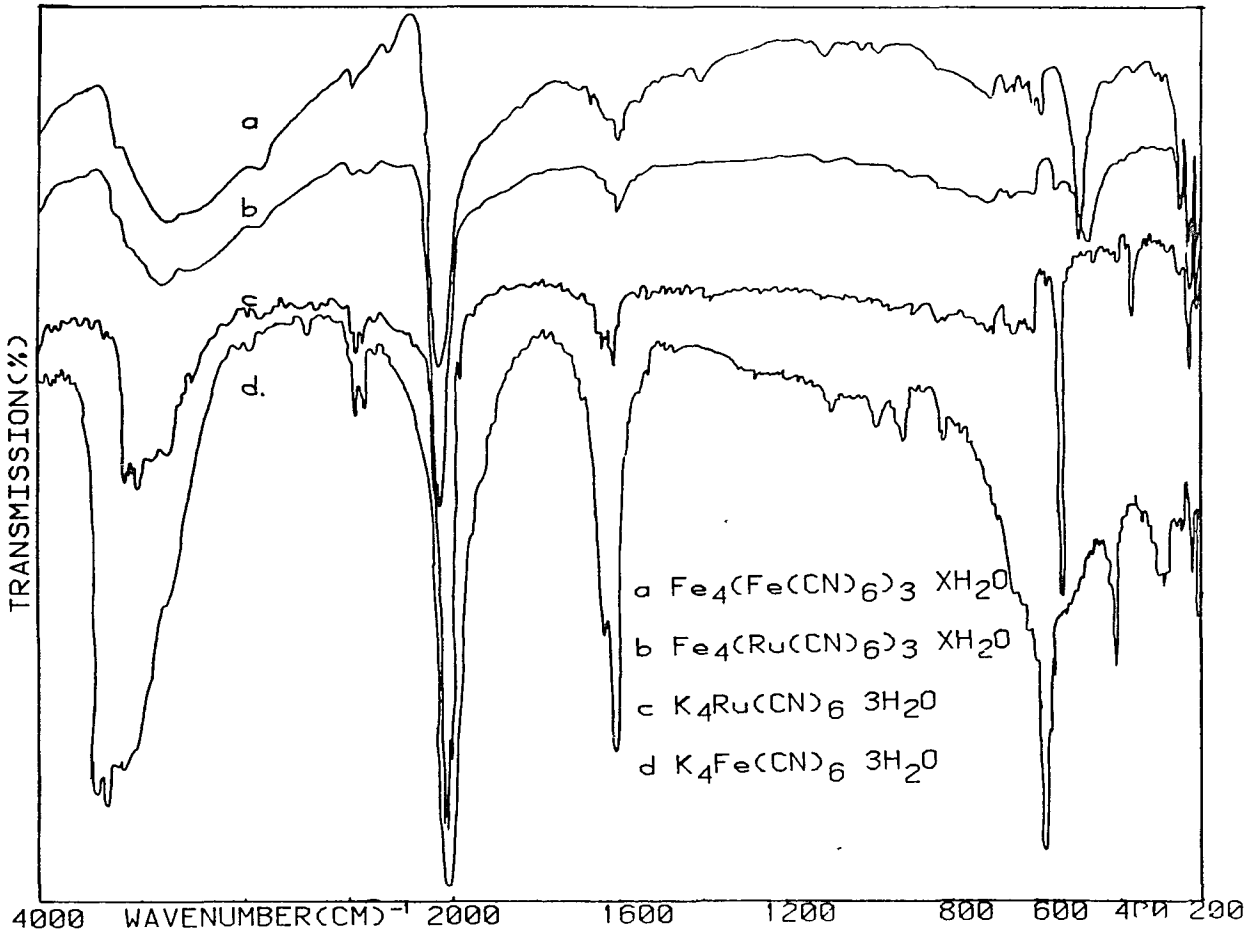

Figure 28. Infrared spectra of iron and ruthenium cyanide complexes.

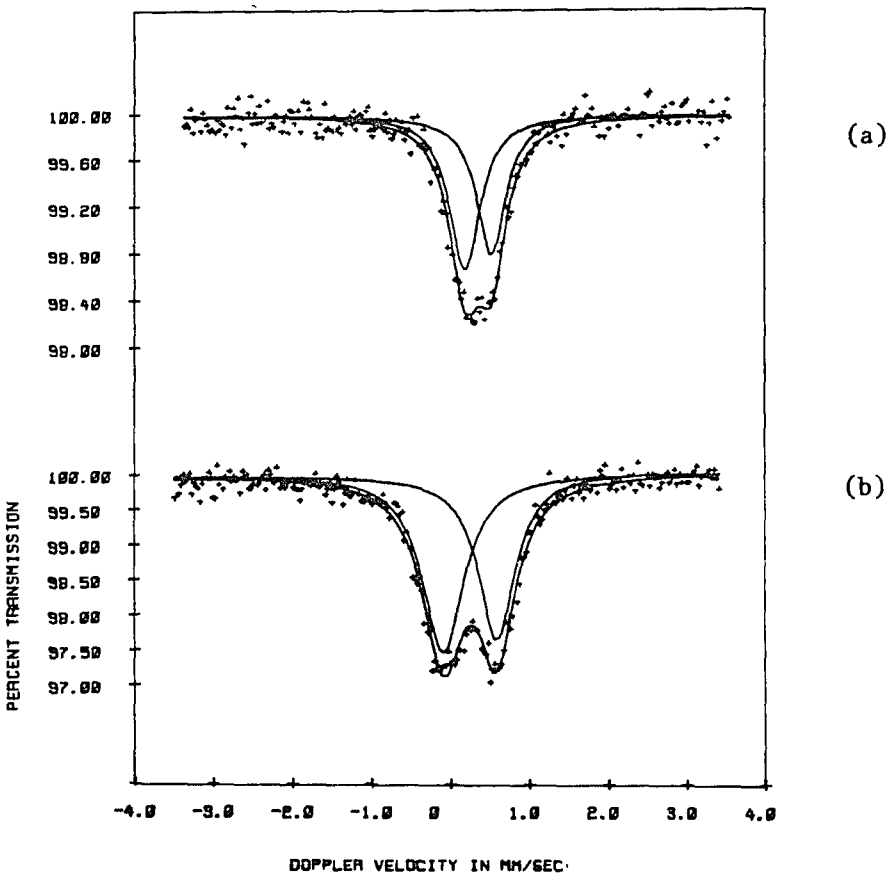

Figure 29. ^{57}Fe Mossbauer spectra: (a) ferric ruthenocyanide, and (b) ferric ruthenocyanide complex on Na-Y zeolite.

when the material was synthesized in Y-zeolite, which may be an indication of entrapment of the particles in the cavities, Fig.29b.

The dehydration product gave completely different spectra as compared with the corresponding dehydrated Prussian Blue specimen, Fig.30b. Ruthenium is expected to be reduced to the metallic state during this treatment, while the iron is reduced to high spin Fe^{2+}. Asymmetric doublets were detected for reduced and air exposed samples as shown in Fig.30c and 30d. To elucidate the nature of the species responsible for the asymmetric doublet spectra, a series of experiments were performed. A specimen was reduced in flowing hydrogen at 450°C for 4 hours without dehydration pretreatment, Fig.31a. This spectrum is analyzed in terms of two doublets due to the presence of Fe^{2+} and Fe^{3+}, and one singlet in the region of zero relative velocity. Reduction of this sample for a longer period increased the Fe^{2+}/Fe^{3+} ratio, while the nature of the singlet was not affected. In addition to the species responsible for the central singlet, only Fe^{2+} was detected, when the sample was dehydrated prior to the reduction treatment, Fig.31d. Asymmetric doublets were observed when the samples were exposed to air at room temperature, Fig.31c and 31e. The nature of the asymmetric doublet was not affected when sample 31e was examined at liquid nitrogen temperatures. Thus the most reasonable assignment is a symmetric doublet, characteristic of high spin ferric species, plus a singlet in the central region of the spectrum. As has been discussed in chapter III and V, the characteristic singlet represents the substitution of iron in the ruthenium lattice and the formation of the bimetallic hcp alloy. The formation of the Fe-Ru bimetallic is potentially attractive in view of a recent report which suggests that the surface structure of this alloy plays a

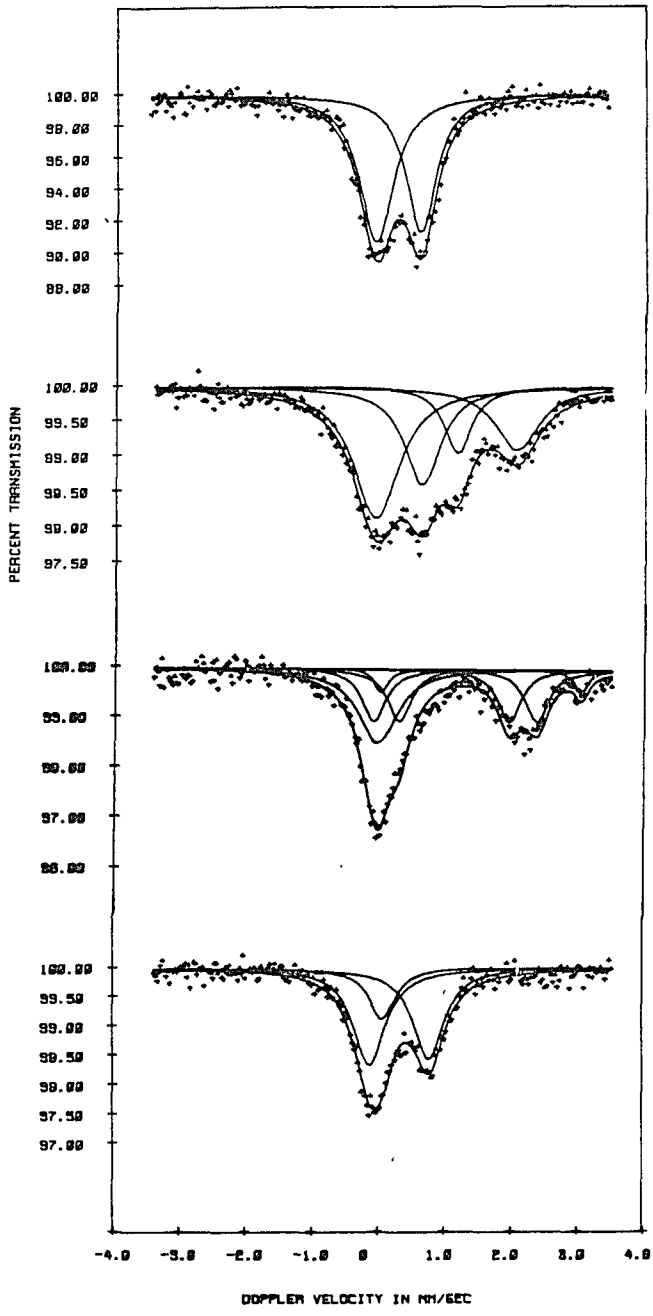

Figure 30. ^{57}Fe Mossbauer spectra of ferric ruthenocyanide complex on Na-Y zeolite as a function of dehydration and reduction-oxidation treatments.

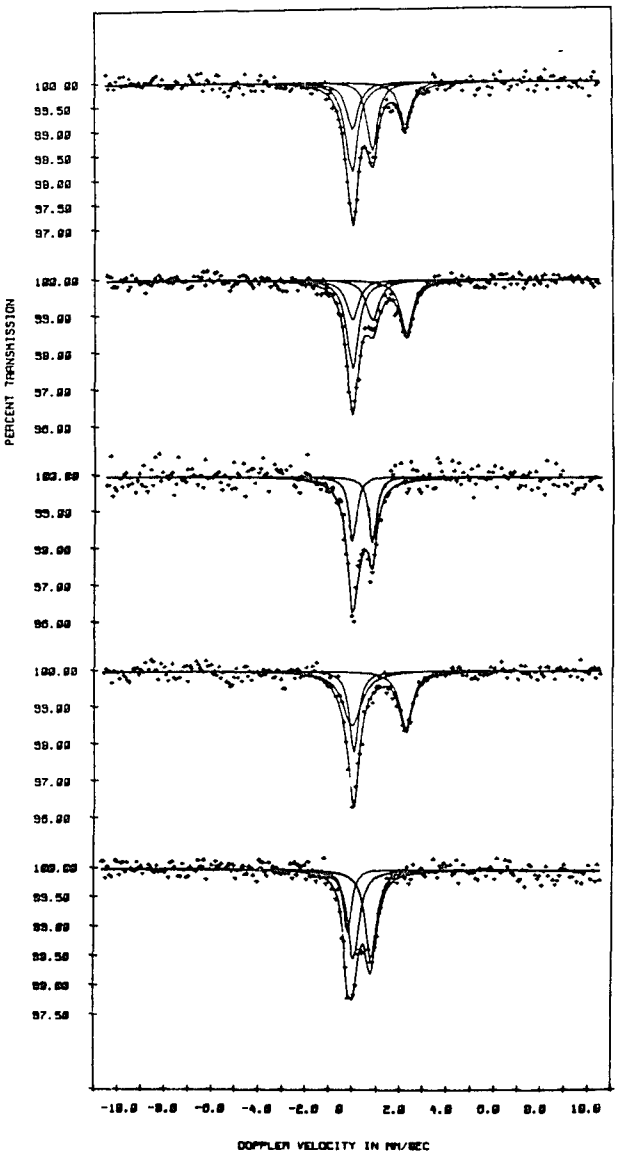

(a)

Catalyst as initially prepared, Reduced 4 Hr. H_2 @ 723°K.

(b) Reduced 9 Hr. H_2 @ 723°K.

(c) Exposed > 24 Hr. air @ R.T..

(d)

Catalyst as initially prepared, dehydrated 3 Hr. @ 723°K and, Reduced 9 Hr. @ 723°K.

(e) Exposed > 24 Hr. air @ R.T.

Figure 31. ^{57}Fe Mossbauer spectra of ferric ruthenocyanide complex on Na-Y zeolite as a function of reduction-oxidation treatments.

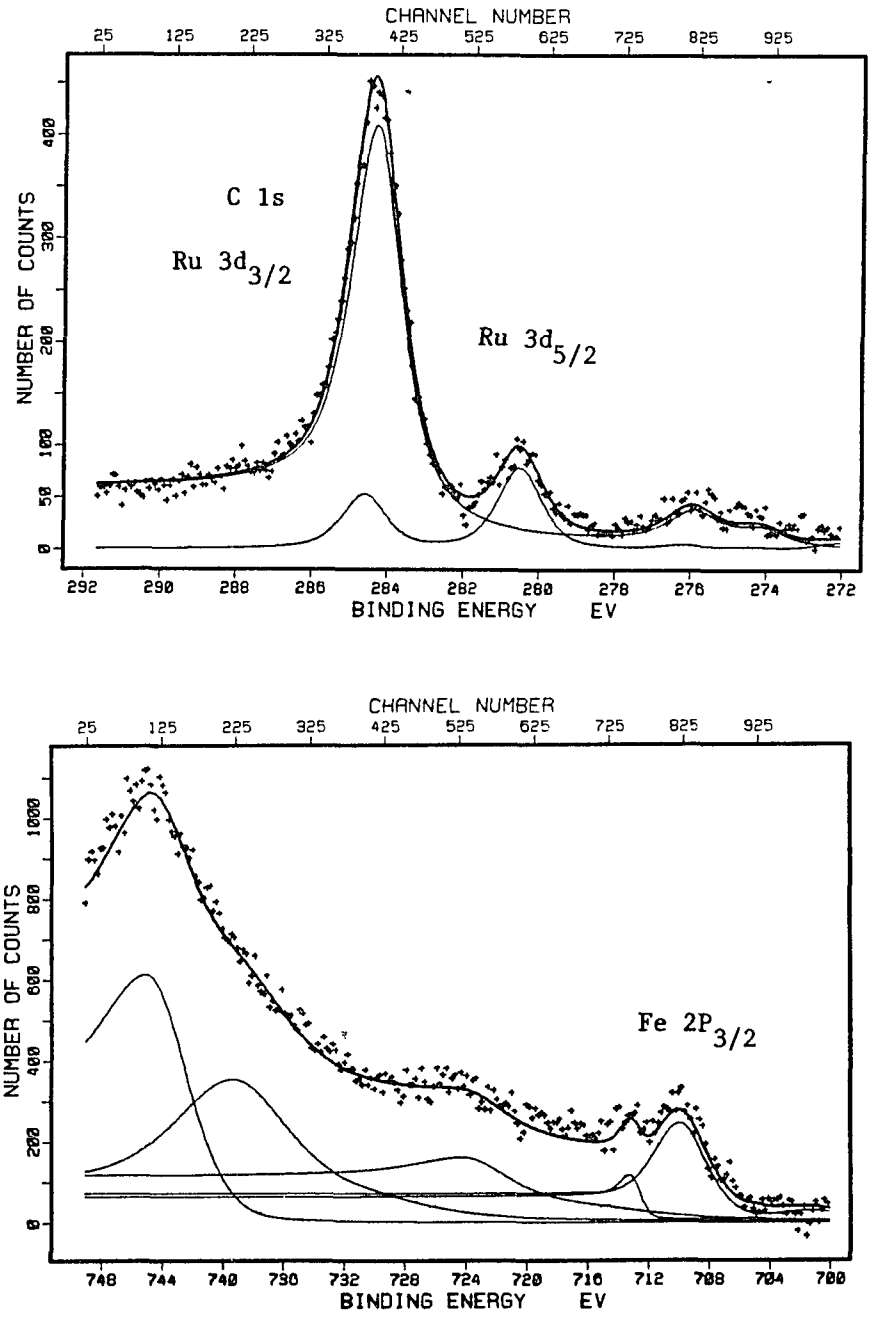

Figure 32. XPS spectra of Ru $3d_{3/2}$, Ru $3d_{5/2}$, Fe $2P_{1/2}$ and Fe $2P_{3/2}$ peak (sample 31e).

catalytic role in the high olefin selectivity during Fischer-Tropsch synthesis (230).

Evidently, several iron-ruthenium polynuclear complexes can be synthesized. Another one was prepared by the addition of 1% solution of $Ru(NH_3)_6Cl_3$ to a 1 weight % solution of $K_4Fe(CN)_6$ according to the following stoichiometric reation:

$$xRu(NH_3)_6Cl_3 + yK_4Fe(CN)_6 \rightarrow [Ru(NH_3)_6]_x[Fe(CN)_6]_y + KCl \qquad [13]$$

Highly dispersed, light blue crystals were formed when the addition of $Ru(NH_3)Cl_3$ solution exceeded the x=4/y=3 stoichiometric ratio. The crystals were not perfect and were very small (5.8 micron). Many attempts were made to grow larger crystals suitable for single crystal X-ray diffraction. The crystals were found to be slightly soluble in oxalic acid and hot hydrochloric acid. Judging from the change of color of the crystals when contacted with hot hydrochloric acid, some chemical interaction was apparent. The I.R. spectrum of the material is represented in Fig.34. In the spectrum the band at 2000.0cm^{-1} is the stretching frequency of the cyanide group. This band is shifted 80 cm^{-1} to lower energy as compared to the characteristic $Fe(CN)_6^{4-}$ band. The band at 1322.0cm^{-1} is attributed to the symmetric deformation of ammonia ligands, identical to that in the $Ru(NH_3)_6Cl_3$ compound. The band at 1600 cm^{-1} is due to retained water. The iron-carbon stretching band at 576.0cm^{-1} is also apparent. The ruthenium-nitrogen stretch is lower in energy and is seen at 410cm^{-1}. The ^{57}Fe Mossbauer spectrum identifies the iron as the low spin ferrous state, Fig.33. X-ray powder diffraction (Fig. 35) revealed that the light blue crystals have a different structure from that these of Prussian Blue and Ruthenium Purple. Final

formulation of this compound would require a nitrogen and carbon analysis and an X-ray single crystal structural determination. Transmission electron microscopy indicated the presence of the hexagonal crystal structure.

These studies have indicated the diverse and rich chemistry which can be expected from the utilization of iron and ruthenium cyanide complexes as catalyst precursors. Specific final catalyst formulations could be designed by proper manipulation of the starting materials and the treatment conditions. The studies also indicate the utility of iron Mossbauer studies in the definition speciation of iron catalysts under reaction conditions.

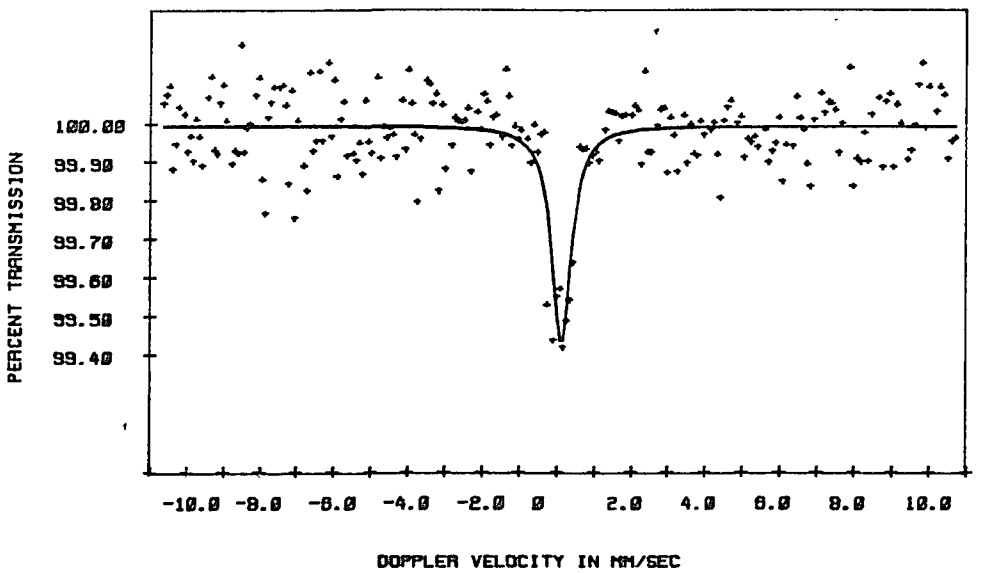

Figure 33. ^{57}Fe Mossbauer spectra of $[Ru(NH_3)_6]_x\ [Fe(CN)_6]_y \cdot zH_2O$

Figure 34. Infrared spectra of $[Ru(NH_3)_6]_x$ $[Fe(CN)_6]_y \cdot zH_2O$.

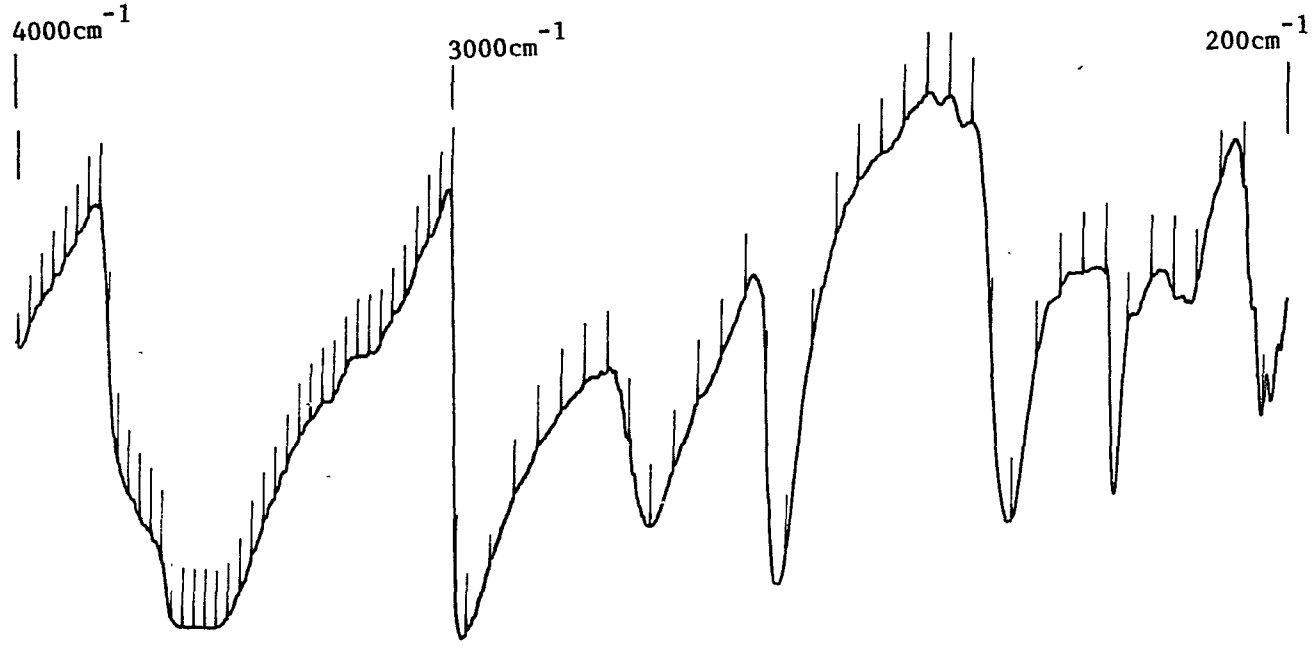

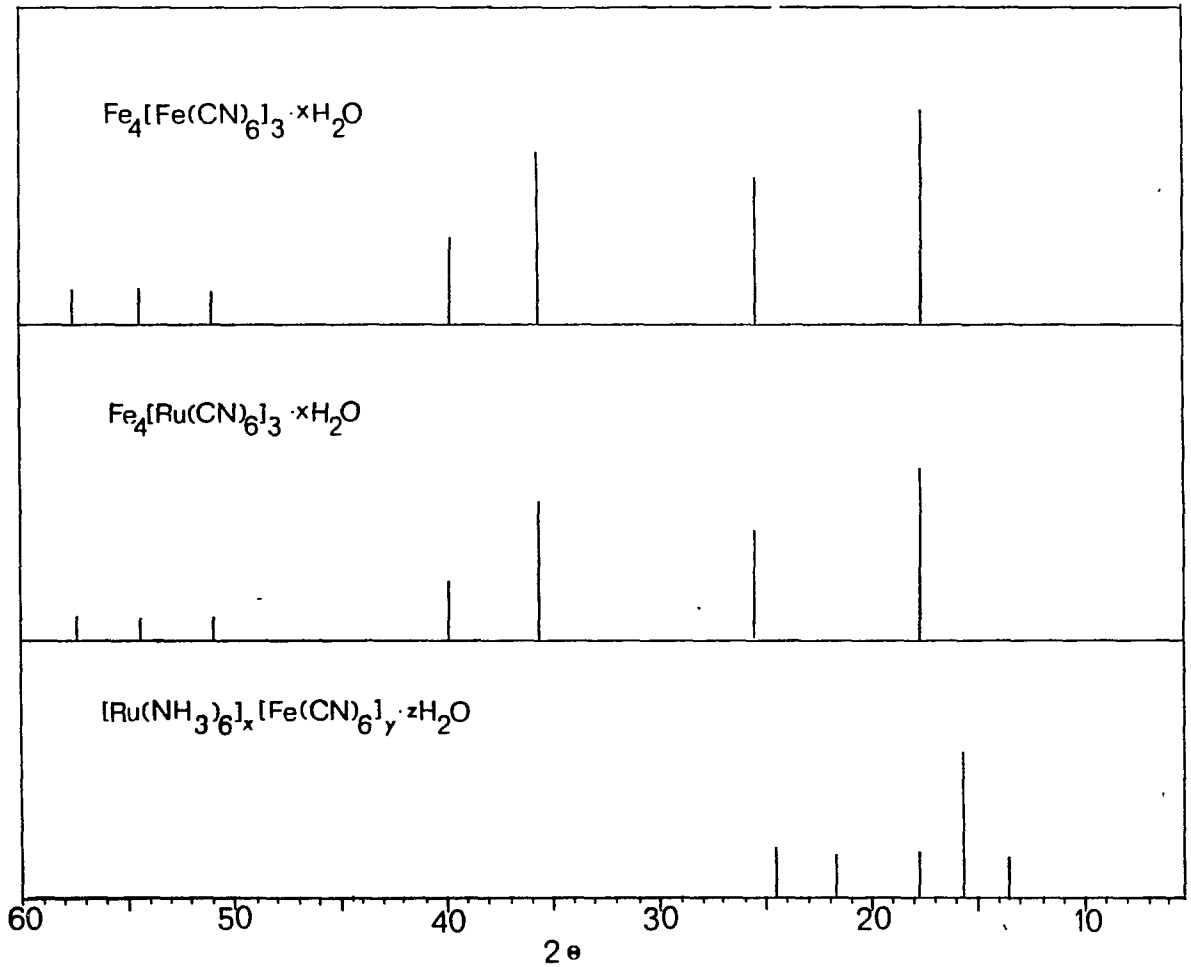

Figure 35. X-ray powder pattern of three Iron-Ruthenium cyanide complexes.

CHAPTER VII

CONCLUSIONS

These studies have indicated very clearly the utility of the iron Mossbauer effect to study iron catalysts and to define the chemical changes which occur during preparation and treatment. They have also indicated the diverse chemistry associated with iron and ruthenium complexes when they are supported on zeolites. The results should be very useful to those groups attempting to design specific supported catalysts of known chemical properties.

The systems studied have included an iron exchanged, ammonium exchanged bifunctional Y-zeolite catalyst. This system was designed to modify the acidic properties of the zeolite as compared to that of the unmodified Na-Y Zeolite. It was also hoped that the use of the ammonia-hydrogen mixture as the reducing agent might facilitate the reduction of iron to the metallic state. However, this modification did not provide any new insight into the reduction behavior of iron.

The reduction of iron to the metallic state may be promoted if hydrogen atoms rather than hydrogen molecules are used as the reducing agent. Since the adsorption of hydrogen takes place to a greater degree on ruthenium, and the reduction process may be accelerated by hydrogen atom spillover, ruthenium metal was added to the system. It was found that the iron had more effect on the chemical behavior of ruthenium than ruthenium had on the chemical behavior of iron. For example, the ruthenium exchanged Y-zeolite was unstable and the yellow color changed

to the characteristic ruthenium-red, when it was exposed to air. With iron present, the formation of "ruthenium red" was inhibited. Since the formation of the red species involved the hydrolysis reaction, the interpetation is that iron favorably competes to draw the water into its coordination sphere and suppresses the ruthenium hydrolysis. The strong bond between iron and oxygen may be responsible for the strong association of the cation with the interchannel water molecules. Furthermore in the presence of iron, a very dispersed ruthenium system was stabilized. The iron apparently prevents the agglomeration of the ruthenium particles. A reversible oxidation-reduction process between ferric-ferrous states was observed, identical to that for the iron only system on Y-zeolite. There is some evidence that the reduction to ferrous state may be enhanced, but the reduction to the metallic state was not accomplished. This effect is attributed to the strong iron-zeolite interaction which is not obstructed by the ruthenium. Contrary to iron, ruthenium reduced easily on the surface of the zeolite and oxidized rapidly at room temperature in air. The lower isomer shift value for the oxidized sample as compared to the correspounding value for bulk ruthenium oxide, is attributed to the association of ruthenium with a few oxygens probably in the form of oxygen bridges. High temperature oxidation of the material leads to the agglomeration of ruthenium oxide outside of the zeolite cavities as shown by ^{99}Ru Mossbauer spectroscopy.

The nearly independent behavior of iron and ruthenium in the zeolite in the first experiments was attributed to the low concentration of the metals and the large surface area of the support. In addition, the metals are introduced by the ion exchange technique and are thus

dispersed at the atomic level in different locations in the zeolite. The interaction between the two metals is expected to be low and the effect on iron of hydrogen spillover on ruthenium is not significant. To increase the extent of interaction between iron and ruthenium, in later experiments the metal solutions were introduced by the method designated as "Homogeneous-Deposition". Under these preparation and subsequent treatment conditions the formation of the hcp ruthenium-iron bimetallic alloy was confirmed. The results have led to the postulation that thick film deposits are formed on the surface of the zeolite during preparation. Under reduction, the layers break up into iron-ruthenium crystallites separated by zeolite, and supported on unreduced iron oxide islands. At least 30% of the total iron in the system is reduced to the metallic state.

These results are a primary indication that the classic problem of the reduction of iron in the Y-zeolite system can be at least partially solved. However, a careful examination of the variables will be needed to develop a reproducible method for controlling the amount of iron reduced and the degree of dispersion. For example, increasing the concentration of the impregnation solution will probably lead to increased metal deposition and decreased dispersion. Other factors which affect the reduction chemistry are: the ruthenium/iron concentration ratio; the initial pH of the depositing solution; reduction time; temperature and hydrogen flow rate; passivation; calcination; and dehydration.

To elucidate the exact nature of the interaction between iron and ruthenium and to evaluate the solid state reactions which take place during bimetallic formation, several iron-ruthenium mixtures were pre-

pared by the addition of ruthenium trichloride to a variety of iron salts and oxides. It was found that the anion present in the starting mixture significantly influenced the final oxidation-reduction products. The chloride-chloride system yielded a clean and uniform product during oxidation-reduction treatments Under reduction conditions, bcc iron and hcp iron-ruthenium were formed. The evaluation of the superparamagnetic relaxation as a function of temperature provided information to estimate the average particle size of the metal crystallites. The product after calcination was totally converted to bulk α-Fe_2O_3.

The nitrate-chloride system behaved very similarly to the chloride-chloride system except that the oxidation-reduction products were not uniform and some unidentified residue remained. Since the iron nitrate is expected to undergo decomposition when heated, the evolved gases may have been trapped in the sample causing the low recoil-free fraction observed for these material.

The sulfate-chloride system behaves quite differently as compared to the nitrate or chloride systems. The role of the sulfate ion is quite interesting since it remains in the structure and provides a cubic-close packed array of oxide ions in which the divalent iron cations with coordination number 4 are in tetrahedral interstices and the three valent iron cations with coordination number 6 are located in the octahedral interstices in a crystal having inverse spinal structure.

The oxidation-reduction behavior of a system containing iron oxide and ruthenium chloride was compared with the corresponding behavior of an iron oxide only system. It was clearly demonstrated that the formation of ε phase iron was only possible in the presence of ruthenium, where the superparamagnetic iron oxide formation was independent of the

presence of ruthenium. The iron enrichment on the surface of the alloy was detected to be about 68%, under reduction conditions. This value reduces to 50% when the sample is exposed to air, which indicates that air quenching of surface region may caused the reversal of segregation phenomenon under oxidation condition. The lattice parameters for hcp iron-ruthenium was calculated as a = 2.681 A° and c/a = 1.583 which are smaller in both the a and c axis than pure ruthenium. This is evidently an effect of the substitution of iron into the hcp ruthenium lattice.

The formation of the mixed spin iron cyanide complexes in the X and Y zeolite was confirmed by Mossbauer spectroscopy. The method was based on the reaction of a ferric exchanged zeolite with an iron cyanide anion complex. It can be speculated that the diffusion of the complex anions to the cavities must be slow due to the repulsion of the negatively charged zeolite sites, but potassium cations can penetrate easily. Thus, the mechanism of formation may involve the back ion exchange of ferric cations from the framework by potassium, and then the mobilization of ferric cations towards the reactive ferrocyanide anion leading to the formation of the complex outside the cavity of the zeolite.

In the process of thermal vacuum dehydration treatment of Prussian Blue on Y-zeolite the H.S. Fe^{3+}, L.S. Fe(II) → H.S. Fe^{2+}, L.S. Fe(III) conversion was observed. This valency reversal mechanism may involve the transfer of one electron from L.S. $Fe(CN)_6^{4-}$ to H.S. Fe^{3+} cation followed by the formation of $KFe^{2+}FeIII(CN)_6$. The potassium cations would have been absorbed from solution to maintain electrical neutrality. Such a formulation requires a close association of potassium with the lattice which is brought about during dehydration treatment. The cyanide ligands may serve as electron mediators.

Upon exposure of the dehydrated material to air $H.S.Fe^{2+} \rightarrow H.S.Fe^{3+}$ oxidation is apparent followed by L.S.Fe(II) → L.S.Fe(III) during hydration of the material in air, consequently the Prussian Blue is reconstituted. Large metallic bcc iron particles are formed during the reduction treatment. This is attributed to the presence of a Prussian Blue deposit on the external surface of the zeolite in the initial material. In order to synthesize the material within the cavities, a modified preparation procedure was proposed. It was suggested that the anion solution should be introduced by incipient wetness impregnation and that the catalyst should be thermally activated to achieve the diffusion of the reactive anion through the zeolitic windows. The amount of anion added should be minimized to promote the formation of microcrystalline "soluble" Prussian Blue and to avoid the peptization to "insoluble" Prussian Blue.

The ferric ruthenocyanide was synthesized in the Y-zeolite by the above procedure. The formation of the complex was confirmed and the material characterized during dehydration-hydration and oxidation-reduction treatments. Two different iron species are detected. One is associated with iron originally ion exchanged in the zeolite and the second form is due to the ferric ruthenocyanide itself. The ion exchanged form reversibly oxidized and reduced between the ferrous and ferric states but the ferric ruthenocyanide reduced to the bimetallic state. The formation of hcp iron-ruthenium was confirmed.

These studies indicate pathways to the production of highly dispersed iron and iron-ruthenium catalysts on zeolites. Such materials are of significant interest in a number of catalytic proceses, particularly those involving syngas conversion.

REFERENCES

1. Vannice, M. A., J. Catal. 37, 449 (1975).

2. Vannice, M. A., J. Catal. 37, 462 (1975).

3. Kirch, M., Lehn., J. M., and Sauvage, J. P. Helv. Chim. Acta - 62, 1345 (1979).

4. Maverick, A. W., and Gray, H. B., Pure Appl. Chem. 55, 2339 (1980).

5. Technology report. C and EN, 44, Sept. 8 (1980).

6. Sinfelt, J. H. Prog. Solid State Chem. 10, 55 (1975).

7. Lunsford, J. H., and Gustafson, B. L., J. Catal. 74, 393 (1982).

8. McKetta, J. J., Chem. Eng. Prog. 69, 51 Aug. (1973).

9. Walters, E. A., and Wewerka, E. M., J. Chem. Edu. 52, 282 (1975).

10. Wender, I., Catal. Rev. - Sci. Eng. 14(1), 97 (1976).

11. King, D. L., Cusumano, J. A., and Garton, R. L., Catal. Rev. - Sci. Eng. 23 (1 & 2), 233 (1981).

12. Vannice, M. A., Catal. Rev. - Sci. Eng. 14(2), 153 (1976).

13. Day, M. E., and Hoogendoorn, J. C., Catal. Rev. - Sci. Eng. 23(1 & 2), 265 (1981).

14. Sabatier, P., Senderens, J. B., C. R. Acad. Sci. 134, 514 (1902).

15. Fischer, F., and Tropsch, H., Brennst. Chem. 4, 276 (1923).

16. Ponec, V., Catal. Rev. - Sci. Eng. 18(1), 151 (1978).

17. Pichler, H., Adv. Catal. 4, 271 (1952).

18. Biloen, P., and Sachtler, W. M. H., Adv. Catal. 30, 165 (1981).

19. Bell, A. T., Catal. Rev. - Sci. Eng. 23, 203 (1981).

20. Bianchi, D., Borcar, S., Teule-Gay, F., and Bennett, C. O., J. Catal. 82, 442 (1983).

21. Dwyer, D. J., and Somorjai, G. A., J. Catal. 52, 291 (1978).

22. Guczi, L., Catal. Rev. - Sci. Eng. 23(3), 329 (1981).

23. Niemantsverdriet, J. W. and van der Kraan, A. M. V., J. Catal. 72, 385 (1981).

24. Bartholomew, C. H., Catal. Rev. - Sci. Eng. 24(1), 67 (1982).

25. King, D. L., J. Catal. 61, 77 (1980).

26. Miyazaki, E., J. Catal. 65, 84 (1980).

27. Blyholder, G., J. Phys. Chem. 79, 756 (1975).

28. Doyen, G., and Ertl, G., Surf. Sci. 43, 197 (1974).

29. Heal, M. J., Leisegang, E. C., and Torrington, R. G., J. Catal. 51, 314 (1978).

30. Gupta, N. M., Kamble, V. S., Annaji Rao, K., and Iyer, R. M., J. Catal. 60, 57 (1979).

31. Gustafson, B. L., and Lunsford, J. H., J. Catal. 74, 405 (1982).

32. Unmuth, E. E., Schwartz, L. H., and Butt, J. B., J. Catal. 63, 404 (1980).

33. Biloen, P., Helle, J. N., and Sachtler, W. M. H., J. Catal. 58, 95 (1979).

34. Bonzel, H. P., and Krebs, H. J., Surf. Sci. 91, 449 (1980).

35. Low, G. G., and Bell, A. T., J. Catal. 57, 397 (1979).

36. Rabo, J. A., Risch, A. P., and Poutsma, M. L., J. Catal. 53, 295 (1978).

37. Ekerdt, J. G., and Bell, A. T., J. Catal. 62, 19 (1980).

38. Ekerdt, J. G., and Bell, A. T., J. Catal. 58, 170 (1979).

39. Brady, R. C., and Petit, R., J. Am. Chem. Soc. 102, 6181 (1980).

40. Bussemeier, B., Frohning, C. D., and Cornils, B., Hydrocarbon Process, P.105, Nov. (1976).

41. Luger, C. R., Hydrocarbon Process, P.105, Jun. (1976).

42. Day, M. E., and Oosthuizen, G. J., J. Catal. 11,18 (1968).

43. Somorjai, G. A., Catal. Rev. - Sci. Eng. 23(1 & 2), 189 (1981).

44. Yang, C. H., and Oblad, A. G. Am. Chem. Soc. Div. Petr. Chem. Prepr., P.513 (1978).

45. Amelse, J. A., Schwartz, L. H., and Butt, J. B., J. Catal. 72, 95 (1981).

46. Jacobs, P. A., Verdonck, J., and Uytterhoeven, J. B., Advan. Chem. Series 178, 15 (1979).

47. Guczi, L., Matusek, K., Eszterle, M., and Schay, Z., Hetro. Catal. 1, 117 (1979).

48. Vannice, M. A., Lam, Y. L., and Garten, R. L., Advan. Chem. Series, 178, 25 (1979).

49. Tkatchenko, D. B., Coudurier, G., and Tkatchenko, I., Am. Chem. Soc. Div. Petro. Chem. Prepr., p.755 (1980).

50. Ott, G. L., Fleisch, T., and Delgass, W. N., J. Catal. 60, 394 (1979).

51. Donner, J. T., Ph. D. Dissertation, Louisiana State University, Baton Rouge, Louisiana, May 1983.

52. Chen, Y. M., Wang, H. T., and Goodwin, J. G., J. Catal. 83, 415 (1983).

53. Delgass, W. N., and Boudart, M., Catal. Rev. 2(1), 129 (1968).

54. Herber, R. H., "The Mossbauer effect and its application in chemistry": Advances in Chemistry Series (R. H. Herber, Eds.), vol. 68, American Chemical Society, Washington, D. C., 1967.

55. Shenoy, G. K., and Wagner, F. E., "Mossbauer Isomer Shifts", North-Holland Co., 1978.

56. Delgass, W. N., Haller, G. L., Kellerman, R., and Lunsford, J. H., "Spectroscopy In Heterogeneous Catalysis", p. 132, Academic Press, Inc., 1979.

57. Dumesic, J. A., and Topsoe, H., Adv. Catal. 26, 121 (1976).

58. Berry, F. J., "Advances in Inorganic Chemistry and Radiochemistry" (H. J. Emeleus, Eds), Vol. 21, p. 255, Academic Press, Inc., 1978.

59. Mourey, C., Marchal, G., and Janot, C., J. DE Phys. C6, 713 (1976).

60. Gol'danskii, V. I., and Suzdalev, I. P., Russ. Chem. Rev. 39(7), 609 (1970).

61. Stevens, J. G., and Stevens, V. E., "Mossbauer Effect Data Index Convering Up to 1976 Literature", Plenum Press, New York, 1978.

62. Garger, H. M., and Hobson, M. C., Jr., Catal. Rev. - Sci. Eng. 11, 117 (1975).

63. Bancroft, G. M, and Platt, R. H., in "Advances in Inorganic Chemistry and Radiochemistry" (H. J. Emeleus, Eds.), Vol. 15, p. 59, Academic Press, Inc., 1972.

64. Mossbauer, R. L., Z. Phys. 151, 124 (1958).

65. Gol'danskii, V. I., and Makarov, E. F., in "Chemical Application of Mossbauer Spectroscopy" (V. I. Gol'danskii, and R. H. Herber, Eds.), p.1, Academic Press, New York, 1968.

66. Danon, J., Report of a Panel on Application of Mossbauer Effect in Chemistry and Solid State Physics, Tech. Rep. Ser. 50, p. 89, Int. Atomic Energy Ag., Vienna, 1966.

67. Bancroft, G. M., Maddock, A. G., and Burns, R. G., Geochim. Cosmochim. Acta, 31, 2219 (1967).

68. Greenwood, N. N., and Gibb, T. C., "Mossbauer Spectroscopy", Chapman and Hall, London, 1971.

69. Wickman, H. H., Klein, M. P., and Shirley, D. A., Phys. Rev. 152, 345 (1966).

70. Wickman, H. H., and Werthem, G. K., in "Chemical Application of Mossbauer Spectroscopy" (V. L. Gol'danskii, and R. H. Herber, Eds.), p. 548, Academic Press, New York, 1968.

71. Gosser, V., Sakai, H., and Keune, W., J. DE Phys. C6(12), 709 (1976).

72. Boudart, M., Dumesic, J. A., and Topsoe, H., In "Physical Basis of Heterogeneous Catalysis", (E. Drauglis and R. I. Jaffe, Eds.), Plenum Press, New York, 1975.

73. Gonser, U., In "An Introduction to Mossbauer Spectroscopy" (L. May, Eds), p. 169, Plenum, New York, 1971.

74. Akaroni, A., Crit. Rev. Solid State Sci., p. 121 (1971).

75. Kittel, C., "Introduction to Solid State Physics", Chapter 16, Wiley, New York, 1971.

76. Morrish, A. H., "The Physical Principles of Magnetism", p. 312, Wiley, New York, 1965.

77. Gager, H. M., Hobson, M. C., and Lefelhocz, J. F., Chem. Phys. Lett. 15, 124 (1972).

78. Kistner, O. C., and Sunyar, A. W., Phys. Rev. Lett. 4, 412 (1960).

79. Kundig, W., and Bommel, H., Phys. Rev. 142, 327 (1966).

80. Schroeer, D., and Nininger, R. C., Jr., Phys. Rev. Lett 19, 632 (1967).

81. Roggwille, P., and Kundig, W., Solid State Comm. 12, 901 (1973).

82. Morup, S., Topsoe, H., and Lipka, J., J. DE Phys. C6(12), 287 (1976).

83. Amulyavichus, A. P., and Suzdalev, I. P., Zh. Eksp. Teor. Fiz. 64, 1702 (1973).

84. Dormann, J. L., Gibart, P., and Renaudin, P., J. DE Phys. C6(12), 281 (1976).

85. Ruppin, R., Phys. Rev. B. 2(5), 1229 (1970).

86. Gibb, T. C., Greatrex, R., and Greenwood, N. N., J. Chem. Soc. A. 890 (1968).

87. Pfannes, H. D., and Gonser, U., Appl. Phys. 1, 93 (1973).

88. Gol'danskii, V. I., and Karyagin, S. V., Phys. Status Solidi A. 68, 693 (1975).

89. Gol'danskii, V. L., Makarov, E. F., and Khrapov, V. V., Phys. Lett. 3(7) 344 (1963).

90. Abras, A., and Mullen, J. G., Phys. Rev. A. 6, 2343 (1972).

91. Delgass, W. N., and Chen, L. Y., Rev. Sci. Instrum. 47(8), 968 (1976).

92. Clausen, B. S., Morup, S., Nielsen, P., Thrane, N., and Topsoe, H., J. Phys. E: Sci. Instrum. 12, 439 (1979).

93. Heineman, H., Catal. Rev. - Sci. Eng. 23(1 & 2), 315 (1981).

94. Naccache, C., and Taarit, Y. B., Acta Phys. Chim. 24, 23 (1978).

95. Rabo, J. A., Bezman, R. D., and Poutsma, M. L., Acta Phys. Chim. 24, 39 (1978).

96. Smith, J. V., Pure and Appl. Chem. 52, 2131 (1980).

97. Sand, L. B., Pure and Appl. Chem. 52, 2105 (1980).

98. Robson, H., Chem. Technol. p.177 (1978).

99. Venuto, P. B., and Habbib, E. T., Catal. Rev. - Sci. Eng., 18(1), 1 (1978).

100. Rabo, J. A., and Poutsma, M. L., Adv. Chem. Ser. 102, 284 (1971).

101. Rabo, J. A., "Zeolite Chemistry and Catalysis", ASC Monograph 171, Washington, D. C., 1976.

102. Meyers, J., Ladriere, J., Chavee, M., and A ?????, J. DE Phys. C6(12), 905 (1976).

103. Csicsery, S. M., in "Zeolite Chemistry and Catalysis", (J. A. Rabo, Eds.), ASC Monograph 171, p. 680, Washington, DC, 1976.

104. Nijs, H. H., Jacobs, P. A., and Uytterhoeven, J. B., J. Chem. Soc. Chem. Comm. 180 (1979).

105. Fraenkel, D., and Gates, B. C., J. Am. Chem. Soc., 102,(7), 2479 (1980).

106. Derouane, E. G., and Gabelica, Z., J. Catal. 70, 238 (1981).

107. Weisz, P. B., Pure and Appl. Chem. 52, 2091 (1980).

108. Kaeding, W. W., Chu., C., Young, L. B., and Butter, S. A., J. Catal. 69, 392 (1981).

109. Pope, C. G., J. Catal. 72, 174 (1981).

110. Schoonheydt, R. A., Vandamme, L. J., Jacobs, P. A., and Uytterhoeven, J. B., J. Catal. 43, 292 (1976).

111. Gallezot, P. and Imelik, B., J. Phys. Chem. 77(5), 652 (1973).

112. Uytterhoeven, J. B., Acta. Phys. Chem. 24, 53 (1978).

113. Rand, B., and Marsh, H., J. Cooloid Interface Sci. 40(1), 121 (1972).

114. Rabo, J. A., Angell, C. L., Kasai, P. H., and Schomaker, V., Discuss. Faraday Soc. 41, 328 (1966).

115. Kasai, P. H., and Bishop, R. J., Jr., in "Zeolite Chemistry and Catalysis", (J. A. Rabo, Eds.), ACS Monograph 171, Chapter 6, Washington, DC, 1976.

116. Rabo, J. A., Catal. Rev. - Sci. Engr. 23(1 & 2), 293 (1981).

117. Beaumont, R., and Barthomeuf, D., J. Catal. 26, 218 (1972).

118. Naccache, C., and Taarit, Y. B., Pure and Appl. Chem. 52, 2175 (1980).

119. Lunsford, J. H., Cata. Rev. - Sci. Eng. 12(2), 137 (1975).

120. Hurst, N. W., Gentry, S. J., and Jones, A., Catal. Rev. - Sci. Eng. 24(2), 233 (1982).

121. Figueras, F., Gomez, R., and Primet, M., Adv. Chem. Sci. 121, 480 (1973).

122. Gallezot, P., Catal. Rev. - Sci. Eng. 20(1), 121 (1979).

123. Baetzold, R. C., J. Chem. Phys. 68, 555 (1978).

124. Naccache, C., Primet, M., and Mathieu, M. V., Adv. Chem. Sci. 121, 266 (1973).

125. Vedrine, J. C., Dufaux, M., Naccache, C., and Imelik, B., J. Chem. Soc. Faradary I. 74, 440 (1978).

126. Beyer, H., Jacobs, P. A., and Uytterhoeven, J. B., J. Chem. Soc. Farraday I. 72, 674 (1976).

127. Chukin, G. D., and Agafonov, Sixth Int. Congr. Catalysis 2, 688 London 1976.

128. Gentry, S. J., Hurst, N. W. and Jones, A., J. Chem. Soc. Faraday I. 75, 1688 (1979).

129. Morice, J. A., and Rees, L. V. C., Trans. Faraday Soc. 64, 1388 (1968).

130. Jacobs, P. A., Tielen, M., Linart, J. P., Uytterhoeven, J. B., and Beyer, H., J. Chem. Soc. Faraday I. 72, 2793 (1976).

131. Gallezot, P., Imelik, B., Adv. Chem. Series 121, 66 (1973).

132. Garten, R. L., J. Catal. 43, 18 (1976).

133. Garten, R. L., and Vannice, M. A., J. Mol. Catal. 1, 201 (1975).

134. Garten, R. L., and Ollis, D. F., J. Catal. 35, 232 (1974).

135. Flinn, P. A., and Ruby, S. L., Science 143, 1434 (1964).

136. Hobson, M. C., Jr., and Gager, H. M., J. Catal. 16, 254 (1970).

137. Dezsi, I., Nagy, D. L., Eszterle, M., and Guczi, L., J. DE Phys. C2 (3), 76 (1979).

138. Amelse, J. A., Butt, J. B., and Schwartz, L. H., J. Phys. Chem. 82 (5), 558 (1978).

139. Raupp, G. B., and Delgass, W. N., J. Catal. 58, 337 (1979).

140. Raupp, G. B., and Delgass, W. N., J. Catal. 58, 348 (1977).

141. Raupp, G. B., and Delgass, W. N., J. Catal. 58, 361 (1979).

142. Unmuth, E. E., Schwartz, L. H., and Butt, J. B., J. Catal. 61, 242 (1980).

143. Kostinko, J. M., 183rd ACS National Meeting, Las Vegas, Nevada, Pete. No. 016, 1982.

144. Charnell, J. F., J. Cryst. Growth 8, 291 (1971).

145. Boudart, M., Delbouille, A., Dumesic, J. A., Khammouma, S., and Topsoe, H., J. Catal. 37, 486 (1975).

146. Dumesic, J. A., Topsoe, H., Khammouma, S., and Boudart, M., J. Catal. 37, 503 (1975).

147. Dumesic, J. A., Topsoe, H., and Boudart, M., J. Catal. 37, 513 (1975).

148. Dumesic, J. A., Topsoe, H., and Derouane, E. G., Clausen, B. S., Morup, S., Villadsen, J. and Torpoe, N., "Preparation of Catalysts II", p. 365, Elsevier Scientific Publishing Co., Amsterdam, 1979.

149. Rubashov, A. M., Fabrichnyi, P. B., Strakhov, B. V., and Babeshkin, A. M., Russ. J. Phys. Chem. 46, 765 (1972).

150. Gao, Z., and Rees, L. V., Zeolites, 2, 72 (1982).

151. Gao, Z., and Rees, L. V. Zeolites, 2, 79 (1982).

152. Dickson, B. L., and Rees, L. V., J. Chem. Soc. Faraday I, 70, 2038 (1974).

153. Dickson, B. L., and Rees, L. V., J. Chem. Soc. Faraday I, 70, 2051 (1974).

154. Dickson, B. L., and Rees, L. V., J. Chem. Soc. Faraday I, 70, 2060 (1974).

155. Segawa, K., Chen, Y., Kubsh, J. E., Delgass, W. N., Dumesic, J. A., and Hall, W. K., J. Catal. 76, 112 (1982).

156. Pearce, J. R., Mortier, W. J., and Uytterhoeven, J. B., J. Chem. Soc. Faraday I, 77, 937 (1981).

157. Lee, J. B., J. Catal, 68, 27 (1981).

158. Huang, Y. Y., and Anderson, J. R., J. Catal. 40, 143 (1975).

159. Garten, R. L., Delgass, W. N., and Boudart, M., J. Catal. 18, 90 (1970).

160. Delgass, W. N., Garten, R. L. and Boudart, M., J. Phys. Chem. 73, 2970 (1969).

161. Flinn, P. A., Ruby, S. L., and Kehl, W. L., Science 143, 1434 (1964).

162. Stone, J. A., in "Mossbauer Effect Methodolgy", Vol. 4, p. 217-236 (1968), Marshall, S. W., Nelson, J. A., and Wilenzick, R. M., Comm. of the ACM, 8, 313 (1965).

163. Kundig, W., and Hargrove, R. S., Solid State Comm. 7, 223 (1969).

164. Mizoguchi, T. and Tanaka, M. J., J. Phys. Soc. Jap. 18, 1301 (1963).

165. Fitch, F. R., and Rees, L. V., Zeolites, 2, 33 (1982).

166. Cotton, F. A., and Wilkinson, G., "Advance Inorganic Chemistry". p. 863, Wiley Inc., New York, 1972.

167. Wang, S. Y., Lu, A. H., and Tseng, P. K., Chinese J. Phys. 2, 50 (1964).

168. Suzdalen, I. P., Plachinda, A. S., Markarov, E., and Dolgopolov, V. A., Russ. J. Phy. Chem. 41, 1522 (1967).

169. Good, M. L. and Clausen, C. A., III, J. Catal. 46, 58 (1977).

170. Shelef, M., and Gandhi, H. S., Platinum Metal Rev. 18(1), 2 (1974).

171. Elliott, D. J., Ph.D. Dissertation, Texas A and M University, Dec. 1977.

172. Lunsford, J. H., and Elliott, D. J., J. Catal. 57, 11 (1979).

173. Gustafson, B. L., Ph.D. Dissertation, Texas A and M University, May 1981.

174. Verdonck, J. J., Jacobs, P. A., and Uytterhoeven, J. B., J. Chem. Soc. Chem. Comm. 181 (1979).

175. Gustafson, B. L., and Lunsford, J. H., J. Catal. 74, 393 (1982).

176. Coughlan, B., Narayanan, S., McCann, W. A., and Carroll, W. M., J. Catal. 49, 97 (1977).

177. McNicol, B. D., and Short, R. T., J. Electroanal. Chem. 92, 115 (1978).

178. Kinoshita, K., and Ross, P. N., J. Electroanal. Chem. 78, 313 (1977).

179. Hadzi-Jordanov, S., Angerstein-Kozlowska, H., and, Conway, B. E., J. Electroanal. Chem. 60, 359 (1975).

180. Koopman, P. G. J., Kieboom, A. P. G., and Bekkum, H., J. Catal, 69, 172 (1981).

181. Chaston, J. C., Platinum Met. Rev. 9, 51 (1965).

182. Hadzi - Jordanov, S., Angerstein-Kozlowska, H., and Conway, B. E., J. Electrochem. Soc. 125, 1471 (1978).

183. Good, M. L., and Clausen, C. A., III, J. Catal. 38, 92 (1975).

184. Muir, A. H., Jr., Ando, K. J., and Coogan, H. M., "Mossbauer Effect Data Index 1958-1965", Interscience Publishers, New York, 1966.

185. Guczi, L., Matusek, K., Manninger, I., Kiraby, J., and Eszterle, M., in "Proceeding of Symposium on Scientific basis for the preparation of Hetrogeneous Catalysts", p. 391, Elsevier Scientific Publ. Co., 1979.

186. Laing, K. R., Leubner, R. L., and Lunsford, J. H., Inorg. Chem. 14 (6), 1400 (1975).

187. Good, M. L., Madhusudhan, C. P., and Patil, M. D., Inorg. Chem. 18, 2384 (1979).

188. Good, M. L., and Clausen, C. A., III, Inorg. Chem. 16, 816 (1977).

189. Good, M. L., Akbarnejad, M. and Donner, J. T., Am. Chem. Soc. Div. Petr. Chem. Prepr., p. 763 (1980).

190. Pedersen, L. A., and Lunsford, J. H., J. Catal. 61, 39 (1980).

191. Verdonck, J. J., Schoonheydt, R. A., and Jacobs, P. A., J. Phys. Chem. 85, 2393 (1981).

192. Uytterhoeven, J. B., Pearce, J. R., Mortier, J. W., J. Chem. Soc. Faraday I, 75, 1395 (1979).

193. Jacobs, P. A., Verdonck, J. J., J. Chem. Soc. Faraday I, 76, 403 (1980).

194. Lunsford, J. H., Dewilde, W., and Peeters, G., J. Phys. Chem. 84, 2306 (1980).

195. McCann, W. A., Coughlan, B., and Caroll, W. M., Chem. Ind. (London), p. 527, 1976.

196. Sigwart, C., and Spence, J. T., J. Am. chem. Soc. 91, 3991 (1969).

197. Guczi, L., Dezsi, I, Nagy, D. L., and Eszterle, M., React. Kinet. Catal. Lett. 3, 301 (1978).

198. Garten, R. L., Mossbauer Effect Methodology, Vol. 10, 1976.

199. Garten, R. L., and Burton, J. J., "Advance Materials in Catalysis", p. 33, Academic Press, New York, 1977.

200. Guczi, L., Dezsi, I., Nagy, D. L., and Eszterle, M., International Conf. on the Appl. of the Mossbauer Effect, Aug. 28, 1978, Kyoto. Japan.

201. Vannice, M. A., Lam, Y. L., and Garten, R. L., Am. Chem. Soc. Div. Pete. Chem. Prepr., p. 495 (1978).

202. Fergusson, J. E., and Love, J. L., in "Inorganic Synthesis" (F. A. Cotton, Eds.), Vol. 13, p. 208, McGraw-Hill Book Company, New York, 1972.

203. Lever, F. M., Powell, A. R., "International Conference on Coordination Chemistry", p. 135, Special Publication number 13, The Chemical Society, London, 1959.

204. Ford, P. C., Coordin. Chem. Rev. 5, 75 (1970).

205. Allen, A. D., and Senoff, C. V., Canadian J. Chem. 45, 1337 (1967).

206. "Scott's Standard Methods of Chemical Analysis" (N. H. Furman Eds.) Fifth Edition, Vol. 1, p. 878-881, D. Van Nostraud Co. Inc.

207. Kistner, O. C., Monaro, S., and Segnan, R., Phys. Letters, 5, 299 (1963).

208. Kistner, O. C., Phys. Rev. 144(3), 1022 (1966).

209. Good, M. L., Clausen, C. A., III, and Prados, R. A., Mossbauer Effect Methodology, 6, 31 (1971).

210. Good, M. L., Mossbauer Effect Data Index, p. 51, 1972.

211. Good, M. L., Clausen, C. A., III, and Prados, R. A., J. Coord. Chem. 2, 201 (1973).

212. Good, M. L., Alexander, C. J., Siddall, T. H., III, and Foyt, D. C., Inorg. Chem. 13, 1793 (1974).

213. Good, M. L., Foyt, D. C., J. Inorg. Nucl. Chem. 37, 1913 (1975).

214. Mossbauer, R. L., Kaindl, G., Potzel, W., Wagner, F., and Zahn, U., Z. Physik 226, 103 (1969).

215. Gibb, T. C., Greatrex, R., Greenwood, N. N., Puxley, D. C., and Snowdon, K. G., Chem. Phys. Lett. 20 (1), 130 (1973).

216. Uytterhoeven, J. B., Christner, L. G., and Hall, W. K., J. Phys. Chem. 69, 2117 (1965).

217. Patil, M. D., Ph.D Dissertation, University of New Orleans, May 1981.

218. Williamson, D. L., Bukshpan, S., and Ingalls, R., Phys. Rev. B, 6 (11), 4194 (1972).

219. Ohno. H., J. Phys. Soc. Jopan, 31(1), 92 (1971).

220. Abrahams, S. C., Guttman, L., and Kasper, J. S., Phys. Rev. 127, 2052 (1962).

221. Johnson, G. J., McGirr, M. B., and Wheeler, D. A., Phys. Rev. B, 1, 3208 (1970).

222. Nicol, M., and Jura, G., Science, 141, 1035 (1963).

223. Williams, J. M., and Pearson, D. I. C., J. DE Phys. C6(12), 401 (1976).

224. Williams, J. M., and Pearson, D. L. C., Physica. 86B, 279 (1977).

225. Rush, J. D., Johnson, C. E., Thomas, M. F., J. Phys. F: Metal Phys. 6(10), 2017 (1976).

226. Giles, P. M., Longenbach, M. H., and Marder, A. R., J. Apply. Phys. 42(11), 4290 (1971).

227. Gordon, P., "Principles of Phase Diagrams in Materials Systems". McGraw-Hill, New York, 1968.

228. Burton, J. J., Hyman, E., and Fedak, D. G., J. Catal. 37, 106 (1975).

229. Ott, G. L., and Delgass, W. N., J. Catal. 56, 174 (1979).

230. Ott, G. L., Fleisch, T., and Delgass, W. N., J. Catal. 60, 394 (1979).

231. Urabe, K., and Ozaki, A., J. Catal. 52, 542 (1978).

232. Zwell, L., Speich, G. R., and Leslie, W. C., Metallurgical Transaction 4, 1990 (1973).

233. Wertheim, G. K., Jaccarino, V., Wernick, J. H., and Buckanan, D. N. E., Phys. Rev. Lett. 12(1), 24 (1964).

234. Good, M. L., Patil, M. D., Donner, J. T., and Madkusudhan, C. P., Adv. Chem. Series, 194, 553 (1981).

235. Good, M. L., Akbarnejad, M., Patil, M. D., and Donner, J. T., "Nuclear and Electron Resonance Spectroscopies Applied to Materials Science", p. 271, Elsevier, North-Holland, Inc., 1981.

236. Delgass, W. N., Hughes, T. R., and Fadley, C. S., Catal. Rev. 4 (2), 179 (1970).

237. Kerkhof, F. P. J. M., and Moulijn, J. A., J. Phys. Chem. 83, 1612 (1979).

238. Fadley, C. S., In "Electron Spectroscopy: Theory Techniques and Applications", (C. R. Brundle and A. D. Baker, Eds.), Vol. 2, p. 1, Academic Press, New York, 1978.

239. Wagner, C. D., Riggs, W. M., Davis, L. E., Moulder, J. F., and Muilenberg, G. E., (Editor), "Handbook of X-ray Photoelectron Spectroscipy". Perkin-Elmer Corp., Eden Prairie, Minn., 1979.

240. Greenwood, N. N, and Howe, A. T., J. Chem. Soc. Dalton Trans., pp. 110, 116 and 122 (1972).

241. Kayo, A., Yamaguchi, T., and Tanabe, K., J. Catal. 83, 99 (1983).

242. Ono, K., Ishikawa, Y., and Ito, A., J. Phys. Soc. Japan, 17 (Suppl. B-I), 125 (1962).

243. Sprenkel-Segel, E. L., and Hanna, S. S., Geochim. Cosmochim Acta, 28, 1913 (1964).

244. Morrish, A. H., Haneda, K., and Schurer, P. J., J. DE. Phys. C6(12), 301 (1976).

245. Raub, E., and Plate, W., Z. Met. 51, 477 (1960).

246. Scofield, J. H., J. Electron Spect. and Related Phen. 8, 129 (1976).

247. Kim, K. S., and Winogard, N., J. Catal. 35, 66 (1974).

248. Carlson, T. A., "Photoelectron and Auger Spectroscopy", p. 262, Plenum, New York, 1975.

249. Cramer, R., J. Am. Chem. Soc. 87, 4717 (1965).

250. Yaskima, T., Ushida, Y., Ebisawa, M., and Hara, N., J. Catal. 36, 320 (1975).

251. Mantovani, E., Palladino, N., and Zanobi, A., J. Mol. Catal. 3, 285 (1977).

252. Griffith, W. P., Quart, Rev. 16, 188 (1962).

253. Home, R. F., and Lunsford, J. H., J. Am. Chem. Soc. 97, 5156 (1975).

254. Gelin, P., Ben Tarrit, Y., and Naccache, C., J. Catal, 59, 357 (1979).

255. Scherzer, J., and Fort, D., J. Catal. 71, 111 (1981).

256. Thompson, R. C., J. Am. Chem. Soc. 70, 1045 (1948).

257. Maer, K., Beasley, M. L., Collins, R. L., and Milligan, W. O., J. Am. Chem. Soc. 90, 3201 (1968).

258. Cosgrove, J. C., Collins, R. L., and Murty, D. S., J. Am. Chem. Soc. 95, 1083 (1973).

259. Bhattacharya, A. K., and Saxend, R., J. Indian Chem. Soc. 28, 145 (1951).

260. Robin, M. B., and Day, P., Adv. Inorg. Chem. and Radiochem. 10, 247 (1967).

261. Fluck, E., Kerler, W., and Neuwirth, W., Angew. Chem. Intern. Ed. (English) 2, 277 (1963).

262. Buser, H. J., and Ludi, A., J. Chem. Soc. Chem. Comm., 1299 (1972).

263. Robin, M. B., Inorg. Chem. 1, 337 (1962).

264. Weiser, H. B., Milligan, W. O., and Bates, J. B., J. Phys. Chem. 45, 701 (1941).

265. Seifer, G. B., Russ. J. Inorg. Chem. (English), 7, 621 (1962).

266. Robinette, R., and Collins, R. L., J. Coord. Chem. 4, 65 (1974).

267. Keggin, J. F., and Miles, F. D., Nature, 137, 577 (1936).

268. Alexander, J. J., and Gray, H. B., Coord. Chem. Rev. 2, 29 (1967).

269. Shriver, D. F., Struct. and Bond, 1, 32 (1966).

270. Adams, D. M., "Metal-Ligand and Related Vibrations", p. 170, St. Martin's Press, New York, 1968.

271. Fung, S. C. and Drickamer, H. G., J. Chem. Phys. 51, 4353 (1969).

272. Wet, J. F., and Rolle, R., Z. Inorg. Allg. Chem. 336, 96 (1965).

273. Klug, H. P., and Alexander, L. E., "X-ray Diffraction Procedures", Wiley, New York, 1967.

VITA

Mohammad Mehdi Akbarnejad was born in Shiraz, Iran on 1950. He educated in Iran until 1973 when he received a Bachelor of Science degree in Chemistry. He then spend two years in military service and subsequently in 1975 he began his education in the United States. In December of 1977 he received a Master of Science degree in the field of Industrial Chemistry from the University of Central Florida. Subsequently he continued his graduate studies at the University of New Orleans. In June of 1979 he transferred to the Department of Chemistry at the Louisiana State University in order to continue working in the field of Inorganic Chemistry under the guidance of Dr. Mary L. Good.

EXAMINATION AND THESIS REPORT

Candidate: M. Mehdi Akbarnejad

Major Field: Inorganic Chemistry

Title of Thesis: Characterization of Iron - Ruthenium Bimetallic Catalyst Systems

Approved:

Mary L. Good
Major Professor and Chairman

William Lowe
Dean of the Graduate School

EXAMINING COMMITTEE:

Geoffrey A. Ozin

Steven F. Watkins

Byron J. Hale

Teresa G. Monger

Francis C. Cartledge

Date of Examination:

April 30, 1984